EXPANDING THE APPLICATIONS OF UTAH ARRAYS:

A NEURAL INTERFACE FOR SMALLER NERVES,

THE CONTROL OF URINATION

AND PROSTHETIC LIMBS

by

Heather Anna Cary Wark

A dissertation submitted to the faculty of
The University of Utah
in partial fulfillment of the requirements for the degree of

Doctor of Philosophy

Department of Bioengineering

The University of Utah

August 2014

The University of Utah Graduate School

STATEMENT OF DISSERTATION APPROVAL

The dissertation of Heather Anna Cary Wark
has been approved by the following supervisory committee members:

Richard Normann , Chair	May 29, 2014 Date Approved
Patrick Cartwright , Member	May 29, 2014 Date Approved
Scott Rogers , Member	May 29, 2014 Date Approved
Richard Rabbit , Member	May 29, 2014 Date Approved
John White , Member	May 29, 2014 Date Approved
Paul House , Member	June 4, 2014 Date Approved

and by Patrick Tresco, Chair of the Department of Bioengineering

David B. Kieda, Dean of The Graduate School

ABSTRACT

Today, we are implanting electrodes into many different parts of the peripheral and central nervous systems for the purpose of restoring function to people with nerve injury or disease. As technology and manufacturing continue to become more advanced, nerve electrodes are being developed to provide more selective access to multiple neurons simultaneously. With the advent of these technologies, it is important that in parallel, their potential clinical impact is investigated, so that both engineering and clinical outcomes can dictate future designs.

Three objectives were carried out to extend the applications of the Utah Slanted Electrode Array (USEAs) for use in the peripheral nervous system. The first objective was to investigate the capabilities and consequences of USEAs with four-fold higher electrode densities for use in smaller ($\leq$ 1 mm) peripheral nerves. Chapters 2 and 3 of this dissertation cover recent work that showed USEAs with 25 electrodes/mm^2 could be developed and implanted into peripheral nerves without causing global nerve injuries. Results from acute (up to 12 hr) and chronic (up to 2 mo) animal implantation studies are presented and discussed.

The second objective was to investigate the use of USEAs implanted into the pudendal nerve as a neural interface for the control of urinary function (Chapters 4-6). Utah Arrays were used to control excitation and inhibition of urinary muscles, and also to record and thereby detect, different genitourinary stimuli. Together, these results demonstrate that USEA-based pudendal nerve prostheses could provide closed-loop

control and restoration of urinary function.

The final objective was to investigate the use of USEAs as a neural interface—implanted into the human median and ulnar nerves—for bidirectional control of future generation prosthetic limbs in people with upper limb amputations. More than 80 different sensory percepts could be evoked with electrical stimulation delivered to individual microelectrodes on a USEA implanted in the ulnar nerve. Recording neural activity during different perceived phantom finger movements, up to 13 different finger movements could be decoded offline. These results showed that, using USEAs, over 10 times the amount of information could be transferred to and from the nervous system than had been previously published for other peripheral nerve electrodes.

In conclusion, we have fabricated and validated a new Utah Array for use in smaller neural structures, and in parallel we have begun investigation of the clinical usefulness of USEA technologies for controlling urination and upper-limb prosthetic devices.

I dedicate this work to all the many supporting facets of my life,
without whom, I wouldn't have been as productive:

Richard Normann, Janet Basset, Dave Warren,
my family, friends, colleagues, dogs, mountains, and
finally, to all the people with nerve injury/disease
whom we are striving to help and who continue
to inspire our work

TABLE OF CONTENTS

LIST OF FIGURES

PREFACE

Within these pages you will find a wide breadth of research, all of which utilized an array of microelectrodes, the Utah Electrode Array, originally developed at the University of Utah in the early 1990s for use in the nervous system. The major theme found throughout the chapters is the advancement of Utah Array technologies by combining aspects of both engineering and clinical medicine. Technologies, even if rudimentary in their design, can at times bring a better quality of life to the people with no or few treatment options, although there must remain a balance between pushing translational medicine when technologies are ready and protecting the patients from technologies that are not ready. We hope the collected work herein serves to inspire the neural engineering and clinical communities to make translational work a priority whenever possible.

We kindly acknowledge the following funding sources: (1) the National Science Foundation (CBET 1134545); (2) the National Center for Advancing Translational Sciences of the National Institutes of Health (award number 1ULTR001067 administered by the University of Utah Center for Clinical and Translational Science); (3) the Defense Advanced Research Projects Agency (contract number N66001-12-C-4042); (4) the University of Utah Research Foundation Seed Grant Award; and (5) the University of Utah MD-PhD program.

CHAPTER 1

INTRODUCTION

1.1 Abstract

In this introduction, an overview is provided of the field of neuromodulation, peripheral nerve anatomy, the foreign body response to indwelling electrodes, as well as currently available peripheral nerve electrodes. The Utah Array and its structural variations are reviewed, as well as the clinical and experimental applications of these devices that were underway prior to the research presented herein. The limitations of the USEA geometry available prior to this research are also discussed, and a proposed new geometry for use in smaller nerves is introduced. Finally, two important clinical problems are discussed: loss of urinary and hand function following nerve injury and amputation, respectively. For each of these clinical problems, the potential for utilizing Utah Array technologies for the restoration of each respective function is introduced and an overview of the work we have done to begin realizing these potentials is reviewed.

This dissertation covers six different studies that have either been published, or are in press, in revisions or submitted for review. The scope of the collected work here is extensive, and therefore, the aim of this introduction is to provide a broad overview, while more detailed introductions are found at the beginning of each chapter. Finally, the dissertation concludes by focusing on the potential future of Utah Array interfaces both from engineering and clinical standpoints.

1.2 Neuromodulation

Neuromodulation of the nervous system for the restoration of normal function has been used throughout history in different forms, such as the ancient eastern therapy of acupuncture to many electrical stimulation devices in the early twentieth century when

electricity was becoming more widespread.[1] Today, neuromodulation is taking on new definitions, with clinical therapies that utilize many means of modulating neuronal activity in the Central (CNS) and Peripheral Nervous Systems (PNS) to achieve better function. Modulation techniques may include chemical, temperature, mechanical, genetic, electrical processes or even a combination of two or more techniques.[2]

Neuromodulation is among the newest and fastest growing areas of medicine with a projected mean market value that grew from under $1 billion to $3 billion (U.S.D.) in six years (from 2004 to 2010).[2] It has been defined in different ways, and one definition is the 'therapeutic alteration of activity in the central, peripheral or autonomic nervous systems, electrically or pharmacologically, by means of implanted or nonimplanted devices'.[3] Several Food and Drug Administration (FDA) approved neuromodulation devices include electrodes implanted to deliver electrical stimulation to the basal ganglia for Parkinson's disease; cochlea for profound deafness; retina for profound blindness; vagal nerve for depression; spinal cord for chronic pain; and the sacral roots for incontinence.[2]

The neuromodulation of interest to our research is the delivery of electrical stimulation to selective axons within a peripheral nerve in order to evoke a desired physiological response. Additionally, we are also interested in recording from selective axons within a peripheral nerve in order to decode activity that can tell us about people's voluntary intentions (e.g., a hand amputee wants to move a finger) or different involuntary states (e.g., the bladder is now full). The ultimate goal is the combination of neural stimulation and recording for closed-loop control of fully implantable neuromodulation devices.

1.3 Peripheral nerves

Peripheral nerves are a collection of nerve axons that are made up of a protective outer layer called the epineurium (Fig 1.1). Within the epineurium are fascicles that contain neuronal axons.[4] These fascicles or axons are the target for neuromodulation in the PNS, and different electrode designs are allowing for targeted delivery of electrical current to subsets of fascicles or neurons within a peripheral nerve.

As a nerve extends more distally, the fascicles may branch off into smaller nerves that eventually reach a targeted end muscle or organ.[4,5] The fascicular structure of a peripheral nerve can vary between and along the length of nerves.[5-9] There may also be variations in the fascicular organization of nerves in different species, such that a nerve in one species may be unifascicular, while it may be multifascicular in another. For example, the feline pudendal nerve trunk has been shown to have 6-10 fascicles[10,11](Fig 1.1A), while we found upwards of 40 fascicles in the porcine pudendal nerve (Fig 1.1B). Such anatomical differences are important to consider when designing neuromodulation studies and choosing neural electrodes, as the fascicular organization can alter the effectiveness by which selective electrical stimulation or recording can be conducted.

In order to assist research in effectively translating to human applications, it is important to consider an animal model that has anatomical similarities to the human. The human pudendal nerve trunk can have 4-6 fascicles that range from 0.5-2 mm in diameter.[9] Therefore, from a purely anatomical standpoint, the feline should be considered a more appropriate animal model than the porcine for investigating neuromodulation of the pudendal nerve for control of urination.

1.4 The foreign body response to indwelling nerve electrodes

Any material intracorporally implanted evokes a Foreign Body Response (FBR) from both the immune and inflammatory systems.[12] Strategies are being developed to contend with the FBR in order to increase the lifetime and effectiveness of neural electrodes. First, we will briefly review the FBR and then discuss some of these strategies as they pertain to Utah Arrays.

The FBR begins with the formation of a provisional matrix, which consists of adsorption of proteins, molecules and cells onto the surface of the material.[13,14] During the acute phases, the adhesion and activation of platelets and complement lead to the release of cytokines, which then serve as chemoattractants for other immune/inflammatory cells.

As the FBR transitions from acute to chronic inflammation (days to weeks), it is marked by a decrease in neutrophils and an increase in monocytes.[15] These new cells include macrophages and fibroblasts, which mediate chronic inflammation and encapsulation at the device-tissue interface, respectively. Macrophages can fuse together to form Foreign Body Giant Cells (FBGCs), which can mediate degradation of the device and tissue through production of reactive oxygen species/intermediates.[13] However, macrophages can produce positive effects, as some phenotypes may help promote healing, and thus, regeneration of nerve axons.[16]

Inhibiting different phases of the FBR may help increase the longevity of indwelling electrodes. For example, devices may last longer if one can selectively inhibit the provisional matrix or chronic inflammation[17-19] while also promoting neuronal survival.[17] Different strategies can be taken to meet these goals and may include

pharmacological interventions or surface modifications. Pharmacological interventions, such as dexamethasone administration either systemically[19] or locally coated onto electrodes,[18] has been shown to decrease the FBR and neural loss in chronically implanted cortical electrodes. Additionally, minocycline has been shown to increase the quality (higher signal-to-noise ratios) and longevity of CNS implanted electrodes.[20] Surface modifications of the electrodes—such as decreasing surface area[21] or adding a hydrogel matrix coating[22]—have also been shown to decrease the FBR to cortical electrodes.

It is important to note that much of the published work in this field has focused on CNS electrodes, and more studies are needed that focus efforts on investigating whether these and other strategies will translate in the PNS. However, it is clear that strategies for modifying the FBR to neural electrodes can help play a key role in the effective translation of indwelling neuromodulation devices for clinical applications. In the following chapters, various experimental designs were implemented in order to decrease the FBR to indwelling electrodes whenever possible. This included administration of systemic minocycline and dexamethasone in the chronic rat (Chapter 3) and human (Chapter 7) studies. Additionally, a new containment system was developed that incorporated an FDA approved nerve wrap to mitigate the immune response by decreasing the surface area of the containment system (Chapters 2 and 7).

1.5 Neural electrodes

More advanced neural interfaces are being developed to assist in reaching new neuromodulation goals. Many different electrodes have been developed over the last few

decades to provide researchers and clinicians with different design choices to meet their research or clinical goals. In order to determine which device to use for a given physiological experiment or clinical application, the neural interface must meet the needs of both the desired physiological outcome and the constraints applied by the targeted neuroanatomy.

Neuromodulation electrodes are generally characterized by low impedances for recording and/or safe charge injection for stimulation.[23,24] Electrical stimulation of the nervous system initiates the flow of ionic current between two sources, such as an electrode and a reference wire return (monopolar configuration) or between two electrodes (bipolar configuration). Different electrode configurations can be used to steer current across targeted fascicles and thus, achieve more selective stimulation.[25,26] Safe stimulation of the nervous system is characterized by the rate of charge injection (or charge density) and charge-balanced waveforms.[24,27,28] The clinical usefulness of a neuromodulation electrode depends on its ability to deliver safe and effective stimulation levels.

Current peripheral nerve interfaces have different numbers, sizes and spacing of electrodes. Some electrodes are separated by hundreds of microns,[29-31] while others by several millimeters.[32-34] The majority of neural interfaces available for intrafascicular peripheral neuromodulation have a relatively low number of electrodes (< 10) compared to the number of axons (up to 8500 myelinated fibers in rat sciatic and 21,000 fibers in the cat sciatic[6]). Some examples include electrodes that are implanted: interfascicularly (e.g., Slowly Penetrating Interfascicular Electrode, SPINE[35]), intrafascicularly (e.g., Longitudinal Intrafascicular Electrode, LIFE[30]), or epineurally (e.g., Flat Interface Nerve

Electrode, FINE[34]). These designs all take advantage of different methods by which to achieve excitation of different fascicles within a peripheral nerve. For example, FINE electrodes flatten a peripheral nerve such that activation of single fascicles is possible by delivering bipolar current across the individual fascicle or section of fascicle.[36]

One of the most important aspects of the field of neuromodulation is the ongoing improvement to nerve electrodes, such that that more selective information can be transferred to and from the nervous system. In order to achieve more selective access to the nervous system, one must consider modifying the size, number, and spacing of electrodes on a single device. The size of mammalian axons may range from 1-20 μm,[37] and one research goal is to modulate a subset of axons within a single fascicle. Thus, one can begin to appreciate that the size and spacing of the electrodes will directly impact the amount of information that can be selectively transferred to and from the peripheral nervous system.

In the early 1990s, Richard Normann's research group recognized this need and pioneered a new type of nerve interface that greatly increased the number of electrodes per millimeter squared, while also decreasing the size of the active sites of the electrodes to less than 100 μm lengths.[31] This new technology, known as the Utah Electrode Array (UEA), helped push the field to a new level: implantation of multiple microelectrodes (up to 100 electrodes/array) simultaneously to allow greater information transfer to and from the central nervous system. A different architecture of this array, known as the Utah Slanted Electrode Array (USEA), was later developed for the peripheral nervous system by grading the lengths of the electrodes in each row so as to achieve different tip penetration depths.[38]

1.6 Expanding applications of Utah Arrays: devices for smaller nerves

The UEA and USEA have 6.25 electrodes/mm^2 with electrodes spaced by 400 μm and lengths from 0.5-1.5 mm. When our work began five years ago, UEAs were being used in many different cortical applications, including implantation into humans with paralysis for the control of remote computers or robotic devices.[39-42] The USEA was being investigated as a neural interface for controlled fatigue-resistant stance in anesthetized felines[43] and control of prosthetic devices in nonhuman primates.[44] Although these were great strides for this device, many potential applications had not been pursued and many questions remained concerning the possible use of this device in peripheral nerves, especially for different sizes of nerves and chronic implantation studies.

The geometry of the USEA was appropriately designed for medium-sized peripheral nerve structures (2-4 mm wide nerves with ≥ 300 μm fascicular diameters), such as the feline sciatic nerve[43] or rhesus macaque.[44] However, implantation of this geometry device into either smaller (≤ 2 mm wide with average fascicle diameters of ≈ 300 μm) or larger nerves (with diameters > 1 mm) would result in lower probabilities that the electrode tips would penetrate into targeted nerve fascicles. Thus, the functionality of USEAs implanted in smaller or larger nerves would become comparable to intrafascicular electrodes with smaller number of electrodes, such as LIFEs. For example, with USEA electrode lengths from 0.5 to 1.5 mm, only the fascicles within this range would be penetrated. Likewise, with electrode spacing of 400 μm, any fascicles with diameters smaller than 400 μm would potentially not be implanted intrafascicularly with USEA electrodes. Thus, in order to extend the capabilities of Utah Array technologies to

smaller and larger neural structures, new USEA geometries were warranted.

One design feature of penetrating neural interfaces that can greatly impact their application is electrode density, or the number of electrodes per mm^2. As researchers begin to investigate more chronic peripheral nerve USEA implants in animals, ideal animal models would be the lesser mammalian species, as they are more cost effective.

Although the UEA has been implanted in human cortex[39] for > 2.7 years, the USEA has historically fallen behind not only in translation into human applications, but also in chronic peripheral nerve implantation times (longest published data = up to 7 months[45]). The rat sciatic nerve has been well characterized anatomically,[46] and this model would provide a cost effective method for studying the effects of chronic USEA implants; however, this nerve is 1 mm in diameter.[46] Additionally, we were considering the feline as an animal model for studying USEA-based pudendal prosthesis for the control of genitourinary muscles; however, the fascicular organization of this nerve would necessitate shorter lengths and more closely spaced electrodes in order to provide high-count numbers (> 20) of intrafascicularly implanted electrode tips. Therefore, we began asking the question, could microelectrode arrays with greater number of electrodes per millimeter squared be developed for smaller nerves or nerves with more complex fascicular structure, and if so, would implantation of the devices cause nerve crush injuries that would negate their use?

Chapters 2 and 3 of this dissertation present and discuss the design, fabrication, and validation of High electrode Density USEAs (HD-USEAs) in acute[11,47] and chronic (up to 2 months)[48] animal models. HD-USEAs increase the number of electrodes per mm^2 for peripheral nerve interfaces by four times the number of electrodes (from 6.25 in

the older arrays to 25 electrodes/mm^2). These two chapters cover physiological and histological assessment of acute implantation of HD-USEAs (Chapter 2) as wells as behavioral, physiological and histological analysis of chronic HD-USEA implants (Chapter 3). Collectively, these studies show that HD-USEAs do not cause global nerve injury that would negate their use in acute or chronic experimentation (up to the 2 mo investigated). As a consequence of the research endeavors covered in Chapters 2 and 3, we now have penetrating microelectrode arrays that can provide the highest degree of information transfer to and from the peripheral nervous system.

Finally, the studies covered in Chapter 3 were also designed to test a new containment system for Utah Arrays that was based on an organic material already FDA approved for human peripheral nerve injury studies.[48] The success of this material in containing Utah arrays implanted chronically in actively behaving animals (rats with voluntary access to wheels) helped open the doors for the translational studies we then pursued in humans (Chapter 7).[49]

1.7 Expanding applications of Utah Arrays: restoration of urination

Many urinary complications can arise from nervous system injury or disease, and may include overactive or underactive neuromuscular changes in the External Urethral Sphincter (EUS) and/or the detrusor bladder muscle.[50-52] The neurophysiology of the urinary system involves both central and peripheral nervous systems, with voluntary urination (micturition) controlled by the CNS in adults.[53] The urinary tract is innervated by three sets of peripheral nerves: sacral somatic nerves bilaterally (pudendal nerves innervate the EUS); sacral parasympathetic (pelvic plexus innervates the detrusor); and

thoracolumbar sympathetic (hypogastric plexus and sympathetic chain innervate the detrusor).[53] Importantly, the urogenital system's dependency on the CNS is rather unique compared to the other visceral organs (e.g., cardiac and gastrointestinal), which function in the absence of voluntary control. Thus, the genitourinary system is sensitive to interruption by CNS or PNS injury/disease.

Urinary function in adults requires pathways in the CNS and spinal cord that control the three nerves innervating the urinary system, such that either storage or voiding is activated. Voiding requires the simultaneous excitation of the detrusor (via increased pelvic nerve drive and decreased hypogastric drive) and inhibition of the EUS (decreased motor output in the pudendal).[54] Urine storage can be switched to the urination phase by either voluntary mechanisms involving the CNS or involuntary mechanisms involving spinal reflexes. The involuntary voiding pathway is demonstrated in the infant[53,55] or in some people with spinal cord injury,[56] and involves reflex bladder-to-EUS pathways. During an involuntary void, a threshold volume is sensed by receptors in the bladder wall, which leads to activation of the pelvic-to-pudendal pathways to allow coordinated contraction of the bladder and relaxation of the EUS. When there is a loss of voluntary control over micturition in the adult, the potential issues can be classified by either 1) the failure to store (e.g., overactive bladder) or 2) the failure to void (e.g., detrusor-sphincter dyssynergia).[53,56]

The loss of urinary function can have a great impact on the patient's quality of life, and the refractory cases are a challenging clinical problem with limited available options.[57] One of the benefits to the emerging neuromodulation therapies for these cases is the reversible nature of the surgical operation, whereas major reconstruction surgeries

carried out today are irreversible.

Sacral neural stimulation is an FDA approved therapy for patients with painful or dysmotility conditions such as neurogenic bladder, overactive bladder, or interstitial cystitis.[58] Complications of sacral nerve stimulation may include lead wire migration (11.8%) or pain (15.3%) at the stimulation site.[59] Refractory overactive bladder can also be treated via tibial nerve stimulation.[60] Neuromodulation of the Pudendal Nerve (PN) is emerging as another potential therapeutic option for the restoration of urinary control.[61-68] To date, the neural interfaces that have been used to investigate neuromodulation of the PN in humans have included extraneurally placed electrodes[66,68-72] or surface electrodes.[69,72-74]

Because there are multiple nerve pathways in the PN—including those that mediate reflex micturition,[73-75] defecation,[75,76] and erection[76]—a multipurpose PN stimulator would be able to selectively activate these different nerve pathways, depending on the clinical needs. Computer modeling studies have shown that whole-nerve cuff electrodes could be designed and electrical stimulation delivered such that selective access to the different fascicles within the PN may be possible.[77,78] However, a closed-loop device based on whole-nerve cuff electrodes would have false-positive detection of different bladder states during tactile stimulation of the genital region or bowel movement related stimulation.[71,79]

Therefore, we hypothesized that Utah Array-based pudendal nerve prostheses would be able to selectively activate the different neural pathways within the nerve trunk Chapters 4 and 6). Additionally, a Utah Array neuromodulation device should be able to selectively record afferent activity arising from tactile or urinary stimuli (Chapter 5). In

the first two studies (Chapters 4 and 5), we demonstrated that Utah arrays implanted in the pudendal nerve trunk can be used to 1) deliver electrical stimulation that can selectively excite the urinary muscles (Chapters 4)); and 2) record neural activity that can differentiate between bladder states and tactile stimulation (Chapter 5). Finally, we extended those results by investigating whether intrafascicular electrode arrays could be used to deliver electrical stimulation to restore urinary function in three different clinical conditions: 1) to restore continence in an acute model of urinary incontinence, 2) to inhibit overactive detrusor contractions and 3) to excite detrusor contractions in underactive states (Chapter 6).

The results presented in Chapters 4-6 demonstrate that a future Utah Array-based pudendal neuroprosthesis could provide closed-loop detection of different genitourinary states, while also providing selective stimulation to allow for excitation or inhibition of different urinary muscles. An exciting avenue for future Utah Array-based pudendal research will be to investigate detection and control of the other pathways within this nerve: reflex erection and defecation (discussed in Chapter 8).

1.8 Expanding applications of Utah Arrays: control of dexterous prostheses

Unidirectional (motor control only) prosthetic limbs are the current gold standard for people with upper-limb amputations and these devices can be myoelectrically or mechanically controlled.[80] New generation prosthetic arms have been developed with more power and over 20 Degrees Of Freedom motion (DOF).[81] One of the new goals of prosthetic research is to achieve higher degrees of information transfer to and from

people with amputations such that they can control such high DOF prostheses. A concurrent goal of upper limb neuroprosthetic research is to establish bidirectional communication between the user and the limb, such that the device is under complete motor control[81-83] by the user, and sensory feedback[84-86] from the limb allows it to be perceived as an extension of the user.

Several neural interface strategies are being investigated for such bidirectional prosthetic limbs and include: surface,[86] extraneural[33] or intraneural[38,84,87-89] electrodes. Another strategy is to implant electrodes directly into the transected peripheral nerves. To date, intraneural interfaces have successfully used a low number of electrodes (1[85,90]; 6[91]; 16[84]; and 20[89] electrodes) to establish bidirectional communication with the user's nervous system. Motor intent has been decoded with up to two DOF online, and three DOF offline control has been achieved using modified LIFE electrodes.[84] Sensory stimulation has also been delivered to the nerves of these amputees, and sensory percepts are evoked and perceived as arising from their phantom limb.[84-86,90,92,93] Importantly and prior to our research, the highest number of movements decoded by a peripheral nerve interface was three DOF offline and the highest number of different percepts evoked by a single nerve implant was five.[84]

Therefore, the next step for advancing bidirectional prosthetic limbs was to increase the amount of information that could be transferred to and from the peripheral nervous system of people with amputations. We hypothesized that USEAs could be used to provide the necessary electrode-to-neuron ratios both to extract highly specific neural information related to phantom-limb movements, as well as to stimulate selective sets of neurons to evoke multiple different sensory percepts across the entire phantom-limb.

Chapter 7 presents the results of the first implantation of microelectrode arrays into the human median and ulnar nerves in two people that had undergone below-the-elbow amputations 2 and 31 years prior to the study, respectively.[49] Using action potentials recorded on the microelectrode arrays, the volunteers were able to independently and proportionally control the fingers of a virtual robotic hand, and up to 13 DOF were decoded offline. By delivering stimulation to individual USEA electrodes, an average of 80 different percepts distributed over the hand were evoked by a single device. The results of the work presented in Chapter 7 demonstrate the feasibility of Utah Array-based prosthesis for providing proportional dexterous control of prosthetic fingers and sensory feedback for future bidirectional prosthetic limbs.

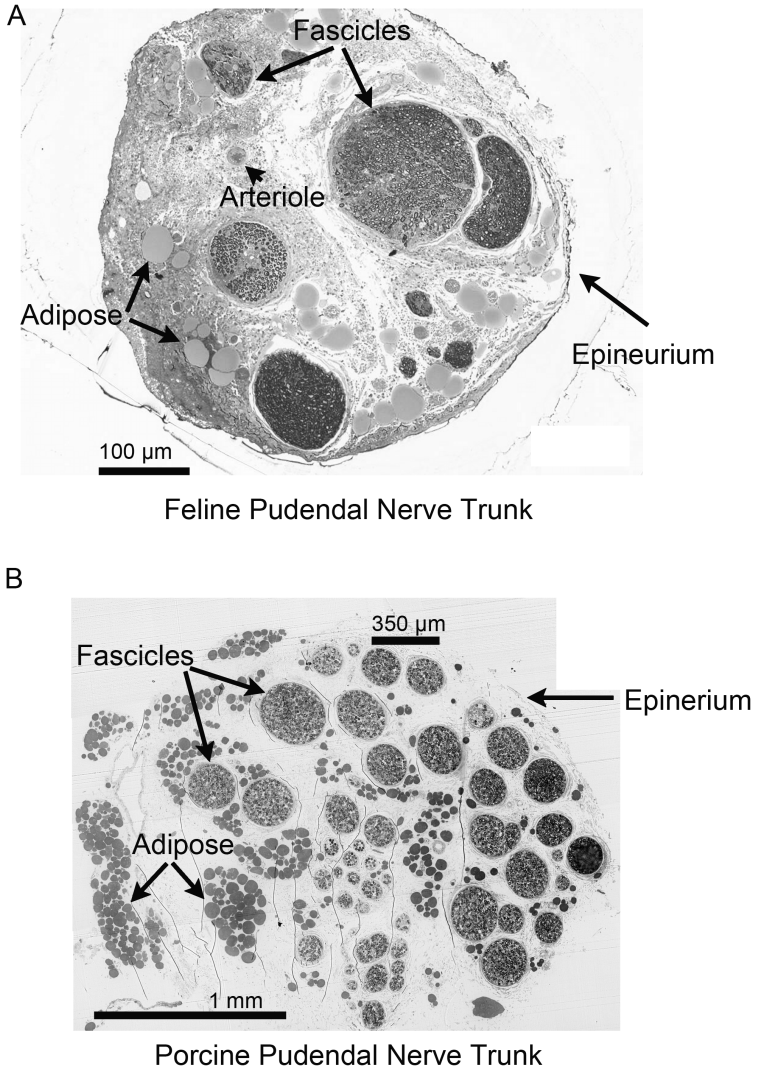

Figure 1.1. Peripheral nerve anatomy. Adult feline (A) and porcine (B) pudendal nerve trunks have similar overall anatomical structures that include an outer connective tissue layer called the epineurium. The inside of the nerve is made up of connective and adipose tissues that surround internal structures called fascicles. Within the fascicles are the neuronal axons that make up the nerve and include myelinated and unmyelinated fibers. Comparison of the feline (A) and porcine (B) pudendal nerve trunks demonstrates that the number and size of the fascicles may be significantly different between species. Such inter-species variations in nerve anatomy is essential to consider when deciding on what neural interface to use for a given neuromodulation goal. The nerve histology shown here was processed in collaboration with: Eduardo Fernandez, University of Alicante, Spain (feline nerve) and Ben Christensen, University of Utah, USA (porcine nerve).

1.9 References

1 Gildenberg PL. Neuromodulation: a historical perspective. In: Neuromodulation, First Edition: Elsevier Ltd, 2009, vol 1, chapter 2:pp9–20.

2 Krames ES, Peckham PH, Rezai AR, et al. What is neuromodulation? In: Neuromodulation, First Edition: Elsevier Ltd, 2009, vol 1, chapter 1:pp3–8.

3 Sakas DE, Simpson B, Krames ES. An introduction to operative neuromodulation and functional neuroprosthetics, the new frontiers of clinical neuroscience and biotechnology. In: Operative Neuromodulation, Springer Wien, vol 1: Functional Neuroprosthetic Surgery. 2007, chapter 1:pp3-10.

4 Stewart JD. Peripheral nerve fascicles: anatomy and clinical relevance. Muscle Nerve 2003;28:525–541.

5 Sunderland S. The intraneural topography of the radial, median and ulnar nerves. Brain 1945.

6 Christensen MB. Doctoral Thesis: Evaluation of inflammation and morphometric parameters associated with neural device implantation in the sciatic nerve. University of Utah 2011.

7 Badia J, Pascual-Font A, Vivó M, et al. Topographical distribution of motor fascicles in the sciatic-tibial nerve of the rat. Muscle Nerve 2010;42:192–201.

8 Gustafson KJ, Pinault GCJ, Neville JJ, et al. Fascicular anatomy of human femoral nerve: implications for neural prostheses using nerve cuff electrodes. Journal of Rehabilitation Res Dev 2009;46:973–984.

9 Gustafson KJ, Zelkovic PF, Feng AH, et al. Fascicular anatomy and surgical access of the human pudendal nerve. World Journal of Urology 2005;23:411–418.

10 Mariano TY, Boger AS, Gustafson KJ. The feline dorsal nerve of the penis arises from the deep perineal nerve and not the sensory afferent branch. Anatomy Histology Embryology 2008;37:166–168.

11 Wark HAC, Sharma R, Mathews KS, et al. A new high-density (25 electrodes/mm^2) penetrating microelectrode array for recording and stimulating submillimeter neuroanatomical structures. Journal of Neural Engineering 2013;10:5003.

12 Abbas AK, Litchtman AH. Cellular and molecular immunology, Fifth Edition. Philadelphia, Pennsylvania: Elsevier Saunders, 2005.

13 Anderson JM, Rodriguez A, Chang DT. Foreign body reaction to biomaterials. Semin Immunol 2008;20:86–100.

14 Luttikhuizen DT, Harmsen MC, Luyn MJAV. Cellular and molecular dynamics in the foreign body reaction. Tissue Engineering 2006;12:1955–1970.

15 Stroncek JD, Reichert WM. Overview of wound healing in different tissue types. : CRC Press, Indwelling Neural Implants Strategies for Contending with the In Vivo Environment 2008: chapter1:pp3–38.

16 Brown BN, Ratner BD, Goodman SB, et al. Macrophage polarization: an opportunity for improved outcomes in biomaterials and regenerative medicine. Biomaterials 2012;33:3792–3802.

17 Grill WM, Norman SE, Bellamkonda RV. Implanted Neural Interfaces: Biochallenges and Engineered Solutions. Annual Review of Biomedical Engineering 2009;11:1–24.

18 Zhong Y, Bellamkonda RV. Dexamethasone-coated neural probes elicit attenuated inflammatory response and neuronal loss compared to uncoated neural probes. Brain Research 2007;1148:15–27.

19 Spataro L, Dilgen J, Retterer S, et al. Dexamethasone treatment reduces astroglia responses to inserted neuroprosthetic devices in rat neocortex. Experimental Neurology 2005;194:289–300.

20 Rennaker RL, Miller J, Tang H, et al. Minocycline increases quality and longevity of chronic neural recordings. Journal of Neural Engineering 2007;4:L1–5.

21 Skousen JL, Merriam SME, Srivannavit O, et al. Reducing surface area while maintaining implant penetrating profile lowers the brain foreign body response to chronically implanted planar silicon microelectrode arrays. Progress in Brain Research 2011;194:167–180.

22 Kim D-H, Wiler JA, Anderson DJ, et al. Soft, fuzzy, and bioactive conducting polymers for improving the chronic performance of neural prosthetic devices. Acta Biomaterialia 2010;6:57–62.

23 Cogan SF. Neural stimulation and recording electrodes. Annual Review of Biomedical Engineering 2008;10:275–309.

24 McCreery DB, Agnew WF, Yuen TG, et al. Charge density and charge per phase as cofactors in neural injury induced by electrical stimulation. IEEE Transactions on Bio-medical Engineering 1990;37:996–1001.

25 Sweeney JD, Ksienski DA, Mortimer JT. A nerve cuff technique for selective excitation of peripheral nerve trunk regions. IEEE Transactions on Bio-medical Engineering 1990;37:706–715.

26 Butson CR, Miller IO, Normann RA, et al. Selective neural activation in a histologically derived model of peripheral nerve. Journal of Neural Engineering

2011;8:036009.

27 Troyk PR, Detlefsen DE, Cogan SF, et al. “Safe” charge-injection waveforms for iridium oxide (AIROF) microelectrodes. Conference Proceedings: IEEE Engineering in Medicine and Biology 2004;6:4141–4144.

28 Cogan SF. Neural stimulation and recording electrodes. Annual Review of Biomedical Engineering 2008;10(1):275-309.

29 Boretius T, Badia J, Pascual-Font A, et al. A transverse intrafascicular multichannel electrode (TIME) to interface with the peripheral nerve. Biosensors and Bioelectronics 2010;26:62–69.

30 Lawrence SM, Larsen JO, Horch KW, et al. Long-term biocompatibility of implanted polymer-based intrafascicular electrodes. Journal of Biomedical Materials Research Part A 2002;63:501–506.

31 Campbell PK, Jones KE, Huber RJ, et al. A silicon-based, three-dimensional neural interface: manufacturing processes for an intracortical electrode array. IEEE Transactions on Bio-medical Engineering 1991;38:758–768.

32 Malagodi MS, Horch KW, Schoenberg AA. An intrafascicular electrode for recording of action potentials in peripheral nerves. Annals of Biomedical Engineering 1989;17:397–410.

33 Polasek KH, Hoyen HA, Keith MW, et al. Spiral nerve cuff electrodes for an upper extremity neuroprosthesis. Conference Proceedings IEEE Engineering in Medicine and Biology 2006;1:3584–3587.

34 Tyler DJ, Durand DM. Functionally selective peripheral nerve stimulation with a flat interface nerve electrode. IEEE Transactions on Neural Systems and rehabilitation engineering : a publication of the IEEE Engineering in Medicine and Biology Society 2002;10:294–303.

35 Tyler DJ, Durand DM. Selective stimulation with a chronic slowly penetrating interfascicular nerve electrode. Conference Proceedings IEEE Engineering in Medicine and Biology, 1997: 351–352.

36 Schiefer MA, Polasek KH, Triolo RJ, Tyler DJ. Selective stimulation of the human femoral nerve with a flat interface nerve electrode. Journal of Neuralengineering 2010; 7(026006):9pp

37 Sunderland S, Bradley KC. The cross-sectional area of peripheral nerve trunks devoted to nerve fibres. Brain 1949;:1–22.

38 Branner A, Stein RB, Normann RA. Selective stimulation of cat sciatic nerve using an array of varying-length microelectrodes. Journal of Neurophysiology 2001;85:1585–1594.

39 Simeral JD, Kim S-P, Black MJ, et al. Neural control of cursor trajectory and click by a human with tetraplegia 1000 days after implantation of an intracortical microelectrode array. Journal of Neural Engineering 2011;8.

40 Simeral J, Hochberg L, Donoghue J, et al. Point-and-click cursor control with an intracortical neural interface system in humans with tetraplegia. IEEE Transactions on Neural Systems and Rehabilitation Engineering 2011. doi:10.1109/TNSRE.2011.2107750.

41 Hochberg LR, Bacher D, Jarosiewicz B, et al. Reach and grasp by people with tetraplegia using a neurally controlled robotic arm. Nature 2012;485:372–375.

42 Hochberg LR, Serruya MD, Friehs GM, et al. Neuronal ensemble control of prosthetic devices by a human with tetraplegia. Nature 2006;442:164–171.

43 Normann RA, Dowden BR, Frankel MA, et al. Coordinated, multijoint, fatigue-resistant feline stance produced with intrafascicular hind limb nerve stimulation. Journal of Neural Engineering 2012;9:6019.

44 Ledbetter NM, Ethier C, Oby ER, et al. Intrafascicular stimulation of monkey arm nerves evokes coordinated grasp and sensory responses. Journal of Neurophysiology 2013;109:580–590.

45 Branner A, Stein RB, Fernandez E, et al. Long-term stimulation and recording with a penetrating microelectrode array in cat sciatic nerve. IEEE Transactions on Bio-medical Engineering 2004;51:146–157.

46 Badia J, Pascual-Font A, Vivó M, et al. Topographical distribution of motor fascicles in the sciatic-tibial nerve of the rat. Muscle Nerve 2010;42:192–201.

47 Mathews KS, Wark HAC, Normann RA. Assessment of rat sciatic nerve function following acute implantation of High Density Utah Slanted Electrode Array (25 electrodes/mm 2) based on neural recordings and evoked muscle activity. Muscle Nerve 2014;in press. doi:10.1002/mus.24171.

48 Wark H, Mathews KS, Normann RA, et al. Behavioral and cellular consequences of high-electrode count Utah Arrays chronically implanted in rat sciatic nerve. *In revision* at Journal of Neural Engineering Apr 2014.

49 Wark H, Davis TS, hutchinson DT, et al. Using a high electrode count intrafascicular peripheral nerve interface to restore motor control and sensory feedback in humans with transradial amputations. *In review* at Journal of Neural Engineering March 2014.

50 Sajadi KP, Gill BC, Damaser MS. Neurogenic aspects of stress urinary incontinence. Current Opinons Obstetrics Gynecology 2010;22:425–429.

51 Benevento BT, Sipski ML. Neurogenic bladder, neurogenic bowel, and sexual

dysfunction in people with spinal cord injury. Physical Therapy 2002;82:601–612.

52 Burks FN, Bui DT, Peters KM. Neuromodulation and the neurogenic bladder. Urology Clinics of North America 2010;37:559–565.

53 Yoshimura N, Chancellor MB. Neurophysiology of lower urinary tract function and dysfunction. Reviews in Urology; 2003;5(8):S3-S10.

54 Roberts MM. Neurophysiology in neurourology. Muscle Nerve 2008;38:815–836.

55 Wen J, Wang Q, Zhang X. Normal voiding pattern and bladder dysfunction in infants and children. Life Science Journal 2007.

56 de Groat WC, Yoshimura N. Mechanisms underlying the recovery of lower urinary tract function following spinal cord injury. In: Autonomic Dysfunction After Spinal Cord Injury. : Progress in Brain Research, 2006: 59–84.

57 McAchran S, Rackley R, Vasavada S. Neuromodulation for voiding dysfunction. In: Krames ES, peckham PH, rezai AR, eds. Neuromodulation. : Elsevier Ltd, 2009: 945–956.

58 van Balken MR, Vergunst H, Bemelmans BLH. The use of electrical devices for the treatment of bladder dysfunction: a review of methods. Journal of Urology 2004;172:846–851.

59 Siegel SW, Catanzaro F, Dijkema HE, et al. Long-term results of a multicenter study on sacral nerve stimulation for treatment of urinary urge incontinence, urgency-frequency, and retention. Urology 2000.

60 van der Pal F, Heesakkers JPFA, Bemelmans BLH. Current opinion on the working mechanisms of neuromodulation in the treatment of lower urinary tract dysfunction. Current Opinions in Urology 2006;16:261–267.

61 Park JH, Kim C-E, Shin J, et al. Detecting bladder fullness through the ensemble activity patterns of the spinal cord unit population in a somatovisceral convergence environment. Journal of Neural Engineering 2013;10:056009.

62 Yoo PB, Woock JP, Grill WM. Bladder activation by selective stimulation of pudendal nerve afferents in the cat. Experimental Neurology 2008;212:218–225.

63 Yoo PB, Grill WM. Minimally-invasive electrical stimulation of the pudendal nerve: A preclinical study for neural control of the lower urinary tract. Neurourology and Urodynamics 2007;26:562–569.

64 Yoo PB, Klein SM, Grafstein NH, et al. Pudendal nerve stimulation evokes reflex bladder contractions in persons with chronic spinal cord injury. Neurourology and Urodynamics 2007;26:1020–1023.

65 Tai C, Wang J, Wang X, et al. Bladder inhibition or voiding induced by pudendal nerve stimulation in chronic spinal cord injured cats. Neurourology and Urodynamics 2007;26:570–577.

66 Peters KM, Killinger KA, Boguslawski BM, et al. Chronic pudendal neuromodulation: expanding available treatment options for refractory urologic symptoms. Neurourology and Urodynamics 2010;29:1267–1271.

67 Uz A, Apan A, Erbil KM, et al. A new approach for pudendal nerve exposure and its clinical significance. Anatomical Science International 2005;80:163–166.

68 Spinelli M, Malaguti S, Giardiello G, et al. A new minimally invasive procedure for pudendal nerve stimulation to treat neurogenic bladder: description of the method and preliminary data. Neurourolology and Urodynamics 2005;24:305–309.

69 Opisso E, Borau A, Rodríguez A, et al. Patient controlled versus automatic stimulation of pudendal nerve afferents to treat neurogenic detrusor overactivity. Journal of Urolology 2008;180:1403–1408.

70 Yoo PB, Klein SM, Grafstein NH, et al. Pudendal nerve stimulation evokes reflex bladder contractions in persons with chronic spinal cord injury. Neurourology and Urodynamics 2007;26:1020–1023.

71 Wenzel BJ, Boggs JW, Gustafson KJ, et al. Detecting the onset of hyper-reflexive bladder contractions from the electrical activity of the pudendal nerve. IEEE Transactions on Neural Systems and rehabilitation engineering : a publication of the IEEE Engineering in Medicine and Biology Society 2005;13:428–435.

72 Vodusek DB, Light JK, Libby JM. Detrusor inhibition induced by stimulation of pudendal nerve afferents. Neurourology and Urodynamics 1986;5:381–389.

73 Boggs JW, Wenzel BJ, Gustafson KJ, et al. Frequency-dependent selection of reflexes by pudendal afferents in the cat. The Journal of Physiology 2006;577:115–126.

74 Gustafson KJ, Creasey GH, Grill WM. A urethral afferent mediated excitatory bladder reflex exists in humans. Neuroscience Letters 2004;360:9–12.

75 Bock S, Folie P, Wolff K, et al. First experiences with pudendal nerve stimulation in fecal incontinence: a technical report. Technique in Coloproctolgy 2010;14:41–44.

76 Pescatori ES, Calabro A, Artibani W, et al. Electrical stimulation of the dorsal nerve of the penis evokes reflex tonic erections of the penile body and reflex ejaculatory responses in the spinal rat. Journal of Urology 1993;149:627–632.

77 Pastelín CF, Zempoalteca R, Pacheco P, et al. Sensory and somatomotor components of the “sensory branch” of the pudendal nerve in the male rat. Brain Research 2008;1222:149–155.

78 Kent AR, Grill WM. Model-based analysis and design of nerve cuff electrodes for restoring bladder function by selective stimulation of the pudendal nerve. Journal of Neural Engineering 2013;10:6010.

79 Wenzel BJ, Boggs JW, Gustafson KJ, et al. Closed loop electrical control of urinary continence. Journal of Urology 2006;175:1559–1563.

80 Zlotolow DA, Kozin SH. Advances in upper extremity prosthetics. Hand Clinics 2012;28:587–593.

81 Resnik L, Klinger SL, Etter K. The DEKA Arm: Its features, functionality, and evolution during the Veterans Affairs Study to optimize the DEKA Arm. Prosthetics and Orthotics International 2013. doi:10.1177/0309364613506913.

82 Pons JL, Rocon E, Ceres R, et al. The MANUS-HAND Dextrous Robotics Upper Limb Prosthesis: Mechanical and Manipulation Aspects. Autonomous Robots 2004;16:143–163.

83 Burck JM, Bigelow JD, Harshbarger SD. Revolutionizing Prosthetics: Systems Engineering Challenges and Opportunities. Johns Hopkins APL Technical Digest 2011;30.

84 Rossini PM, Micera S, Benvenuto A, et al. Double nerve intraneural interface implant on a human amputee for robotic hand control. Clinical Neurophysiology 2010;121:777–783.

85 Dhillon GS, Horch KW. Direct neural sensory feedback and control of a prosthetic arm. IEEE Transactions on Neural Systems and Rehabilitation Engineering 2005;13:468–472.

86 Schultz AE, Marasco PD, Kuiken TA. Vibrotactile detection thresholds for chest skin of amputees following targeted reinnervation surgery. Brain Research 2009;1251:121–129.

87 Boretius T, Badia J, Pascual-Font A, et al. A transverse intrafascicular multichannel electrode (TIME) to interface with the peripheral nerve. Biosens Bioelectron 2010;26:62–69.

88 Yoshida K, Horch K. Selective stimulation of peripheral nerve fibers using dual intrafascicular electrodes. IEEE Transactions on Bio-medical Engineering 1993;40:492–494.

89 Gasson M, Hutt B, Goodhew I. Invasive neural prosthesis for neural signal detection and nerve stimulation. International Journal of Adaptive Control and Signal Processing 2005;19:365–375.

90 Horch K, Meek S, Taylor TG, et al. Object discrimination with an artificial hand using electrical stimulation of peripheral tactile and proprioceptive pathways with

intrafascicular electrodes. IEEE Transactions on Neural Systems and Rehabilitation Engineering 2011;19:483–489.

91 Jia X, Koenig MA, Zhang X, et al. Residual motor signal in long-term human severed peripheral nerves and feasibility of neural signal-controlled artificial limb. The Journal of Hand Surgery 2007;32:657–666.

92 Benvenuto A, Raspopovic S, Hoffmann KP, et al. Intrafascicular thin-film multichannel electrodes for sensory feedback: Evidences on a human amputee. Conference Proceedings IEEE Engineering in Medicine and Biology 2010;2010:1800–1803.

93 Dhillon GS, Lawrence SM, Hutchinson DT, et al. Residual function in peripheral nerve stumps of amputees: implications for neural control of artificial limbs. The Journal of Hand Surgery 2004;29:605–15; discussion 616–8.

CHAPTER 2

A NEW HIGH-DENSITY (25 ELECTRODES/MM^2) PENETRATING MICROELECTRODE ARRAY FOR RECORDING AND STIMULATING SUBMILLIMETER NEUROANATOMICAL STRUCTURES

Reprinted with permission by the Journal of Neural Engineering & co-authors

Publication Reference:

Wark HAC, Sharma R, Mathews K, Fernandez E, Yoo J, Christensen B, Tresco P, Rieth L, Solzbacher F, Normann RA, Tathireddy P. J Neural Eng. 2013. v 10(045003). 1-10

Author contributions: HACW, RS, LR, FS, RAN, PTa designed HD-USEA ; RS, JY fabricated HD-USEAs; HACW, KM, RAN validated arrays *in vivo*; BC, PTr, EF validated arrays ex vivo; HACW, KM, RAN, PTa wrote the manuscript.

2.1 Abstract

Among the currently available neural interface devices, there has been a need for a penetrating electrode array with a high electrode count and high electrode density (the number of electrodes/mm^2) that can be used for electrophysiological studies of submillimeter neuroanatomical structures. We have developed such a penetrating microelectrode array with both a high electrode density (25 electrodes/mm^2) and high electrode count (up to 96 electrodes) for small nervous system structures, based on the existing Utah Slanted Electrode Array (USEA). Such high electrode density arrays are expected to provide greater access to nerve fibers than the conventionally spaced USEA especially in small diameter nerves. One concern for such high density microelectrode arrays is that they may cause a nerve crush-type injury upon implantation. We evaluated this possibility during acute (< 10 h) *in vivo* experiments with electrode arrays implanted into small diameter peripheral nerves of anesthetized rats (sciatic nerve) and cats (pudendal nerve). Verification of successful intrafascicular implantation and of viable nerve function was made via microstimulation, single-unit recordings and histological analysis. Device fabrication quality was assessed by measuring the electrode impedances and by quantifying electrode dimensions. The results of these experiments show that such high density neural interfaces can be implanted acutely into neural tissue without causing a complete (neurotmesis) nerve crush injury, while mediating intrafascicular access to fibers in small diameter peripheral nerves. This new penetrating microelectrode array has characteristics unmatched by other neural interface devices currently available for peripheral nervous system neurophysiological research.

2.2 Introduction

A variety of neural interfaces have been developed over the last few decades, which have provided researchers and clinicians with an ever-expanding repertoire of design choices to meet their research or clinical goals [1-7]. High-count microelectrode arrays have proven useful in basic physiology research [8], and for clinical applications such as the restoration of function in people with nervous system injury [9] or stroke [10]. In order to determine which device to use for a given physiological experiment or clinical application, the neural interface must meet the needs of both the desired physiological outcome and the constraints applied by the targeted neuroanatomy. Current peripheral nerve interfaces have electrodes that vary in their number of contacts, which can be separated by hundreds of microns [2, 4, 5, 11-13] or several millimeters [3, 7, 14]. Many of the devices have a low number of electrodes (<10) that are implanted interfascicularly (e.g., Slowly Penetrating Interfascicular Electrode, SPINE[6]), intrafascicularly (e.g., Longitudinal Intrafascicular Electrode, LIFE[15]), or epineurally (e.g., Flat Interface Nerve Electrode, FINE[7]). Recent penetrating neural interface applications are requiring a greater number of electrodes (>60) to achieve complex neuromodulation [9, 10, 16] or neurophysiological [8] goals.

One design feature of penetrating neural interfaces that greatly impacts their application is electrode density, or the number of electrodes per mm^2. Some neural interface devices have been fabricated with high electrode densities; however, their designs have limited the use of these arrays to specific central nervous system structures, such as cortical grey matter (6.25 electrodes/mm^2 [12, 13]; > 150 electrodes/mm^2 [17, 18] or hippocampal slices (< 11 electrodes/mm^2) [19]. Other high electrode density devices

include nonpenetrating electrode arrays [20], which will not be discussed herein. Currently, there is one high electrode density (6.25 electrodes/mm^2), high electrode count (96 electrodes) penetrating device available for neuromodulation of large structures (> 4mm) in the peripheral nervous system [1]. However, penetrating electrode arrays with higher densities have been needed to expand neurophysiology research and to investigate future clinical applications in submillimeter neuroanatomical structures, such as small diameter peripheral nerves or ganglia (e.g., the 1 mm cat pudendal nerve). Moreover, higher density microelectrode arrays would improve the access to closely spaced individual or subpopulations of neurons and/or nerve fibers in order to investigate the mechanisms underlying more complex spatial neural interactions.

We have recently developed a penetrating electrode array with a 25 electrodes/mm^2 density (called the High-Density Utah Slanted Electrode Array or HD-USEA). The grid of electrodes used in these studies had graded electrode lengths ranging from 300 to 800 μm with neighboring electrodes separated by 200 μm. We have shown that the production of a defined geometric surface area (GSA) of the electrode tips was possible using either an oxygen plasma etching technique [1, 21] or by excimer laser ablation [22]. This paper describes the fabrication techniques used for the production of these arrays as well as the results of *in vitro* and *in vivo* electrode characterizations.

One of the main concerns regarding the use of penetrating microelectrode arrays that have such high electrode densities is that a nerve crush injury may result from their implantation. Physiological and histological evaluations showed no evidence of neurotomesis (complete disruption of entire nerve trunk [23]) type of a crush injury after acute (< 10 h) implantation of HD-USEAs. We observed that electrical stimulation of rat

sciatic nerve fibers delivered via individual HD-USEA electrodes could selectively evoke hind limb muscle twitches. In the same rat preparations, we were also able to record afferent neuronal activity via individual electrodes that was evoked by tactile and proprioceptive stimuli. Histological analysis of the implantation sites verified that multiple HD-USEA electrodes penetrated into the individual fascicles (< 500 μm in diameter) of both the rat sciatic and feline pudendal nerves with little or no evidence of nerve fiber compression around the electrode tips. Collectively, these results show that HD-USEAs are safe and effective for acute neurophysiology studies (we have yet to investigate their use in chronic experimentation). The architecture of this device makes it a unique and useful addition to the neural interfaces currently available, as it provides unprecedented nerve fiber access in submillimeter structures outside the central nervous system.

2.3 Methods

2.3.1 Device Fabrication

High-density electrode arrays were fabricated using techniques that were previously described [13, 24-26]. In brief, fabrication of these devices proceeded in the following steps (described subsequently): back-side dicing, glassing, back-side metallization, front-side dicing, wet etching, dicing of individual arrays from the wafer, tip metallization, parylene-C deposition, tip deinsulation, and finally, wirebonding to a connector. The devices used in this study were fabricated from 2 mm thick boron-doped (p-type) single crystal silicon wafers (76.2 mm diameter) with high boron concentrations (resistivity of silicon wafers < 0.0025 Ω-cm). The fabrication procedures were designed to cover the entire wafer with sets of 400 electrodes (sets of 20×20 square grids). The initial

back-side dicing—to form a square grid of kerfs—was done using a Disco dicing saw (DAD - 3220) with a 50 μm thick resin blade (Semicon - FSN1600508). The resulting kerfs had a pitch of 200 μm and a depth of 500 μm. These kerfs were later filled with glass to electrically isolate the electrodes[25, 26]. Metalized bond pads for wirebonding to the electrodes were formed on the squares between the kerfs using standard photolithographic techniques. Bondpads were sputter deposited as individual layers of titanium (Ti), platinum (Pt), titanium tungsten (TiW), then Pt, with respective thicknesses of 100/150/550/350 nm (1150 ± 100 nm total thickness).

The front side of the wafer was then diced in one direction to form sequences of 20 steps. The steps were subsequently diced in two orthogonal directions to produce the high aspect-ratio columns that would become electrodes following the etching procedure. This dicing step was also done using the Disco dicing saw, but with a 70 μm Ni bound blade with a 3 μm diamond mesh size (NBC-Z 1050). The postdicing dimensions of these columns were approximately 110×110 μm with lengths that ranged from 200 to 1500 μm in each 20 x 20 array. The wafer was then cut into quarters to facilitate etching. A two-step wet acid etching process using a homogeneous mixture of 95% HNO_3 and 5% HF was used to produce the final shape of the electrodes in the array. The first and second etching steps were performed on each quarter of the wafer for 3 min (in an agitated solution) and 3.45 min (in a nonagitated solution), respectively. The wafer was then diced into individual 20×20 arrays and prepared for tip metallization by pushing the electrode shanks through a thin square of aluminum foil (to protect the bottom of the electrode shanks from becoming metalized). One wafer yields approximately 20 arrays that do not have any broken electrodes. A film stack of Ti/IrOx (100/500 nm) was sputter deposited

using pulsed DC at a 10 mTorr process pressure and at a power of 90 and 100 W for the Ti and IrOx films, respectively. These Sputtered Ti and Iridium Oxide Films (SIROF) were deposited for 5 and 40 min, respectively, with gas flows of 150 sccm Ar for the Ti, then 100 sccm each of Ar and O_2 for the IrOx deposition.

Annealing of the metalized tips and parylene-C coating (6 μm thick) of the shanks was carried out as previously described [22]. Arrays were deinsulated with either an oxygen plasma etch of aluminum-foil-masked electrode shanks (March Plasmod, March Plasma Systems, Inc.; 150 W, 400 mTorr, n = three arrays) [13, 27] or with an excimer laser (200 pulses, 248 nm wavelength, 1440 mJ/cm^2, n = one array) [22]. The carbon debris generated by the laser ablation was removed by a shorter (2 min) oxygen plasma etch using the parameters described above. The 20×20 electrode arrays were then custom diced and a subset of these electrode arrays were wirebonded using insulated wire (Isonel Au:Pd (with 2% Pd), Kanthal) to a Tucker-Davis Technologies (TDT) 96-pin ZIF-Clip connector. The final wired electrode arrays used herein consisted of 4 or 5 by 10 electrodes with targeted lengths from 300 to 800 μm along the long axis of the array with 2-4 electrodes wired as reference electrodes. This number of electrodes was chosen to best fit the dimensions of the peripheral nerves tested in this work, but up to 96 electrodes could be wirebonded for use in other nerve structures. An external reference wire (5 mm Pt, PTFE insulated) was also bonded to the TDT reference pads.

2.3.2 In vitro and in vivo HD-USEA characterization

Impedance testing and Scanning Electron Microscopy (SEM) were used to characterize the HD-USEAs. Impedances were measured using an automated impedance

tester as described previously [28]. In brief, the impedance of each electrode was measured with a 1 kHz, 10 mV sine wave [28]. Impedance tests were performed with the array, the driving electrode, and the sensing electrode placed in a dish of sterile 0.9% normal saline. Impedances were tested over the course of 2-3 days. *In vivo* impedance testing was also performed after implantation of the arrays. The Geometric Surface Area (GSA) of the electrode tips was calculated for the electrodes that were deinsulated via plasma etching and laser ablation. The surface area of the tips was approximated using the area of a cone [29], and the values for tip height and radius were determined from SEMs that included >15 tips/image. Tips without any insulation removed were excluded from the calculations (< 5 tips per image). The diameter of electrodes across 10 devices were determined via optical microscopy by measuring diameters at 20%, 50% and 90% of the electrode length measured from the electrode tip.

2.3.3 Surgical and experimental procedures for in vivo validation of HD-USEA functionality

All procedures were approved by the Institutional Animal Care and Use Committee of the University of Utah. Sprague-Dawley rats (350-500 g) were used for the sciatic nerve preparations, and anesthesia was induced using either Isoflurane (2-5% gas in an induction chamber) or a cocktail of Xylazine (7.5 mg/kg IP) and Ketamine (65 mg/kg IP). Felines were used for the pudendal nerve preparations, and anesthesia was induced using Telazol (9-12 mg/kg IM) or Ketamine (10-20 mg/kg IM). Anesthesia was maintained with Isoflurane (1-2% gas) for both rats and felines, with the addition of α-Chloralose (30 mg/kg initial dosage, 15 mg/kg maintenance dosage, IV) for felines. Vital

signs (heart rate, blood oxygen saturation, and rectal temperature) were monitored and recorded to assess the depth of anesthesia and condition of the animal.

The surgical procedures followed those previously described for exposing the sciatic [1, 30] and pudendal nerves [31]. The electrode arrays were inserted using a high-velocity pneumatic pulse insertion technique [32]. Electrical currents were injected via HD-USEA electrodes using a custom-built 1100-channel stimulator [33]. Constant-voltage, monophasic cathodic stimuli with varying amplitudes (-2 to -3 V) and pulse-width durations (0.2 to 1024 μs) were used. A custom built program (MATLAB, MathWorks) was used to control stimulation via individual electrodes [34, 35]. Electromyography (EMG) wires (California Fine Wire Co., Model #M146240) were custom made as previously described [31]. Two EMG wires were inserted into each targeted muscle in the rat hind limb in order to record bipolar EMG responses to electrical stimulation. EMG responses were normalized to maximal muscle twitches evoked by either stimulating all electrodes simultaneously or by delivering stimulation through a single microelectrode. Electrodes that activated only flexor or extensor muscles at greater than 0.5 of the normalized EMG response were considered to be selective. Data collection was done using a Cerebus data acquisition system (Blackrock Microsystems, Inc.). In the rat preparations, recordings were taken from all wired electrodes while applying various mechanical stimuli to the lower limb. These stimuli included brushing areas of the foot and rotating the foot around the ankle joint. Signal-to-Noise Ratios (SNR) were determined by dividing the amplitude of the average waveform by two times the standard deviation of the waveforms [36]. Data analysis was carried out using MATLAB and Microsoft Excel.

Electrode arrays were acutely implanted (1-10 h) into small diameter peripheral nerves. Rat preparations were used for histology and physiology, while the feline preparations were used for histology only. After the animals were sacrificed, the exposed nerve containing the HD-USEA implant site was soaked in 4% paraformaldehyde for 30 min, and the arrays were then explanted.

Nerves were excised from the animal and stored in 4% paraformaldehyde for 24 h, then rinsed and stored in 1% phosphate buffer solution with 0.01% sodium azide. Tissue was then stained with 1-2% OsO_4 in a 0.1M sodium cacodylate buffer, dehydrated in graded concentrations of ethanol, cleared with propylene oxide, and embedded in Embed 812 (Epon, Electron Microscopy Science). Serial 0.5-0.6 μm semithin sections (Ultracut EMUC6, Leica) were stained and examined with an Olympus AX70 Microscope. Scatic nerves were stained with toluidine blue and pudendal nerves were stained with thionin and acridine orange (Sigma-Aldrich). Sciatic nerve image fields were digitized using a high-resolution Olympus DP12 camera. Pudendal nerve images were obtained using ImagePro Plus 4.0 (MediaCybernetics) and a color CCD camera (Photometrics) attached to a Nikon E600 microscope. The whole pudendal nerve images were obtained at 200x final magnification, while fascicle images were obtained at 1000x final magnification. For the pudendal nerve imaging, serial overlapping images were taken over the entire nerve or fascicle. Serial images were reconstructed to form a mosaic image using the photomerge command in Adobe Photoshop CS.

2.4 Results

2.4.1 Precision of HD-USEA device fabrication

Figure 2.1 shows a scanning electrode micrograph of the new HD-USEA device located next to a conventional USEA. The desired GSA of the exposed SIROF electrode tips was achieved by oxygen plasma etching and laser ablation techniques. The average GSA of electrode tips deinsulated with the oxygen plasma etching (Fig. 2.1b) and laser ablation (Fig. 2.1c) methods were 4543 ± 526 μm^2 (mean ± sd; n = 17 tips from one device) and 473 ± 365 μm^2 (n = 22 tips from one device), respectively. The *in vitro* mean tip impedances of the electrodes deinsulated by laser (n = one array) and plasma etching (n = three arrays) were 440 ± 340 and 179 ± 216 (mean ± sd) kΩ, respectively. The device deinsulated using the excimer laser technique had a large drop in mean tip impedance to 232 ± 150 kΩ when measured *in vivo*.

The quality of the manufacturing techniques used was assessed by comparing the electrode dimensions [13] from ten different nonwirebonded HD-USEAs produced from the same silicon wafer (Fig. 2.2). The diameter of the electrodes along the length of each shaft was measured at three different points for each electrode and across 10 devices (Fig. 2.2). The average lengths of the longest and shortest electrodes measured from these 10 devices ranged from 884 ± 39 to 310 ± 60 μm, respectively. The quality and reproducibility of HD-USEAs is comparable to that of the conventional arrays currently being manufactured.

2.4.2 Selective recordings from afferent nerve fibers in rat sciatic nerve

In order to learn if such high electrode density arrays could be implanted into a nerve and subsequently used for neurophysiological research, we recorded the neuronal response to different tactile or proprioceptive stimuli in three rats with sciatic nerves acutely implanted with HD-USEAs. In each experiment, there were > 25 electrodes out of the 48 wired electrodes that were able to record either single unit or multiunit waveforms. In each preparation, there were neural units that fired spontaneously, and different neural units that could be selectively driven by tactile or proprioceptive stimuli. Figure 2.3 shows an example of two neural units that were recorded via two different HD-USEA microelectrodes on one implanted device and that were driven specifically by dorsiflexion (Fig. 2.3a, electrode 21) or by plantarflexion (Fig. 2.3b, electrode 14) of the ankle, respectively. The mean SNR for all three preparations across all recording channels was > 4.

2.4.3 Selective motor fiber activation achieved by electrical stimulation of rat sciatic nerve

Delivering voltage-controlled stimulation via individual electrodes on the implanted HD-USEA evoked selective muscle twitches in the ankle flexor and extensor muscles. In all three rat preparations, there were 15 ± 6 and 17 ± 8 (mean ± sd) electrodes that selectively evoked ankle flexion and extension, respectively. Figure 2.4 shows selective muscle activation using recruitment curves generated in the ankle flexor muscle—Tibialis Anterior (TA)—and the ankle extensor muscles—Lateral Gastrocnemius (LG) and Medial Gastrocnemius (MG)—by cathodic stimulation (-2V, up to 1024 μs

pulse-widths) delivered via two different HD-USEA microelectrodes on one implanted device. This selective activation of flexor versus extensor muscles was achieved by delivering stimulation via two catercornered electrodes with an approximate tip-to-tip separation of 208 μm.

2.4.4 Histological evaluation of HD-USEA implants

A fixed sample of the rat sciatic nerve that was implanted with an HD-USEA is shown in Figure 2.5a-b. The suture in Fig 2.5a marks the distal portion of the nerve. The nerve was sectioned through the middle of the implant site. A microscopic cross section of the 1.8 × 0.8 mm nerve shows penetration of the shorter HD-USEA microelectrodes (< 400 μm in length) with preservation of the intrafascicular anatomy (epineurial, endoneurial, and perineurial) between electrode penetration tracks into the nerve (Fig. 2.5c). Figures 2.5d-f show the microelectrode tracks of several HD-USEA electrodes. Sections taken through the center of an electrode track show no compression of the axons around the electrode tips (Fig. 2.5d-e). A section taken adjacent to the center of the electrode track shows no compression of axons around the electrode shank (Fig. 2.5f).

Figure 2.6a shows a cross-section of a feline pudendal nerve that was implanted with an HD-USEA. This section was taken from the portion of the nerve that was implanted with longer electrodes (> 400 μm in length). As with the sciatic nerve implant, there is preservation of the intrafascicular anatomy in the region between electrode tracks. One electrode was broken prior to implantation and does not penetrate into the fascicular space (track marked with an arrowhead; Fig 2.6a).

2.5 Discussion

2.5.1 Array fabrication

We have successfully fabricated 25 electrodes/mm^2 penetrating microelectrode arrays with varying length electrodes designed to access nerve fibers that are found at different depths in small peripheral nerves. The electrode proportions, impedances, number of functionally distinct electrodes, and SNR of HD-USEAs are comparable to the conventionally spaced Utah electrode arrays. Implantation of the regularly spaced Utah arrays into submillimeter structures would result in neural interfaces that have a functionally low-count number of electrodes that could stimulate and record from nerve fibers. For example, implantation of a 5×10 conventional array (0.4 mm electrode spacing with lengths from 0.5 to 1.5 mm) into a 1 mm nerve would result in partial coverage with at most only two electrode rows penetrating into the nerve (20 electrodes). Additionally, the shortest electrode row (0.5 mm in length) would be too long to access fibers within the upper half of the nerve and the longest electrodes would pass through the nerve. Thus, as few as 6 electrodes of the conventionally spaced arrays might be functionally implanted into a 1 mm nerve. In contrast, implantation of a 5×10 HD-USEA would result in more complete coverage (from 0.2 to 1.0 mm) of the nerve and with a high-count number of electrodes (48 electrodes). For physiological testing of these arrays, we chose to wirebond two different grids: a 5×10 grid of electrodes to custom-fit the size of the rat sciatic nerve (1.2 mm in diameter [37]) and a 4×10 grid to custom-fit the feline pudendal nerve (1 mm in diameter [38]).

For the fabrication of these arrays, low resistivity silicon wafers were used to reduce the ohmic contact resistance between the metal-semiconductor interfaces (the

metalized tips and bond pads) and produce reliable contacts at lower annealing temperatures. The initial grid of electrodes was made bigger than the required grid to facilitate uniform acid etching of these columns in the middle regions of the 20×20 grid. The wet etching times were optimized to produce narrow shanks and rounded electrode tips. Wafers were cut into quarters for the wet etching steps in order to reduce the number of cuts made down from approximately 1000 to 250, which provides more uniform kerfs widths and depths. Analysis of the widths of the electrode shanks at different locations along their lengths across 10 electrodes on 10 different devices demonstrates the uniformity that was achieved during fabrication of these devices.

Electrode impedances were measured *in vitro* and *in vivo* to characterize the quality of the arrays. One concern in development of this device was whether we would have difficulty fabricating arrays with deinsulated tips and electrode impedances in the range needed for stimulation and recording (with SNRs > 4), while producing an overall electrode geometry that would meet our anatomical goals (penetrating into fascicles that are 50-200 μm diameter [37, 38]). Deinsulation of the HD-USEA microelectrode tips was carried out using two different methods and we assessed the ability of each to produce low and uniform GSAs. Deinsulation using the conventional plasma etching technique requires a foil mask to protect the rest of the array from becoming deinsulated. This process can be carried out on individual electrode arrays [13] or—for microelectrode arrays that have uniform electrode lengths—on the wafer scale [24]. Deinsulating HD-USEAs using the foil mask and oxygen plasma etching resulted in uniform GSAs (small distribution with standard deviation of 526 μm^2), but relatively large areas (4543 μm^2). Excimer laser ablation [22] was performed on one HD-USEA in order to decrease the GSA of the

electrode tips and thereby, increase the selectivity of neuronal recordings or evoked motor responses. In this work, we used a novel hybrid laser technique that included an additional plasma etching step. The mean GSAs obtained with the laser ablation deinsulation (473 ± 365 μm^2) were significantly lower (alpha = 0.05; $p = 1.06 \times 10^{-26}$; 2-tailed student t-test); however, this technique produced much less uniform tip exposures (larger distribution around the mean) likely due to the manual nature of the process. Deinsulation via laser ablation was done manually for each individual electrode; however, future work is aimed at developing an automated process.

The excimer laser ablation technique used in this work required the use of oxygen plasma etching to remove the carbon debris generated by the laser ablation. The carbon debris layer is thinner than the parylene-C layer [22], and thus, we hypothesized that the etching of the carbon debris could be carried out in 2 min without the need of a foil mask. The laser ablation technique (laser spot-size) was optimized for lower-density (6.25 electrodes/mm^2) microelectrode arrays, and more work is needed to optimize the parameters for performing laser ablation on higher-density neural interfaces. The mean GSAs for the laser deinsulated electrodes were well within the safe limits established for penetrating microelectrodes (GSA $\leq$ 2000 μm^2) [29]; however, more work is needed to decrease the GSA of electrodes deinsulated using the foil mask technique.

2.5.2 In vivo characterization of HD-USEAs

The conventionally spaced, lower density USEA can be implanted both acutely (< 1 days) [1] and chronically (> 6 months) [40, 41] with insult to the epineurium or perinerium limited to the areas penetrated by the microelectrodes. The main concern for

using the newly fabricated high-density arrays of electrodes is that the high-velocity pneumatic pulse insertion [32] of the device could cause a partial or complete nerve crush injury. We were able to record spontaneous and stimulus driven neuronal units on > 25 electrodes with an average SNR > 4 in all animal preparations, indicating the nerve remained viable for at least the duration of these experiments (< 10 h). Importantly, histological analyses of the HD-USEA implant sites showed the nerve axons and fascicles appear to manifest no global damage. Tissue insult was limited to that which was produced by the penetrating electrode tips, similar to implantation of arrays that were four times less dense. If these arrays produced an acute nerve crush injury, rather than a limited penetrating injury, we would have expected to see evidence of traumatic injury to the anatomical structure of the nerve, which may have included the loss of myelinated axons surrounding the electrodes (neurapraxia); the loss of continuity of axons around the electrodes with preserved connective tissue between the electrode tracks (axonotmesis); or the complete transection of the nerve (neurotmesis) [23, 42]. The cross-sections of acutely implanted rat sciatic nerves (n = 2) and a feline pudendal nerve (n =1) showed no signs of these types of nerve injuries outside the tracks of the penetrating electrodes. Moreover, there was little compression of the nerve fibers around the tips and shanks of the HD-USEA electrodes, as had been previously noted for the conventionally spaced USEAs [1]. Future studies will be needed to assess any chronic damage to the nerve and whether any such damage is followed by nerve regeneration, as in other nerve crush injury studies[42].

We also investigated the degree of selective motor fibers access in the rat sciatic nerve by delivering voltage-controlled stimulation via individual HD-USEA electrodes. In all three rat preparations, we were able to evoke selective contractions of ankle flexor and

extensor muscles, and importantly, such selectivity could be achieved in electrodes with a tip-to-tip separation as low as 208 μm between electrodes. One advantage of the use of penetrating microelectrodes is that less current is needed to stimulate nerve fibers once the tips are inside the fascicle. Selective and complete recruitment of rat hind limb muscles was possible by delivering stimulation amplitudes of only -2 V with 50% recruitment of muscle twitches seen in some trials for pulse-widths < 100 μs. Lower voltages were not investigated, as this is the lowest limit of the 1100 channel stimulator used in these studies [33].

The devices used in these experiments were designed, in part, to investigate the hypothesis that large numbers of electrodes with 200 μm spacing could penetrate intrafascicularly into peripheral nerves, and that such delicate electrodes would be not damaged (broken) by the epineurium and perineurium or vice versa. Further, experiments were designed to test the hypothesis that 200 μm spacing provided selective access both for stimulation and recording from small diameter neuroanatomical structures. In the rat preparation, selective activation of ankle flexor and extensor muscles was achieved by delivering stimulation via two neighboring electrodes in adjacent rows (≈ tip-to-tip separation of 208 μm). Another concern was that the shortest electrodes would not penetrate into the fascicles. Figure 2.5 shows that, in fact, the shortest electrodes were able to do so. In addition, we were able to record either single or multiunit waveforms from the 300-μm-long-electrodes in one animal. We were also able to selectively stimulate flexor or extensor ankle muscles by delivering low amplitude (-2V, steps of increasing pulse-width of 50 μs) stimulation to the 300 μm length electrodes. Together, these results demonstrate HD-USEAs should provide a useful neural interface for small, delicate

nervous system structures where access to nerve fibers and/or cell bodies at depths of 200 μm is needed, such as retinal ganglion cells [43], mitral cells of the rat olfactory bulb [44], or dorsal root ganglion neurons [45].

2.6 Conclusion

We have developed a novel, high electrode density (25 electrodes/mm^2), high electrode count (48-96 electrodes) penetrating neural interface, designed for use in stimulation and recording in submillimeter neuroanatomical structures, such as small diameter nerves (< 2mm) like the rat sciatic [37], feline pudendal [38], or feline/human cochlear nerves [46]. The results reported herein illustrate that such a delicate architecture can be fabricated consistently, and importantly, that implantation of such high-density electrode arrays does not cause nerve damage, at least on the acute time frame (<10 h) studied here. Furthermore, the HD-USEA provides selective access to the fibers of small diameter peripheral nerves. The high electrode density array described in this study adds a novel and useful architecture to currently available neural interfaces. Future studies will be needed to assess long-term efficacy and biocompatibility of these arrays for their potential use in clinical applications.

2.7 Acknowledgments

This work was supported by the National Science Foundation CBET-1134545, the Spanish National Organization of the Blind and the Ministry of Economy and Competitiveness.

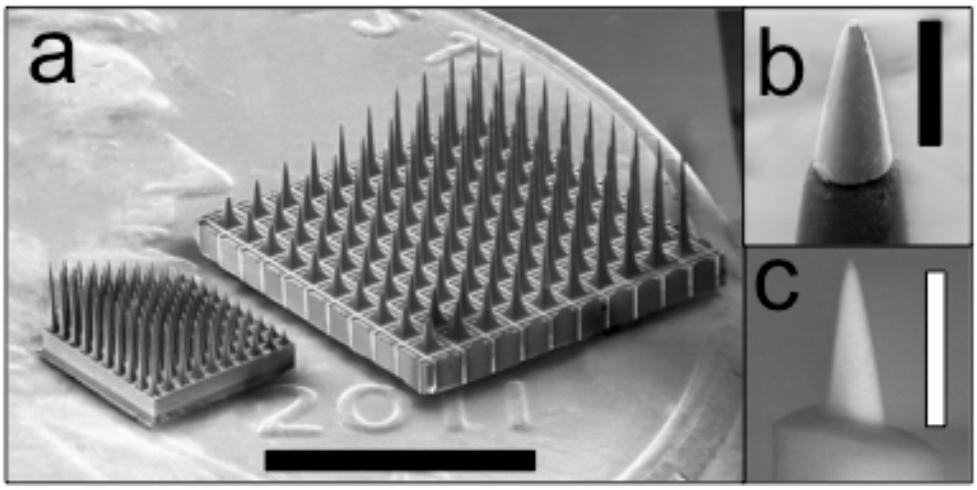

Figure 2.1 The High-Density Utah Slanted Electrode Array (HD-USEA). (a) A scanning electron microscopy (SEM) image of the conventionally spaced USEA (right) and the new HD-USEA (left) located atop a U. S. penny (scale bar = 3 mm). The inset SEM images were taken of HD-USEA tips that have the biocompatible parylene-C insulation removed using (b) an oxygen plasma etching technique (geometric surface area (GSA) = 4367 μm^2; scale bar = 50 μm) and (c) a novel hybrid excimer laser and plasma etching technique (GSA = 297 μm^2; scale bar = 25 μm).

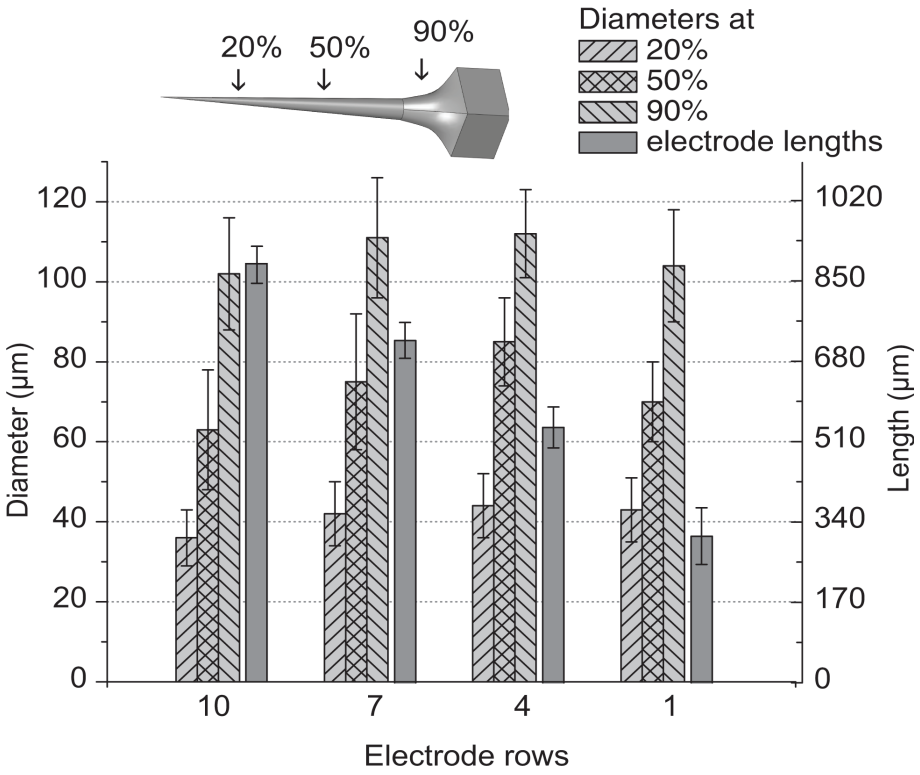

Figure 2.2 Structural variability of 10 HD-USEA devices. The diameters of 4 electrodes from 10 different HD-USEA devices was measured at 20%, 50%, and 90% the distance from the tip down the shaft of the electrode (from Rows 1, 4, 7 & 10; short to long electrodes). Diameters and electrode lengths are shown on the left and right ordinates, respectively. Bars represent the standard deviation for each set of measured diameters and lengths.

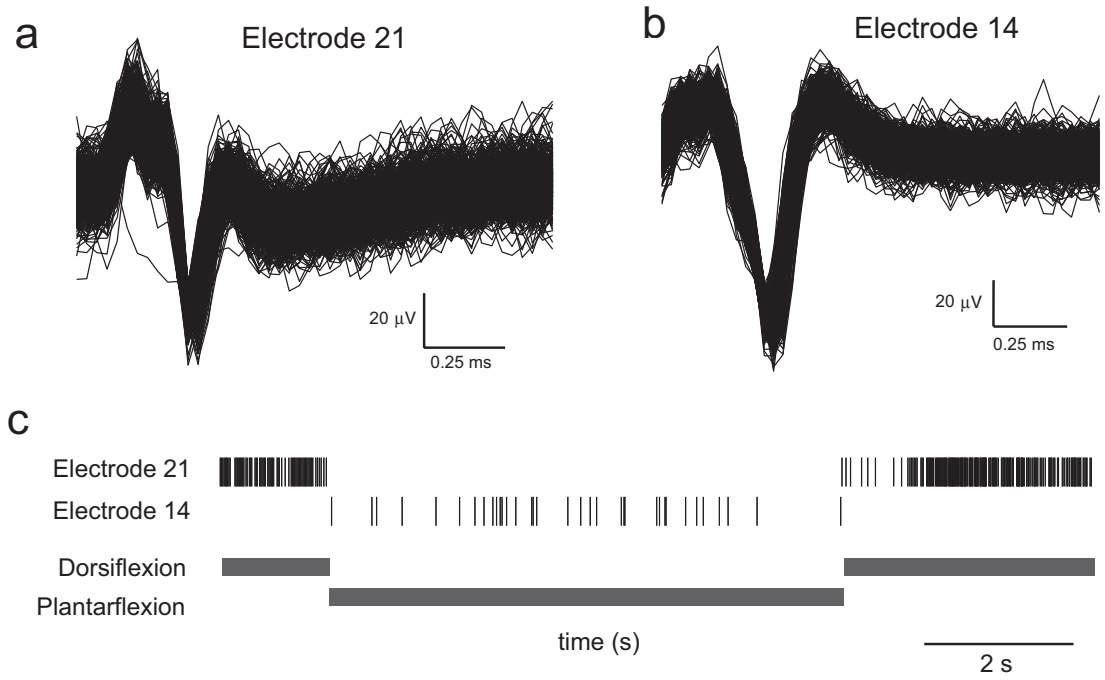

Figure 2.3 Neural units recorded from two HD-USEA electrodes on a single implanted array. (a) 968 waveforms show the summation of the responses from two units to dorsiflexion of the foot around the ankle joint recorded by electrode 21 (SNR = 5.9). (b) 1416 waveforms show a unit recorded on electrode 14 that was driven by plantarflexion (SNR = 10.8). (c) The neural events recorded by electrodes 21 (top) and 14 (bottom) during both dorsiflexion and plantarflexion (shown below raster plot). Note that electrode 21 recorded neural responses only during dorsiflexion, while electrode 14 recorded responses only during plantarflexion.

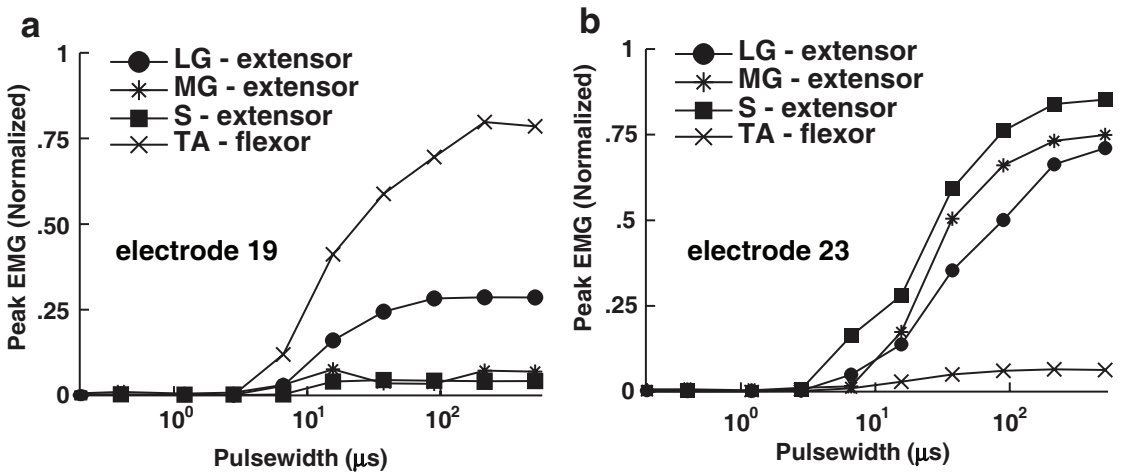

Figure 2.4 Selective ankle flexor and extensor muscle contractions. Normalized EMG peak amplitude was recorded in response to increasing stimulation amplitude (via increasing pulsewidth) delivered via single electrodes on HD-USEA. (a) Stimulation delivered via HD-USEA electrode 19 evoked selective contractions in the ankle flexor muscle, tibialis anterior (TA). (b) Similarly, stimulation delivered via electrode 23 evoked selective contractions in the ankle extensor muscles: lateral gastrocnemius (LG), medial gastrocnemius (MG), and soleus (S).

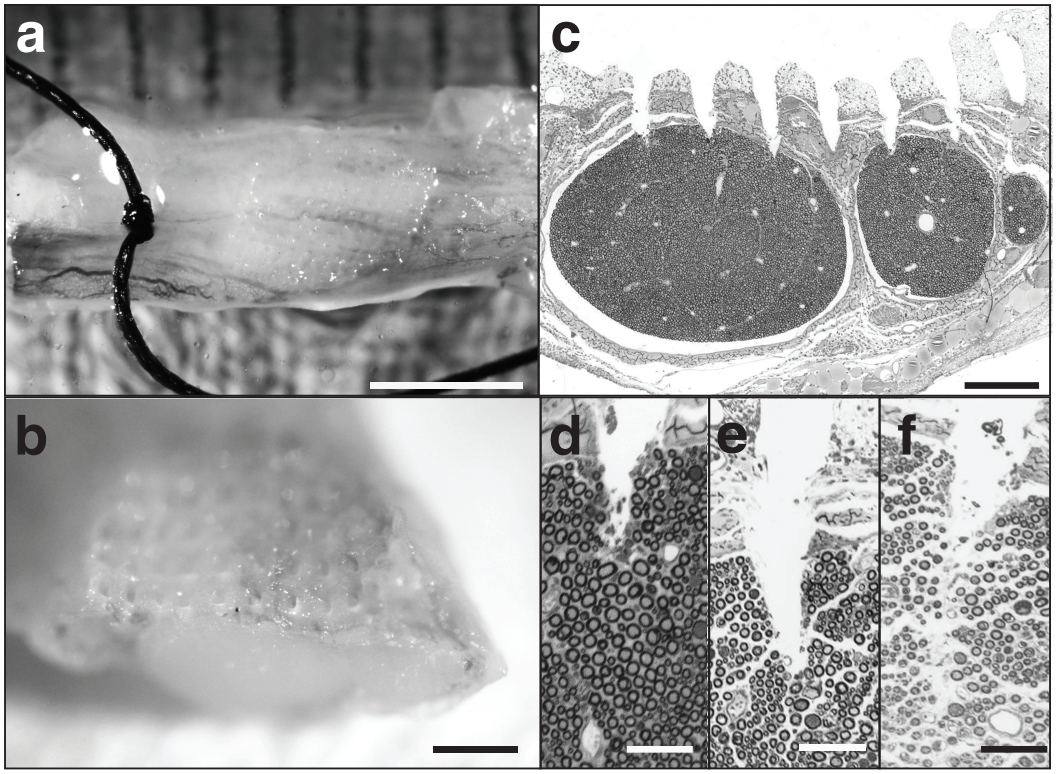

Figure 2.5 Evaluation of implant site. (a-b) HD-USEA electrode tracks are visible on macroscopic inspection of the nerve (a, scale bar = 2 mm; b, scale bar = 0.5 mm). (c) Microscopic cross section of the nerve shows penetration of a row of shorter length electrodes into the top portion of the rat sciatic nerve fascicles (scale bar = 200 μm). (d-f) show a close up of the tips of the short electrodes penetrating into a fascicle. (f) shows a section taken adjacent to an electrode shank. Notice there is no axonal compression around the tips (d-e) of the electrodes or around the shanks (f) of the electrodes (d-f, scale bars = 50 μm)

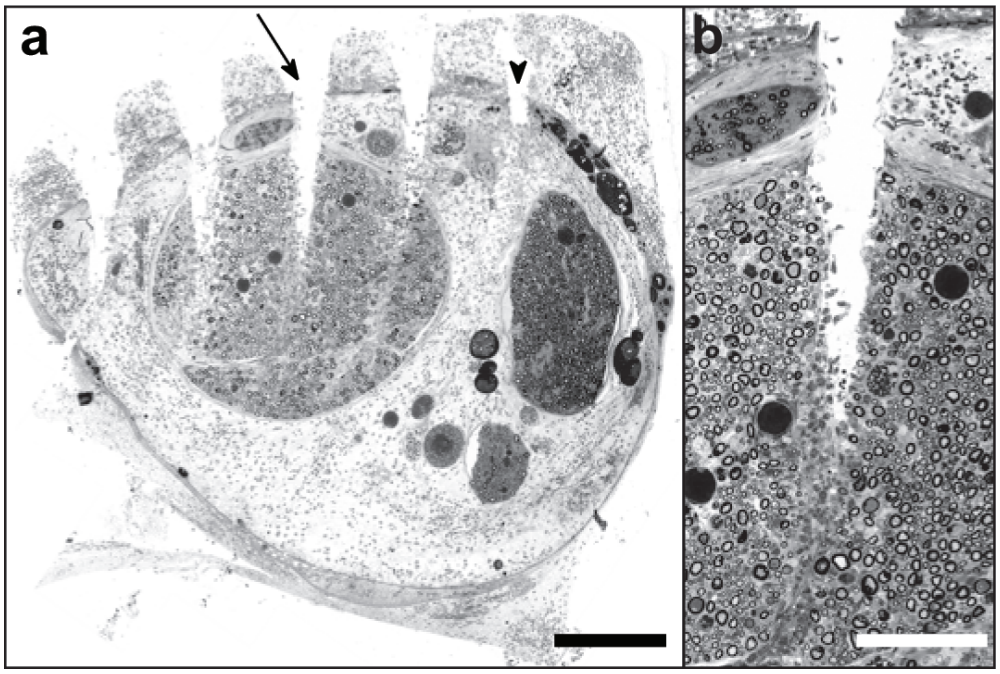

Figure 2.6 Cross-section of cat pudendal nerve implanted with HD-USEA for <10 h. (a) Low-resolution image showing penetration of four electrodes into the nerve, three of which penetrated the fascicular space. The far right track (arrowhead) is from an electrode that was broken prior to implantation. The three tracks that penetrate into the endoneurium extend approximately 450-500 μm from the edge of the epineurium to the electrode tips (scale bars = 200 μm). (b) Close up view of an electrode track from (a) (denoted by arrow) showing penetration of the electrode through the epineurium and perineurium into the endoneurial space (scale bars = 100 μm). While substantial loss of fibers in the electrode track is observed, fibers immediately surrounding the track show minimal signs of acute damage. Additionally, no evidence of complete crush injury (neurotmesis) or nerve compression (neurapraxia) is observed.

2.8 References

1. Branner A, Normann RA. 2000 A multielectrode array for intrafascicular recording and stimulation in sciatic nerve of cats. *Brain Res Bull*. **51**(4) 293-306.

2. Boretius T, Badia J, Pascual-Font A, Schuettler M, Navarro X, Yoshida K, Stieglitz T. 2010 A transverse intrafascicular multichannel electrode (TIME) to interface with the peripheral nerve. *Biosens Bioelectron*. **26**(1) 62-9.

3. Foldes EL, Ackermann DM, Bhadra N, Kilgore KL, Bhadra N. 2011 Design, fabrication and evaluation of a conforming circumpolar peripheral nerve cuff electrode for acute experimental use. *J Neurosci Methods*. **196**(1) 31-7.

4. Lawrence SM, Dhillon GS, Horch KW. 2003 Fabrication and characteristics of an implantable, polymer-based, intrafascicular electrode. *J Neurosci Methods*. **131**(1-2) 9-26.

5. Malagodi MS, Horch KW, Schoenberg AA. 1989 An intrafascicular electrode for recording of action potentials in peripheral nerves. *Ann Biomed Eng*. **17**(4) 397-410.

6. Tyler DJ, Durand DM. 1997 A slowly penetrating interfascicular nerve electrode for selective activation of peripheral nerves. *IEEE Trans Rehabil Eng*. **5**(1) 51-61.

7. Tyler DJ, Durand DM. 2002 Functionally selective peripheral nerve stimulation with a flat interface nerve electrode. *IEEE Trans Neural Syst Rehabil Eng*. **10**(4) 294-303.

8. Csicsvari J, Henze DA, Jamieson B, Harris KD, Sirota A, Barthó P, Wise KD, Buzsáki G. 2003 Massively parallel recording of unit and local field potentials with silicon-based electrodes. *J Neurophys*. **90**(2) 1314-23.

9. Simeral JD, Kim S-P, Black MJ, Donoghue JP, Hochberg LR. 2011 Neural control of cursor trajectory and click by a human with tetraplegia 1000 days after implant of an intracortical microelectrode array. *J Neural Eng*. **8** 1-24.

10. Hochberg LR *et al*. 2012 Reach and grasp by people with tetraplegia using a neurally controlled robotic arm. *Nature*. **485**(7398) 372-5.

11. Mitsui M *et al*. 2005 Development of a novel intrafascicular nerve electrode. *ASAIO J*. **51**(6) 692-5.

12. Bai Q, Wise KD, Anderson DJ. 2000 A high-yield microassembly structure for three-dimensional microelectrode arrays. *IEEE Trans Biomed Eng*. **47**(3) 281-9.

13. Campbell PK, Jones KE, Normann RA. 1990 A 100 electrode intracortical array: structural variability. *Biomed Sci Instrum*. **26** 161-5.

14. Polasek KH, Hoyen HA, Keith MW, Tyler DJ. 2007 Human nerve stimulation thresholds and selectivity using a multicontact nerve cuff electrode. *IEEE Trans Neural Syst Rehabil Eng*. **15**(1) 76-82.

15. Lawrence SM, Dhillon GS, Jensen W, Yoshida K, Horch KW. 2004 Acute peripheral nerve recording characteristics of polymer-based longitudinal intrafascicular electrodes. *IEEE Trans Neural Syst Rehabil Eng*. **12**(3) 345-8.

16. Normann RA, Dowden BR, Frankel MA, Wilder AM, Hiatt SD, Ledbetter NM, Warren DA, Clark GA. 2012 Coordinated, multijoint, fatigue-resistant feline stance produced with intrafascicular hind limb nerve stimulation. *J Neural Eng.* **9**(2) 026019.

17. Du J, Blanche TJ, Harrison RR, Lester HA, Masmanidis SC. 2011 Multiplexed, high density electrophysiology with nanofabricated neural probes. *PLoS ONE*. **6**(e26204).

18. Seidl K HS, Torfs T, Neves H, Paul O, Ruther P 2011 CMOS−based high−density silicon microprobe arrays for electronic depth control in intracortical neural recording. *J Microelectromech Sys*. **20** 1439−48

19. Kibler AB, Jamieson BG, Durand DM. 2012 A high aspect ratio microelectrode array for mapping neural activity in vitro. *Neurosci Methods*. **204**(2) 296-305.

20. Pine J. 1980 Recording action potentials from cultured neurons with extracellular microcircuit electrodes. *J Neurosci Methods*. **2**(1) 19-31.

21. Cogan SF, Ehrlich J, Plante TD, Van Wagenen R. 2009 Penetrating microelectrode arrays with low-impedance sputtered iridium oxide electrode coatings. *Conf Proc IEEE Eng Med Biol Soc*. **2009** 7147-50.

22. Yoo J, Sharma A, Tathireddy P, Rieth L, Solzbacher F, Song J. 2012 Excimer-laser deinsulation of Parylene-C coated Utah electrode array tips. *Sensors Actuators B: Chemical*. 777-86.

23. Lee SK, Wolfe SW. 2000 Peripheral nerve injury and repair. *J Am Acad Orthop Surg*. **8**(4) 243-52.

24. Bhandari R, Negi S, Rieth L, Solzbacher F. 2010 A wafer-scale etching technique for high aspect ratio implantable MEMS structures. *Sensors Actuators A: Physical*. **162**(1) 130-6.

25. Bhandari R, Negi S, Solzbacher F. 2010 Wafer-scale fabrication of penetrating neural microelectrode arrays. *Biomed Microdevices*. **12**(5) 797-807.

26. Jones KE, Campbell PK, Normann RA. 1992 A glass/silicon composite intracortical electrode array. *Ann Biomed Eng*. **20**(4) 423-37.

27. Hsu J-M, Rieth L, Normann RA, Tathireddy P, Solzbacher F. 2009 Encapsulation of an integrated neural interface device with Parylene C. *IEEE Trans Biomed Eng*. **56**(1) 23-9.

28. Gunalan K, Warren DJ, Perry JD, Normann RA, Clark GA. 2009 An automated system for measuring tip impedance and among-electrode shunting in high-electrode count microelectrode arrays. *J Neurosci Methods*. **178**(2) 263-9.

29. Cogan SF. 2008 Neural stimulation and recording electrodes. *Ann Rev Biomed Eng*. **10** 275-309.

30. Dowden BR, Wark HAC, Normann RA. 2010 Muscle-selective block using intrafascicular high-frequency alternating current. *Muscle Nerve*. **42**(3) 339-47.

31. Wark HAC, Dowden BR, Cartwright PC, Normann RA. 2011 Selective activation of the muscles of micturition using intrafascicular stimulation of the pudendal nerve. *IEEE J Emerg Topics Sys Circuits*. **1**(4) 631-37.

32. Rousche PJ, Normann RA. 1992 A method for pneumatically inserting an array of penetrating electrodes into cortical tissue. *Ann Biomed Eng*. **20**(4) 413-22.

33. Hiatt SD, et al. 2010 1100-Channel neural stimulator for functional electrical stimulation using high-electrode count neural interfaces. *IFESS Abstract*. (July 26) 1-3.

34. Wilder AM, Hiatt SD, Dowden BR, Brown NAT, Normann RA, Clark GA. 2009 Automated stimulus-response mapping of high-electrode count neural implants. *IEEE Trans Neural Syst Rehabil Eng*. **17**(5) 504-11.

35. Frankel MA, Dowden BR, Mathews VJ, Normann RA, Clark GA, Meek SG. 2011 Multiple-input single-output closed-loop isometric force control using asynchronous intrafascicular multielectrode stimulation. *IEEE Trans Neural Syst Rehabil Eng*. **19**(3) 325-32.

36. Kelly RC, Smith MA, Samonds JM, Kohn A, Bonds AB, Movshon JA, Lee TS. 2007 Comparison of recordings from microelectrode arrays and single electrodes in the visual cortex. *J Neurosci*. **27**(2) 261-4.

37. Badia J, Pascual-Font A, Vivó M, Udina E, Navarro X. 2010 Topographical distribution of motor fascicles in the sciatic-tibial nerve of the rat. *Muscle Nerve*. **42**(2) 192-201.

38. Mariano TY, Boger AS, Gustafson KJ. 2008 The feline dorsal nerve of the penis arises from the deep perineal nerve and not the sensory afferent branch. *Anat Histol Embryol*. **37**(3) 166-8.

39. Parker RA, Davis TS, House PA, Normann RA, Greger B. 2011 The functional consequences of chronic, physiologically effective intracortical microstimulation.

Prog Brain Res. **194** 145-65.

40. Branner A, Stein RB, Fernandez E, Aoyagi Y, Normann RA. 2004 Long-term stimulation and recording with a penetrating microelectrode array in cat sciatic nerve. *IEEE Trans Biomed Eng*. **51**(1) 146-57.

41. Torab K, Davis TS, Warren DJ, House PA, Normann RA, Greger B. 2011 Multiple factors may influence the performance of a visual prosthesis based on intracortical microstimulation: nonhuman primate behavioural experimentation. *J Neural Eng.* **8**(3) 035001.

42. Luís AL *et al*. 2007 Long-term functional and morphological assessment of a standardized rat sciatic nerve crush injury with a non-serrated clamp. *J Neurosci Methods*. **163**(1) 92-104.

43. Guillory KS, Shoham S, Normann RA. 2006 Discrete stimulus estimation from neural responses in the turtle retina. *Vision Res*. **46**(12) 1876-85.

44. Lehmkuhle MJ, Normann RA, Maynard EM. 2003 High-resolution analysis of the spatio-temporal activity patterns in rat olfactory bulb evoked by enantiomer odors. *Chem Senses*. **28**(6) 499-508.

45. Stein RB. 2004 Coding of position by simultaneously recorded sensory neurones in the cat dorsal root ganglion. *J Physiol*. **560**(3) 883-96.

46. Badi AN, Hillman T, Shelton C, Normann RA. 2002 A technique for implantation of a 3-dimensional penetrating electrode array in the modiolar nerve of cats and humans. *Arch Otolaryngol Head Neck Surg*. **128**(9) 1019-25.

CHAPTER 3

BEHAVIORAL AND CELLULAR CONSEQUENCES OF HIGH-ELECTRODE COUNT UTAH ARRAYS CHRONICALLY IMPLANTED IN RAT SCIATIC NERVE

Reprinted with permission by the Journal of Neural Engineering & co-authors

Publication Reference:

Wark HAC, Mathews K, Normann RA, Fernandez EF. J Neural Eng.

Accepted May 2014. In press.

Author contributions: HACW, KM, RAN designed and carried out the experiments; HACW and EF carried out the histology; HACW and RAN wrote the manuscript; all authors edited the manuscript.

3.1 Abstract

Before peripheral nerve electrodes can be used for the restoration of sensory and motor functions in patients with neurological disorders, the behavioral and histological consequences of these devices must be investigated. These indices of biocompatibility can be defined in terms of desired functional outcomes; for example, a device may be considered for use as a therapeutic intervention if the implanted subject retains functional neurons postimplantation even in the presence of a foreign body response. The consequences of an indwelling device may remain localized to cellular responses at the device-tissue interface, such as fibrotic encapsulation of the device, or they may affect the animal more globally, such as impacting behavioral or sensorimotor functions. Here we investigate the overall consequences of high-electrode count intrafascicular peripheral nerve arrays, High Density Utah Slanted Electrode Arrays (HD-USEAs; 25 electrodes/mm^2), that were implanted in rat sciatic nerve for one- and two-month periods. We monitored wheel running, noxious sensory paw withdrawal reflexes, footprints, nerve morphology, and macrophage presence at the tissue-device interface. In addition, we used a novel approach to contain the arrays in actively behaving animals that consisted of an organic nerve wrap. A total of 500 electrodes were implanted across all 10 animals. The results demonstrated that chronic implantation (≤8 weeks) of HD-USEAs into peripheral nerves can evoke behavioral deficits that recover over time. Morphology of the nerve distal to the implantation site showed variable signs of nerve fiber degeneration and regeneration. Cytology adjacent to the device-tissue interface also showed a variable response, with some electrodes having many macrophages surrounding the electrodes, while other electrodes had few or no macrophages present. This variability was also seen

along the length of the electrodes. Axons remained within the proximity of the electrode tips at the distances required for theoretically effective stimulation and recording (≤100μm). We conclude from these studies that HD-USEAs do not cause overall global effects on the animals, at least up to the two-month period investigated here. These results demonstrate for the first time that the consequences of high-electrode count intrafascicular arrays compare with other peripheral nerve electrodes currently available for clinical or investigational neuromodulation.

3.2 Introduction

The use of peripheral nerve electrodes offers new therapeutic approaches for the restoration of sensory and motor function following nerve injury or disease [1]. Assessment of the behavioral and histological consequences of implantation of such neural interfaces is an important milestone in the development of this technology as it progresses from acute animal experimentation to clinical applications. For a device to be considered for use as a potential therapeutic intervention, it must meet a predetermined set of criteria after implantation into living tissue.

Nerve electrode arrays have recently been developed that contain a large number of electrodes, allowing for more information to be transferred to and received from the nervous system for neuromodulation studies and applications [2]. To date, larger peripheral nerves (>3 mm diameter) have been implanted with devices that have between 16 [3] and 96 [4] electrodes. For smaller peripheral nerves (≤1 mm), three different multielectrode neural interfaces have been manufactured and chronically implanted (≤3 months), including high channel-count regenerative sieve electrodes (19 electrodes [5]),

27 electrodes [6]), Transverse Intrafascicular Multichannel Electrodes (TIMEs; 5 electrodes [7]), and thin-film Longitudinal Intrafascicular Electrodes (tfLIFEs; 8 electrodes [8]). The behavioral and cellular consequences of chronic implantation of these devices have been investigated [6-8]. However, no studies have been carried out that investigate the consequences of chronically implanted peripheral nerve high-electrode count penetrating microelectrode arrays.

A new high electrode count neural interface, the High Density Utah Slanted Electrode Array (HD-USEA; 25 electrodes/mm^2), has recently been fabricated and tested in acute experiments (<12 hr) for its use in small peripheral nerves (<2 mm) [2,9]. The motivation for developing such a high electrode count array was to increase the selective intrafascicular access to nerve fibers in millimeter and submillimeter nervous system structures. In order to expand application of HD-USEAs to chronic preparations, we assessed the behavioral outcomes and cytology at the tissue-device interface in rats that had nonwired HD-USEAs implanted into their sciatic nerves. This study was motivated by the concern that implantation of such a high spatial density of penetrating microelectrodes could severely damage or crush the nerve, negating their use in short-term chronic experimentation. The behavioral and histological criteria we used in this study to assess the use of such high-electrode density arrays in chronic experimentation included: 1) that the devices must have remained implanted in actively behaving animals, 2) that the devices did not permanently interfere with overall animal behavior, and 3) that axons remained within 100 μm of the electrode tips. Nonwired devices were used in this study in order to assess the effects of the implanted electrodes alone, without confounding factors that may arise from wire bundles or a percutaneous connector.

The rat model was chosen for these studies as it has frequently been used in chronic peripheral nerve injury models [10-12], and for standard histological [13-16] and behavioral [10,15,17-20] quantification studies. Because functional recovery in the rat has been observed within three to four weeks after nerve crush injury and within six to eight weeks after nerve transection repair, we implanted two cohorts of rats for durations of four and eight weeks to focus on assessing damage and recovery during these early phases of nerve injury [10,20].

We found that HD-USEAs caused mild behavioral changes that recovered within days to weeks postimplantation and that there was a mild chronic inflammatory response characterized by a nonuniform distribution of macrophages surrounding the tissue-device interface. The novel containment system (an organic nerve wrap) that was used in these studies successfully protected the arrays, and nine of the arrays remained completely implanted in the nerve at the end of the two study periods. Morphology of the nerves was assessed both proximally and distally to the implant site, and signs of degeneration and regeneration were seen. Quantification of these sections showed no significant difference in the myelin thickness, while there was a significant difference the area and diameter of the nerve fibers or axons. Morphology was also assessed at the device tissue interface, and axons remained in close proximity ($\leq$ 100μm) to the tips of the intrafascicular electrodes in both study cohorts. Future studies are now warranted to assess the capabilities of HD-USEAs that are implanted for > eight weeks and for devices that are wired for electrophysiological experimentation.

3.3 Materials and methods

3.3.1 Animal groups and behavioral protocols

All studies were approved by the University of Utah Institutional Animal Care and Use Committee. Ten Wistar-Kyoto rats (Charles-River Laboratories International, Inc., USA) were randomly assigned to either four- or eight-week implant cohorts (n = 5 for each cohort). Wistar-Kyoto rats were chosen as they have been shown to have increased voluntary wheel running over other rat strains [21]. Rats (age ≈ 40 days postnatal at the start of the study) were placed in separate cages each night and provided with food, water, and an exercise wheel *ad libitum*. Each wheel was equipped with a cyclometer that measured running distance (km), maximum speed (km/hr), average speed (km/hr), and total elapsed running time. Rats were returned to shared housing (3-4 rats/cage) with the same litter mates each morning. All rats were allowed to run voluntarily for nine weeks prior to implantation of HD-USEAs in order to establish preimplant peak and average running distances [22]. The distances ran nightly were averaged for a weekly distance. For statistical analysis, average weekly distances were compared using t-test statistics for nine weeks of preimplant data and for either four or eight weeks of postimplant data. Data analysis was carried out using MATLAB (The MathWorks, Inc., MA, USA) and Microsoft Excel (Microsoft, WA, USA).

3.3.2 Surgical procedures

Unwired HD-USEAs were cut to form a 5x10 grid of electrodes (lengths ranged from 200 to 800 μm with 200 μm spacing) and then coated in paralyene-C [2]. Prior to implantation, electrodes were cleaned and sterilized. HD-USEAs were implanted into the

left sciatic nerve using previously described methodology [2,9]. In brief, anesthesia was induced and maintained with Isoflurane (5.0% and 0.2% gas, respectively) and vital signs were monitored. The sciatic nerves were exposed and HD-USEAs were pneumatically implanted [23]. The implantation site was then wrapped with a commercially available nerve wrap (AxoGen Inc., Alachua, FL). Nerve wraps were trimmed to fit around the nerves and arrays, with approximately 5 mm of wrap extending both proximally and distally from the HD-USEA. The wraps were closed with sutures (8-0 Nylon, Ethicon) to minimize gaps between the wrap and the nerve. The ends of the wraps were then sutured to the epineurium in order to prevent slippage of the wrap along the length of the nerve. Rats were given minocycline (100 mg/L) dissolved in water *ad libitum* for two days before and for five days after implantation of the HD-USEAs [24]. Dexamethasone (200 μg/kg) was administered by a subcutaneous injection on the day of surgery [25].

3.3.3 Assessment of sensorimotor reflexes

Assessment was evaluated using the paw Withdrawal Reflex Latency (WRL) test, defined as the time it took for the animals to withdraw their paw from a hot plate set to ≈ 50°C (with a cut-off time of 12 sec) [10,19]. Tests were performed with rest intervals > 1 min to prevent sensitization and average weekly WRLs were calculated from > 3 tests on each hindlimb [10]. Our methodology differed from previous methods only in that we tested the WRL for both hindlimbs in order to control for any small differences in hot plate temperature that may have occurred between testing times. The ratio of WRLs for implanted and control hindlimbs were calculated and expressed as percentages [((Implanted-Control)/Implanted) × 100]. The sensorimotor reflexes were assessed one

week before surgery, but not weekly during the control period when peak running distances were obtained. Footprint analysis was carried out using the ratio of the toe-spread length from the first to the fifth digit in the implanted versus the control limb, which has been shown to be an efficient and sensitive test for footprint deficits [18]. Briefly, the rats were placed in a box with a clear bottom and photographs were taken of the standing rats. In order to decrease the chance of any postural tone which could affect footprint stance, the testing room was free of startling noises and the animals were allowed to acclimate in the box before photos were taken [18].

3.3.4 Histological procedures

Animals were sacrificed by injection of pentobarbital and perfused with 4% paraformaldehyde. The nerves around the implant site and nerve wrap were excised, the nerve wrap was dissected from the nerve, and the HD-USEAs were explanted under a dissecting microscope. The nerves were then transferred to 0.01 M phosphate buffer solution (PBS) with 0.1% sodium azide. Each rat nerve was assigned to a morphological and/or immunohistochemistry processing group, which included light microscopy cross- and longitudinal sections through the implanted array site; light microscopy cross-sections proximal and distal to the implanted array site; and cross- and longitudinal sections of the array site for immunohistochemical assessment of macrophages. The light microscopy designated samples were incubated for 1 h in 2% OsO_4 and further processed for embedding in Epon 812 resin. Semithin sections (0.5 μm thick) were stained with toluidine blue and examined by light microscopy. Images of the whole sciatic nerve were acquired at various magnifications with a microscope (Olympus AX70) using a high-

resolution digital camera (Olympus DP-11).

Images were analyzed using the Image J software (National Institutes of Health, Bethesda, MD) and a custom-modified version of software designed to study axonal morphometry (Cavalieri 3.0 macros by G. MacDonald, Virginia Merrill Bloedel Hearing Research Center, University of Washington, Seattle, WA). Morphometrical evaluation was performed in sets of images chosen by systematic random sampling of squares representing at least 20-30% of the nerve cross-sectional area. Because it was difficult to automatically select the boundary between the nerve fibers and the surrounding background for small axons and thinly-myelinated fibers using standard image analysis techniques, each digitized image was analyzed using a semiautomatic method. The axonal contour and the external contour of the myelin sheath (fiber contour) were manually traced on enlarged images. A set of custom macros allowed the calculation of the lengths of the major and minor axes of the best fitting ellipse and the cross-sectional area. Fiber diameters and axonal diameters were deduced from the fiber and axonal perimeters assuming a cylindrical shape of axons. These data were used to derive the form factor, roundness of fiber, and myelin sheath thickness. Fibers were defined as the outer diameter of the neuron including the myelin. Axons were defined as the inner diameter of a neuron, not including the myelin. These diameters were calculated from the area of each assuming a circular geometry. Because many of the fibers had elliptical geometry, the form factor, roundness and mean diameter (major axis diameter + minor axis diameter/2) were calculated to quantify differences that could be due to changes in elongation. The ratio of the axon diameter to the fiber diameter (g-ratio) was calculated using two different methods: 1) using the diameters derived from area of the axon and

fiber, assuming circular geometry, and 2) using the mean diameter of the major and minor axes.

Samples designated for immunohistochemical processing were washed in PBS, cryoprotected in 30% sucrose at 4ºC and mounted in optimal cutting temperature compound (OCT). Longitudinal and traversal sections were cut at 16 μm with a minus 20ºC cryostat (Micron HM505E) and mounted directly onto Superfrost Plus (Thermo Fisher Scientific) slides. Slides were removed from the cryostat, air-dried, blocked for 30 min (0.1M PBS, 10% normal donkey serum, and 0.5% Triton X-100) and incubated overnight at room temperature in the following primary antibodies (in 0.1 M PBS, pH 7.4, plus 0.5% Triton X-100): mouse antirat monocytes/macrophages clone ectodermal dysplasia-1 (ED1; Millipore 1:100); and rabbit antirat neurofilament-200 (NF-200; Sigma 1:300). After three 10 min washes in PBS, the corresponding secondary antibodies to IgG (Invitrogen) conjugated to Alexa Fluor 488 (green), 555 (red), 633 (far red) or 647 (far red) were applied at a 1:100 dilution for 1 h at room temperature. Finally slides were washed three times (10 min each) in PBS before being cover-slipped in fluorescent mounting medium. All fluorescent images were captured with a confocal laser-scanning microscope (TCS SPE, Leica Microsystems, Wetzlar, Germany). Mosaic images were created using Photoshop (Adobe Photoshop CS5, Adobe Systems Inc., USA).

3.4 Results

3.4.1 Behavioral assessment of rats implanted with HD-USEAs

Rat toe-spread lengths were measured for each hindlimb between the first and fifth digits (denoted as ‘1-5 toe-spread’). An example of one rat’s static footprint is

shown in Figure 1a (rat #7, eight-week cohort). This rat showed a decreased toe-spread postimplantation (middle photograph; star indicates implanted side). By the third week after surgery there was a full recovery of the 1-5 toe-spread length. For the four- (Fig 3.1b) and eight-week (Fig 3.1c) cohorts, a total of four rats manifested no decreases in their 1-5 toe-spread lengths for the duration of their implants. The remaining six rats had decreased initial toe-spread lengths in their implanted hindlimbs, but these returned to normal lengths compared to the contralateral foot (mean time for full recovery = three weeks; range = one to four weeks).

Paw WRLs were measured weekly for each rat beginning the week prior to surgery and weekly thereafter. The presurgical value for the WRL manifests no differences in the latency times between left and right hindlimbs as they reflexively withdrew from the hot plate. Figures 3.1d-e show the mean value (computed from three measurements) of the ratio of WRLs in the implanted versus the control leg for the four and eight-week cohorts. A total of three rats had WRL ratios that increased above baseline within the first week after HD-USEA implantation, with latencies returning to normal by the second week. Two rats had increases in WRL times in their implanted leg 3-4 weeks after surgery, with times returning to baseline within 1-2 weeks. The mean recovery time for the five rats with increased WRL in their implanted leg was 1.5 weeks.

Average distances in kilometers ran per night over the course of one week were plotted for rats that had no significant (Fig 3.2a; two-tailed t-test; $p > 0.05$ for each rat) and significant (Fig 3.2b; two-tailed t-test; $p < 0.05$ for each rat) differences in running distances before and after HD-USEA implantation. Note that here the rats have been grouped according to significant (3 rats) and nonsignificant (7 rats) running changes and

not by implanted time periods. For the rats that had significant changes in running distances after surgery, two of these rats had decreased weekly running distances (rat #8, 8-wk group, preimplant average = 7.44 km/night, postimplant average = 4.45 km/night, $p = 0.0294$; rat #4, 4-wk group, preimplant average = 7.64 km/night, postimplant average = 2.87 km/night, $p << 0.0005$), while one rat had increased average nightly distances ran (rat #9, preimplant average = 4.94 km/night, postimplant average = 8.73 km/night, $p = 0.0005$). There were no significant differences ($p = 0.70$; two-tailed t-test;) in the mean and standard deviations of the weekly distances ran across all rats when comparing preimplantation (6.24 ± 2.3 km/night; mean ± std) and postimplantation (6.07 ± 2.45 km/night) groups (Fig 3.2c).

3.4.2 Tissue assessment of rats implanted with HD-USEAs

Nerves were dissected in postperfused animals and the organic nerve wraps were subjectively assessed for the quality of the nerve tissue and the extent of fibrotic encapsulation surrounding the implant site. A representative example of a control nerve and the contralateral implanted nerve is shown in Figure 3.3a. In all of the rats, the organic nerve wraps remained in place and each of the nonwired arrays were still contained within the organic material at the end of the study period. Furthermore, no major adhesions between the wrap and the epineurium were formed. Each HD-USEA implantation was dissected under a microscope and assessed for the extent by which the arrays remained implanted in the sciatic nerve. Figures 3.3b-c show two nerves with the HD-USEA exposed for the qualitative assessment of the extent of end-point implantation. An implant was categorized as ‘complete’ if the entire substrate of the array was located

immediately adjacent to the epineurium (Fig 3.3b). Implants were characterized as 'partial' if the substrate had backed away from the nerve with any portion of the electrode shanks visible outside the epineurium (Fig 3.3c). Nine rats were found to have devices that were completely implanted post sacrifice. After removal of the HD-USEAs, a waffle-like pattern produced by the electrodes was visible (third photograph Fig 3.3b-c). One rat had an HD-USEA that had partially migrated out of the nerve (Fig 3.3c; rat 4; four-week cohort). Note the waffle-like pattern from this device appeared to have an enhanced fibrotic response with suspected hemosiderin-laden macrophages or erythrocytes causing pigmentation on the epineurium. None of the implants had electrode arrays that had completely migrated out of the nerve. Scanning electrode microscopy (SEM) images were taken of several HD-USEAs after explantation and organic material adhering to the surface of the device was evident (Fig 3.3d).

Representative proximal and distal nerve cross-sections are shown in Figure 3.4 for a rat in each of the implant cohorts. For each of the samples processed for proximal and distal morphology (n= seven rats; four-week cohort rat#s 1-4; eight-week cohort rat#s 6, 7 & 10), the distal nerve showed more signs of nerve degeneration and regeneration, consistent with local damage to the axons at the implant site. Such axonal degeneration was characterized by encroachment of axoplasm, redundant myelin (including collapse of the myelin into the axoplasm; thick arrowheads Fig 3.4d & h), and presumptive presence of phagocytic immune cells (thin arrowheads Fig 3.4d &h). These injuries left the endoneurium and perineurial tubes intact, which presumably facilitated the regeneration of damaged axons. In the nerve distal to the implant, regenerating axons are seen with their characteristically thin myelin (arrows in Fig 3.4d & h). An example of

the organic nerve wrap material used to contain the arrays can be seen in the light microscopy images for each rat (double headed arrow Figs 3.4a & g).

Nerve morphology was assessed in nerve sections taken proximal and distal to the HD-USEA implant site for two rats representative of each group (number of fibers: four-week proximal = 534, distal = 483; eight-week proximal = 520, distal = 499). There was no significant difference (two-tailed homoscedastic t-test) found in the thickness of myelin ($p_{rat\ 1} = 0.64$; $p_{rat\ 10} = 0.17$) or the g-ratio (Fig 3.5.a & c; $p_{rat\ 1} = 0.24$; $p_{rat\ 10} = 0.25$) between proximal and distal sections for both rats. We calculated g-ratios using two different methods to obtain the fiber and axon diameters. The first method used diameter measurements derived from the fiber and axon areas, assuming a circular geometry, and there was no significant difference in the g-ratios for both rats (Fig 3.5.a & c; $p_{rat\ 1} = 0.24$; $p_{rat\ 10} = 0.25$). The second method used diameter measurements derived by measuring the mean diameter from both the major and minor axes for a given fiber and axon, and there was a significant different in the g-ratio of the distal tissue for the eight-week implant ($p = 0.02$; proximal = 0.62 ± 0.07; distal = 0.63 ± 0.08), but there was no significant different for the four-week implant ($p = 0.63$; proximal = 0.61 ± 0.07; distal = 0.60 ± 0.10).

In the tissue implanted for four weeks, no significant difference between the proximal and distal morphology was found for axon diameter (Fig.5b; $p = 0.18$; proximal = 5.25 ± 1.39; distal = 5.11 ± 1.86 μm), fiber area ($p = 0.47$; proximal = 65 ± 26, distal = 64 ± 37 μm^2; mean ± std) or axon area ($p = 0.94$; proximal = 23 ± 12; distal = 23 ± 17 μm^2). In the tissue implanted for eight weeks, there were significant differences in the axon diameter (Fig.5d; $p < 0.005$; proximal = 5.73 ± 1.31; distal = 5.38 ± 1.33 μm), fiber

area ($p < 0.005$; proximal = 70 ± 24; distal = 62 ± 26 μm^2), axon area ($p < 0.005$; proximal = 27 ± 13; distal = 24 ± 12 μm^2), and fiber diameter ($p < 0.005$; proximal = 9.3 ± 1.56; distal 8.68 ± 1.85 μm). Morphometric parameters with significant differences in proximal and distal segments for tissue implanted for four or eight weeks included form factor (increased for both groups indicating elongation; $p << 0.001$), mean fiber and axon diameter (decreased for both fiber and axon measurements in both groups indicating smaller fibers; $p < 0.05$), and roundness of the fiber (decreased for both groups; $p << 0.001$).

Figure 3.6a shows a representative cross-section through a row of electrodes from a rat that was implanted for four weeks (rat #1). Magnification of the electrode tracks shows myelin-stained axons that were still intact and within 50 μm of the electrode tracks (Fig 3.6b). Antibodies were used to identify the presence of ED1 positive macrophages at the device-tissue interface. Macrophages and neurons were found along the electrode tracks (Fig 3.6c; ED1 positive cells = green; Neurofilament positive cells = red; rat #8; eight-week cohort). Figure 3.6d-e shows a longitudinal section taken from the same rat shown in Figs 3.6a-b (rat #1) and the osmium-stained myelin again shows that many of the axons are within 100 μm of the electrode tips. A longitudinal section that was exposed to antibodies for ED1 positive macrophages demonstrates again the presence of macrophages at the electrodetissue interface (Fig 3.6f; rat #7; eight-week cohort). The presence of macrophages around the electrode shafts was found to be nonuniform, with some electrode tracks having a greater number of macrophages then others.

3.4.3 Overall assessment of the functional and histological consequences of implanted HD-USEAs

Table 3.1 summarizes the overall results for each implanted rat. Grades were given for the following categories: sensorimotor tests ('Sensorimotor'), running distance ('Running'), macroscopic assessment of the depth of implantation of the electrode arrays at the end of the study period ('Implant'), and an assessment of the proximity of axons to electrode tracks ('Axons'). None of the rats had deficits across all of the categories. Overall scores were given with one point for each severity of deficit so that a total of seven points would indicate major deficits in each category (major biocompatibility issues) and a score of zero indicated no deficits across all the categories (no biocompatibility issues). The mean scores were 1.2 and 1.8 for the four- and eight-week cohorts, respectively.

3.5 Discussion

3.5.1 Effect on animal behavior

In order to quantify animal behavior and sensorimotor changes that may result as a consequence of electrode array implantation, we chose standard tests that have been previously reported to accurately reflect nerve crush or transection injuries (WRL and standing 1-5 toe-spread). In addition, we also measured nightly running behavior in each rat in order to obtain a quantification of the more global effects the devices may have had on animal behavior. The results of these studies suggest each of the tests utilized here were useful for measuring the consequences of these devices on animal behavior and sensorimotor function.

The peak times of the deficits in the WRL and 1-5 toe-spread lengths did not correlate in time across all of the rats. One of the two rats in the four-week cohort (rat #1) and one in the eight-week cohort (rat #7) that showed impaired toe-spreads on their implanted side also had impaired WRL times in this limb. However, the times corresponding to each deficit did not overlap, suggesting that the sensorimotor fibers needed for stance were damaged or inhibited first, while impairment of the sensorimotor fibers needed for noxious withdrawal reflexes occurred subsequently. However, this trend was not consistent for rat 9, where both WRL and toe-spreads showed deficits within the first week postimplantation. The different assessment sensitivities of the WRL and toe-spread ratio suggest these two methods for assessing sensorimotor function are specific to different types of nerve injury. We speculate that the 1-5 toe-spread ratio reflects acute nerve injury resulting from HD-USEA implantation, as all deficits revealed by this test were seen immediately following implantation. However, the WRL test showed deficits that appeared at varying times throughout the study period, which could be reflective of different stages of inflammation, nerve compression or injury.

The two rats that had decreased weekly running distances (rat #8, eight-week cohort; rat #4, four-week cohort) did not show any major deficits in their sensorimotor tests towards the end of the study periods. Rat #8 had transient deficits in both its toe-spread and WRL, but both sensorimotor tests returned to normal while its average weekly distances continued to decline. Finally, the rat (#4) with the HD-USEA that had partially migrated out of the nerve by the end of the study also had decreased weekly running distances, but did not have deficits in the other sensorimotor tests.

The nightly enrichment cages used in these studies were larger than standard

AAALAC holding cages and had wire walls to encourage rat-climbing activity. These enrichment cages allowed for substantially more activity both on the exercise wheel and during wall climbing than standard cages. One motivation for using these cages was to increase the possible mechanical stress on or around the implant system and to provide a challenging environment in which to test the ability of HD-USEAs to remain implanted in peripheral nerves, especially while using the novel organic nerve wrap containment system. However, forced treadmill running in rats has been shown to increase healing after peripheral nerve injury [26], and therefore, the time required by nerves to recover following HD-USEA implantation may be shortened in our rats compared to more sedentary animals.

3.5.2 Containment of the HD-USEAs using an organic nerve wrap

In previous studies using a lower electrode density version of the HD-USEA (the USEA with 6.25 electrodes/mm^2), chronic feline sciatic nerve implants were contained using a three-step containment system: silicone elastomer cuffs were wrapped around the implant and nerve, surrounded by a gold screen (to minimize EMG interference), and then the entire system was coated with surgical-grade adhesive [27,28]. In order to investigate a new containment system that would have less foreign material surrounding the implant, and thus, a potentially decreased foreign body response, we used a decellularized organic nerve wrap that has been approved for use in human nerve repair or protection surgeries [29]. Because few or no adhesions between the organic nerve wrap and the epineurium were formed, the wrapping material could easily be dissected away from the nerve after being implanted for four or eight weeks. Such a containment

system for HD-USEAs would be important for applications in semichronic human experiments where the implanted arrays would need to be explanted from the nerve at the end of the study.

3.5.3 Morphology and cytology at the tissue-device interface

Tissue damage after implantation and/or the formation of a large fibrotic scar can effectively displace the indwelling electrodes from the nerve axons, negating their use in chronic studies [7,30-33]. Fibrotic scarring can also increase the distance from the tip of the electrodes to active neural tissue, potentially placing the electrode outside its effective recording distance (150 μm) [34]. Also, an extensive fibrotic or granulation response surrounding the device could require higher stimulation currents in order to evoke a given response over time, and thus, may lead to stimulation levels that would no longer be safe for the electrodes or the surrounding neural tissue [35]. The results of this study showed that the tips of the electrodes remained within distances that would be useful for stimulating and recording from these fibers on the time scales investigated herein. Although axons were found within such useful ranges, it is unknown whether these axons were functional; however, Rushton pointed out that g-ratios (of peripheral nerves) close to 0.6 provide fiber geometries that allow for the optimal spread of current between nodes of Ranvier [36]. The g-ratios reported herein were all between 0.59-0.63, and thus, we hypothesize these axons would be functional for electrophysiological recording or stimulation studies, and future studies using wired HD-USEA are warranted to investigate this hypothesis.

Quantification of the nerve morphology at an electrodetissue interface has

historically been carried out for neural interfaces with either a low number of electrodes, such as long intrafascicular electrodes, or with many electrodes along a single plane, such as the Michigan probe [37]. However, the electrode arrays here differed in that many electrodes are distributed along multiple planes. Our results—and other previous results from conventionally spaced Utah Arrays implanted in the peripheral and central nervous systems [28,38]—indicate that much variability of the tissue adjacent to the electrode tracks is observed in both light microscopy and immunohistochemical samples. A total of 500 electrodes were implanted across 10 animals in this study, and the tips of some of these electrodes penetrate into fascicular space, while others penetrate into endoneural space. This results in variability in the number of axons within distances needed for recording or stimulation, as well as variability in the number of macrophages at the electrodetissue interface (both between electrodes and along the length of a single electrode). Some electrodes had many macrophages surrounding the shaft/tip of the electrode, while other electrodes had few or no macrophages present. With such variability, it was difficult to obtain quantification of the morphology or immunology that would be representative of all of the 500 implanted electrodes.

As with the immunohistochemistry, there was variability in the morphology of the distal nerve sections, depending on which section of the nerve was magnified. Some areas within the fascicles had nerve morphology that showed little to no signs of degenerating/regenerating fibers, while others showed marked differences. In Figure 4 we did our best to show regions of the nerve that had the most marked signs of degeneration/regeneration, although we note that other areas of the nerve remained free from such changes. Quantification of the nerve tissue proximal and distal to the

implanted devices supported such variability, with significant differences seen for some parameters (such as increases in form factor and decreases in mean axon diameters in the distal tissue), while there were no significant differences in other factors (such as the thickness of the myelin). Thus, the quantified morphometric data did not support overall degeneration/regeneration throughout the entire section of the distal nerve.

The g-ratio has been traditionally used as a method for quantifying nerve morphology and is defined as the ratio of the axon to the fiber (axon and myelin) diameters [39]. Many of the axons in the proximal tissue closely approximated circular geometries, whereas many regenerating axons in the distal tissue approximated more elliptical geometries. When we calculated the g-ratio using diameters back-calculated by the area of the fiber/axon, assuming circular geometry, we did not find significant differences in the proximal and distal g-ratios for rats implanted for 4 or 8 weeks. However, when we calculated the g-ratio using mean diameters by measuring the major and minor axes, we found a significant difference in the g-ratio of the distal tissue (8-week implant). Future studies that utilize the g-ratio as a metric for quantification of nerve morphology following nerve injury or implantation of nerve electrodes should consider calculation of g-ratios using the mean of major and minor axes, which may better reflect geometric changes in regenerating axons.

Immunohistochemistry was performed to obtain additional information about the distribution of macrophages surrounding the device. The tissue reaction to HD-USEA implantation was characterized by a mild to moderate inflammatory response localized mainly around the device-tissue interface, an observation consistent with previously published results for electrode arrays implanted in the peripheral [6-8,28] and central

[32,38,40,41] nervous systems. Macrophages were nonuniformly distributed at the device-tissue interface, a finding that may reflect localized impalement of blood vessels in the nerve. Macrophages are known to differentiate into different subsets that are either inflammatory (referred to as M1 cells) or reparative (referred to as M2 cells) [42] and future studies are warranted to assess which subtype is found at the device-tissue interface and whether the subtype changes over different postimplantation times.

The variability seen in the immunohistochemistry and the morphometric analysis of the nerves is in agreement with previous studies that were carried out using Utah Arrays with 400μm electrode spacing implanted for various time periods in the cat sciatic nerve [28]. Future studies are warranted to determine what causes this variability among arrays of electrodes (possibly a result of localized blood vessel impalement or positioning of the electrodes within the nerves either intrafascicularly or interfascicularly). Methods for automating such quantification for high electrode count devices across three-dimensional space within the nerves would facilitate studying this question.

3.5.4 Overall assessment of the histological consequences of HD-USEAs

In this study, an overall subjective evaluation was made across the data collected using behavioral assays, assessment of the extent that the devices remained intrafascicularly implanted, and the distance of nerve axons from the electrode tips. Compilation of the data in Table 3.1 resulted in an overall rating for the consequences of chronic implantation of HD-USEAs for four and eight weeks, and for each cohort, these devices were considered to have minor consequences. Future studies need to investigate not only longer duration implants, but also devices that are wired to a percutaneous

connector for electrophysiological studies. Such wired electrode arrays may produce additional tethering forces that could exacerbate the immune response as seen for tethered devices in the central nervous system [32]. There may also be increased mechanical strain on the implant site for wired devices, which may result in differences in tissue damage and/or explantation of the devices.

3.5.5 Modifying the cellular response at device-tissue interface

Previous research has shown that the cellular response to chronically implanted brain electrodes can be attenuated by systemic or local delivery of antiinflammatory drugs [24,25,43]. The rats in this study were given both oral minocycline and injected dexamethasone, and although it was not the aim of this study to investigate the effects of these drugs, the administration of these drugs was carried out to potentially provide a more neuroprotective environment in the face of indwelling HD-USEAs. Future studies are warranted to assess whether administration of these drugs can help modify the sensorimotor and/or cellular responses to chronically implanted peripheral nerve electrodes. Additionally, modifications to the surface chemistry [43-45] or surface area [37] of HD-USEAs could assist in altering the host response to these devices.

3.6 Conclusion

The present study was aimed at evaluating the consequences of HD-USEA implantations in actively behaving animals in terms of overall animal behavior and cytology at the tissue-device interface. Using a combination of behavioral assessment tools, the results showed that HD-USEAs evoke mild deficits that generally returned to

normal within days to weeks. Cytological analysis showed that although macrophages were present at the device-tissue interface, nerve axons remained within distances needed for neural recording or stimulation. Signs of axonal damage were observed in all animals, with the distal nerve showing signs of regenerating neurons. Our results indicate that unwired high count (25 electrodes/mm^2) microelectrode arrays passed the biocompatibility criteria defined for this study. Future studies are now warranted to investigate longer duration implants, devices that are wired to a connector, and histological analysis of the variability in morphometric and immune cell changes throughout the nerve and along the device-tissue interface.

3.7 Acknowledgments

This work was supported by the USA National Science Foundation (CBET-1134545), the Spanish National Organization of the Blind, and the Spanish Ministry of Economy and Competitiveness. We would also like to acknowledge Meredith Gibbons for her assistance with the perfusions and Rebecca Pfeiffer for her assistance with some of the histology.

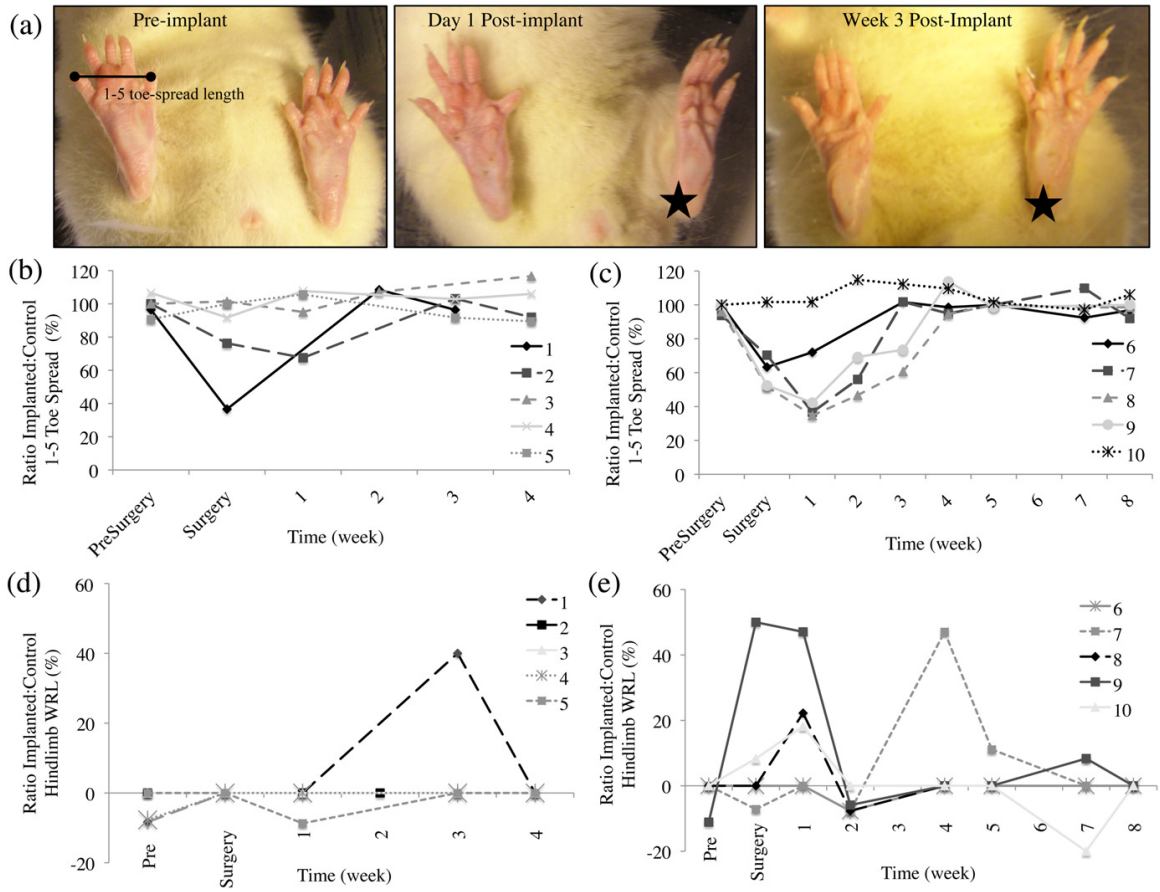

Figure 3.1. Functional assessment of sensorimotor pathways in rats with HD-USEAs chronically implanted into their sciatic nerves. (a) Footprint analysis of a rat (#7, eight-week cohort) before and after HD-USEA implantation. The preimplant photograph shows an example of the 1-5 toe-spread length measurement taken from a standing rat. The left sciatic nerve was implanted with an HD-USEA (indicated by a star in postimplant photographs). In this rat, the 1-5 toe-spread length decreased in the implanted leg for two weeks, then returned to control lengths. (b-c) The 1-5 toe-spread lengths are plotted for rats implanted for four (b) and eight weeks (c). Six rats had decreased 1-5 toe-spread lengths that returned to normal lengths within 2-4 weeks. (d-e) The sensorimotor reflexes were assessed in rats implanted with HD-USEAs for (d) four and (e) eight weeks by measuring the paw withdrawal reflex latency (WRL) times. Five rats had transient increases in WRL times in their implanted hindlimb, which recovered within three weeks (mean = 1.5 weeks). Across all rats, there was no correlation between decreased toe-spread lengths and increased WRL times.

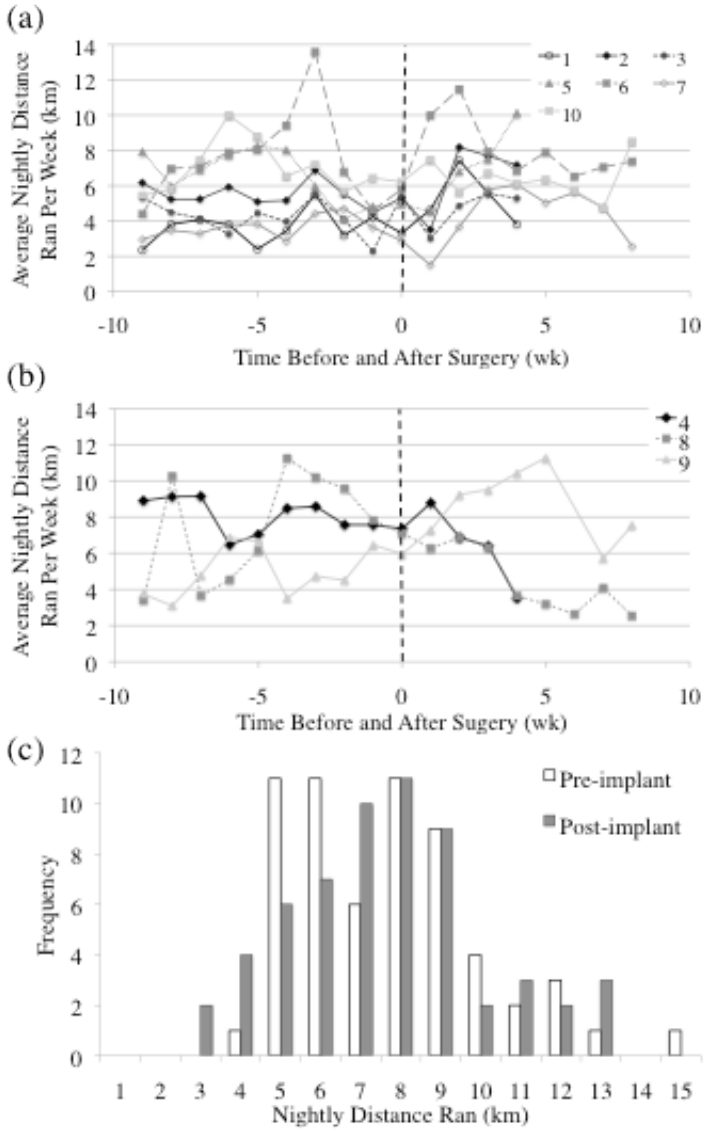

Figure 3.2. Voluntary running in rats implanted with HD-USEAs. Average nightly distance ran per week for (a) rats that had no significant changes ($p > 0.05$) and (b) rats with significant changes ($p < 0.05$) in the distances ran after implantation of HD-USEAs. Rat identifications are shown in the legends. Note for the rats in the four-week cohort, the last data points are four-weeks post surgery. (c) No significant differences ($p = 0.70$; two-tailed t-test) were seen in the distribution of nightly distances ran by all the rats (both time period groups combined) for four weeks before (preimplant; white bars; mean ± std = 6.24 ± 2.3 km/night) and four weeks after (postimplant; grey bars; 6.07 ± 2.45 km/night) HD-USEA implantation. Note that both groups are included in this distribution data, but only the first four weeks of the eight-week group are included in the data set for statistical comparison.

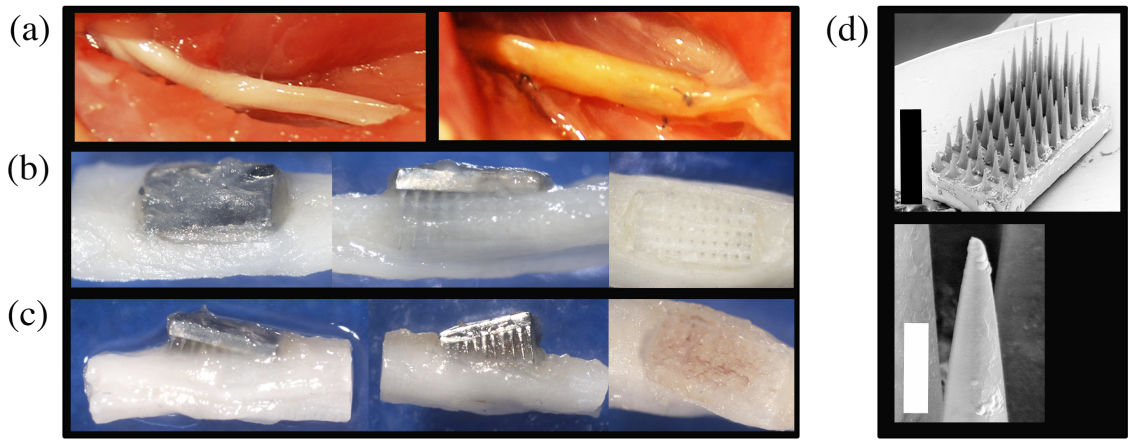

Figure 3.3. Macroscopic assessment of chronic HD-USEA implantations. (a) After 4-8 weeks of implantation in actively behaving animals, HD-USEAs all remained within the confines of the organic nerve wrap containment system (left image = control nerve; right image = implanted nerve). Black suture can be seen in the image, which was used to close the wrap around the implant site and to tack the wrap to the epineurium. The distal ends of the nerves are on the right sides of the images. (b-c) Dissection of each implant site allowed for a qualitative characterization of implants as either: complete; partial; or explanted. Nerve wraps were completely dissected away from the nerve for the examples shown. (b) Example of an HD-USEA that remained completed implanted into the nerve (rat 2; four-week implant). The last image shows the waffle-like pattern seen after array explantation. Nine rats had implants characterized as complete at the end of the study period. (c) One rat had a partially implanted HD-USEA at the end of the study period and the waffle pattern after array explantation on these devices showed marked increases in fibrosis (rat 4; four-week cohort). (d) Scanning electron microscopy (SEM) image for an HD-USEA device that was implanted for eight weeks (top image). The image on the bottom shows a close up of one of the electrode tips with sparse organic material adhering to the surface of the device. None of the electrodes were broken across all 10 devices implanted. Scale bars = 1mm top image; 50 μm bottom image

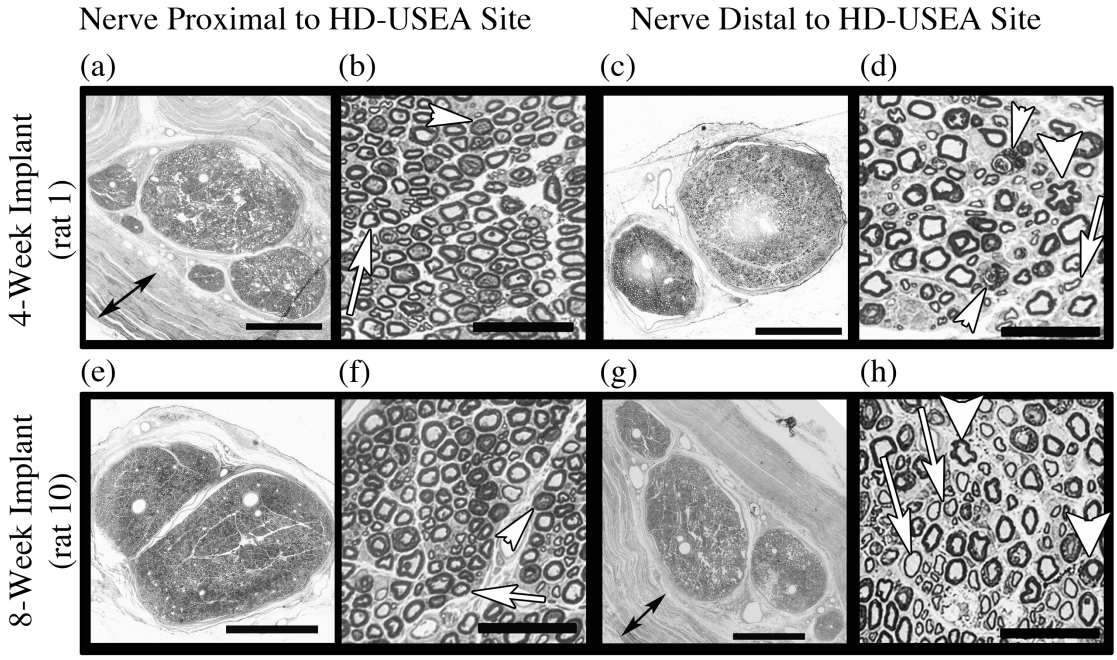

Figure 3.4. Nerve morphology of the tissue proximal and distal to the HD-USEA implant site. Assessment of the whole-nerve shows intact epineurium and perineurium adjacent to (< 5mm) the site of device implantation (4-week implant a & c; 8-week implant e & g). These rats were chosen as representative samples that included some deficits in their sensorimotor testing. The organic nerve wrap used to contain the HD-USEAs can be seen as multiple layers surrounding the nerve (a & g; double-headed arrows). Magnification of the neuronal fibers (proximal- b & f; distal- d & h) within the largest fascicle showed an overall decrease in fiber packing in the distal section (rat 1_{distal}= 723 & rat 10_{distal}= 951 fibers/mm^2) compared to the proximal sections (rat $1_{proximal}$= 1357 & rat $10_{proximal}$= 1146 fibers/mm^2). (b & f) The proximal nerve had normal myelinated fibers (arrows) and presumptive regenerating/degenerating fibers indicated by dilation of the Schmidt-Lanterman incisures and/or myelin collapse (arrowheads). (d & h) The distal nerve showed normal myelinated axons, presumptive regenerating axons (thinly myelinated; arrows), degenerating axons (myelin collapse; thick arrowheads) and phagocytic macrophages (thin arrowheads in d). scale bars a, c, e, g = 500 μm; b, d, f, h = 50μm

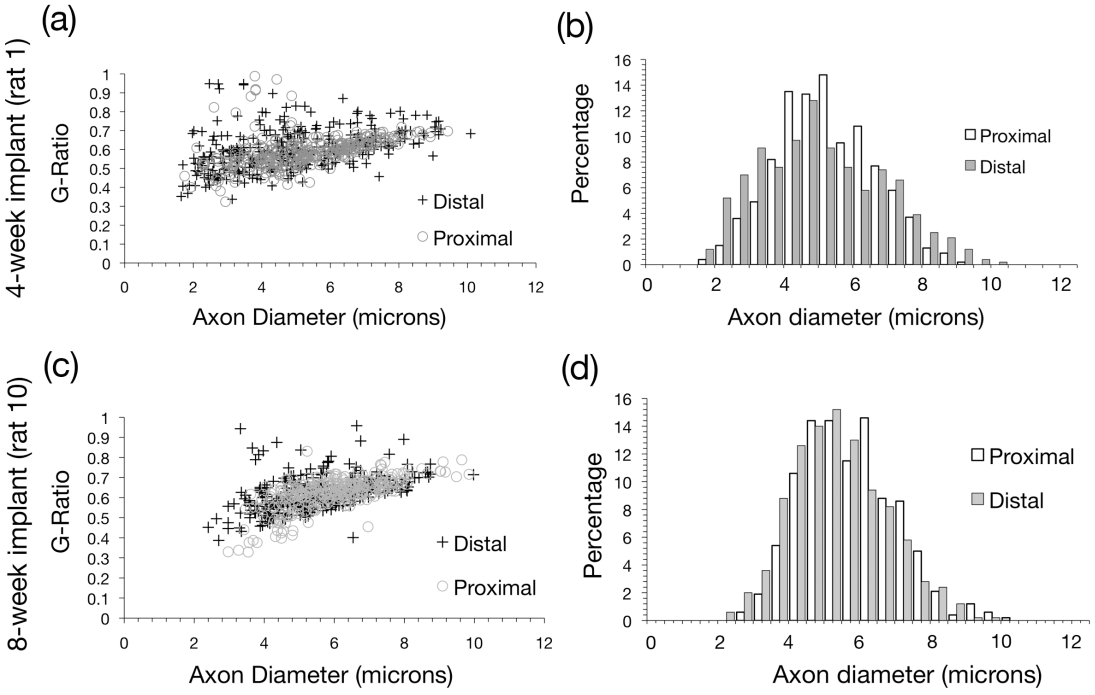

Figure 3.5. Quantification of the nerve morphology of the tissue proximal and distal to the HD-USEA implant site. The top two graphs represent data from a 4-week implant (rat 1; a-b) and the bottom graphs represent data from an 8-week implant (rat 10; c-d). (a, c) The g-ratios (back-calculated from area, assuming circular geometry) are plotted against the axon diameters measured in nerve sections proximal and distal to the implants. No significant difference in the g-ratio was measured ($p > 0.2$ both rats; rat $1_{proximal} = 0.59 \pm 0.08$; $rat1_{distal} = 0.59 \pm 0.1$; rat $10_{proximal} = 0.61 \pm 0.07$; $rat10_{distal} = 0.62 \pm 0.08$; mean ± std). There was a significant difference ($p = 0.02$) in the g-ratios for rat 10 when they were calculated from mean major and minor axes. (b) There was no significant difference in the proximal and distal axon diameters ($p = 0.18$; proximal = 5.25 ± 1.39; distal = 5.11 ± 1.86) in rat 1, although there was a significant difference in axon diameters for rat 10 ($p < 0.005$; proximal =5.73 ± 1.31; distal = 5.38 ± 1.33). The smaller diameter axons seen in rat 10 may reflect more regenerating axons in an 8-week nerve. Note these are the same rats shown in Figure 3.4

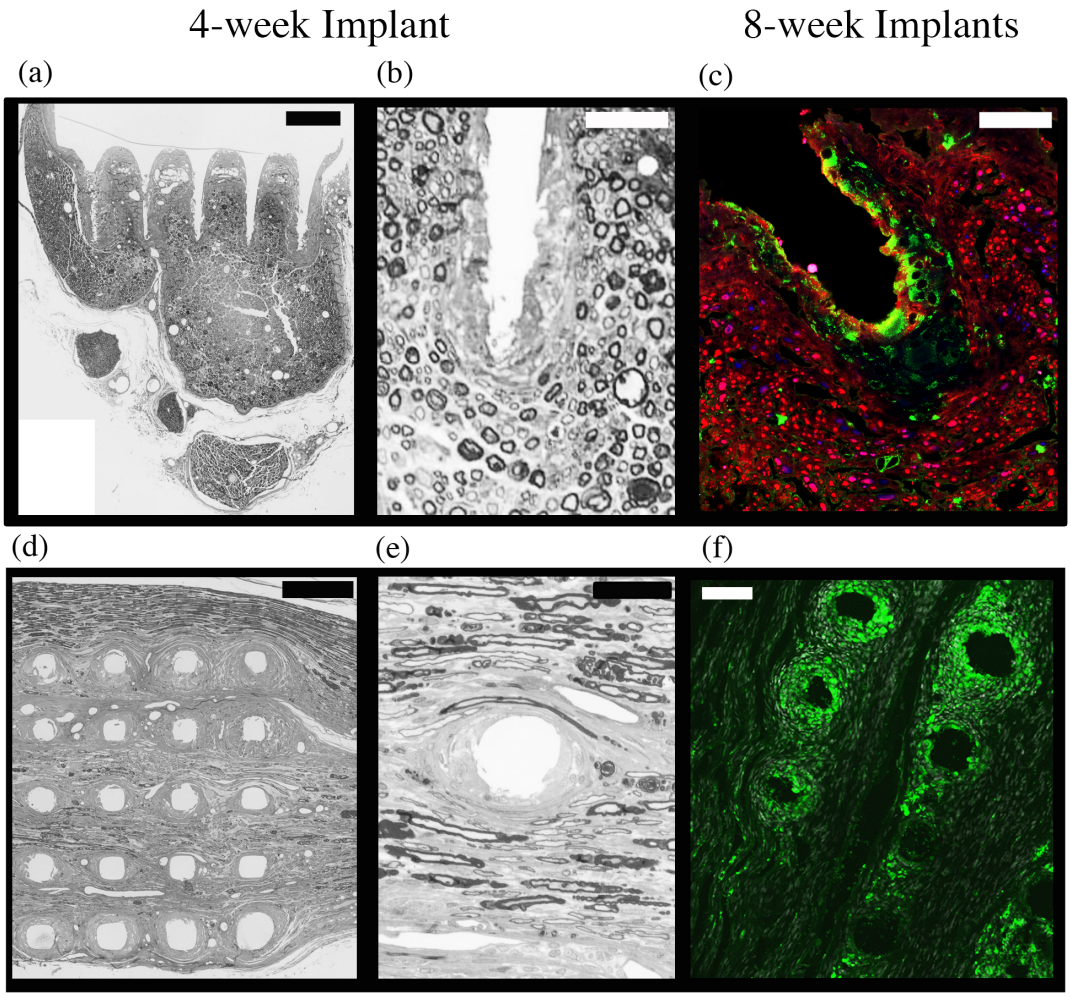

Figure 3.6. Morphometric and immunological assessment of the tissue adjacent to the electrode tracks. Transverse (a-b) and longitudinal sections (d-e) of the implant sites were stained for myelin and show axons within 25 µm of the electrode tracks (rat #1; 4-week cohort). (c) An electrode track from a rat implanted for eight weeks (rat #8) was stained for macrophages (ED1 = green) and neurons (NF200 = red). The macrophages lined some of the electrode tracks (as shown in this example); however, despite the presence of these immune cells, axons were still found within 50 µm of the electrode tip, with some axons as close as 25 µm. (f) A representative longitudinal section was stained for macrophages (ED1 = green) of a rat sciatic nerve that was implanted for eight weeks (rat #7). The distribution of macrophages around the HD-USEA microelectrodes varied across the electrode tracks, and in this image two rows of electrodes are shown that each have varying degrees of macrophage infiltration. Note that electrode diameters differ along the length of an electrode, such that near the tip the diameter is smaller (smaller holes in the tissue) while closer to the substrate the diameters are larger. Scale bars are as follows: a & d = 200µm; b-c & e = 50 µm; f = 100 µm.

Table 3.1: Overall assessment of rats chronically implanted with electrode arrays

Animal #	Sensorimotor	Running	Implant	Axons	Overall
4-week cohort:					
1	++	-	-	-	2
2	+	-	-	-	1
3	-	-	-	-	0
4	-	+	+	N/A	2
5	+	-	-	-	1
					Mean = 1.2
8-week cohort:					
6	+	-	-	-	1
7	++	-	-	-	2
8	++	+	-	N/A	3
9	++	*	-	-	2
10	+	-	-	-	1
					Mean = 1.8

Sensorimotor Grade:
- No damage
+ Transient deficit on one test
++ Transient deficit on both tests
+++ Permanent deficit on ≥ one test

Sensorimotor tests = WRL & Toe-spread length

Running Behavior Grade:
- No change in running
* Increased running
+ Decreased running

Array Implant Grade:
- Array base adjacent to the nerve
+ Array base partially explanted
++ Array completely explanted

Axon Grade:
- Axons ≤ 100μm of electrode tips
+ Axons > 100μm of electrode tips

Overall Grade:
One point was given for each '+'
0 = no consequences overall
7 = major behavioral & neuronal consequences

Abbreviations:
N/A = data not available

3.8 References

[1] Navarro X, Krueger T B, Lago N, Micera S, Stieglitz T and Dario P 2005 A critical review of interfaces with the peripheral nervous system for the control of neuroprostheses and hybrid bionic systems *Journal of the Peripheral Nervous System* **10** 229–58

[2] Wark H A C, Sharma R, Mathews K S, Fernandez E, Yoo J, Christensen B, Tresco P, Rieth L, Solzbacher F, Normann R A and Tathireddy P 2013 A new high-density (25 electrodes/mm^2) penetrating microelectrode array for recording and stimulating submillimeter neuroanatomical structures *Journal of Neural Engineering* **10** 5003

[3] Rossini P M, Micera S, Benvenuto A, Carpaneto J, Cavallo G, Citi L, Cipriani C, Denaro L, Denaro V, Di Pino G, Ferreri F, Guglielmelli E, Hoffmann K-P, Raspopovic S, Rigosa J, Rossini L, Tombini M and Dario P 2010 Double nerve intraneural interface implant on a human amputee for robotic hand control *Clinical Neurophysiology* **121** 777–83

[4] Branner A, Stein R B and Normann R A 2001 Selective stimulation of cat sciatic nerve using an array of varying-length microelectrodes. *Journal of Neurophysiology* **85** 1585–94

[5] Stieglitz T, Ruf H H, Gross M, Schuettler M and Meyer J-U 2002 A biohybrid system to interface peripheral nerves after traumatic lesions: design of a high channel sieve electrode *Biosensoors and Bioelectronics* **17** 685–96

[6] Lago N, Udina E, Ramachandran A and Navarro X 2007 Neurobiological assessment of regenerative electrodes for bidirectional interfacing injured peripheral nerves *IEEE Transactions on Biomedical Engineering* **54** 1129–37

[7] Badia J, Boretius T, Udina E, Stieglitz T and Navarro X 2011 Biocompatability of chronically implanted transverse intrafascicular multichannel electrode (TIME) in the rat sciatic nerve *IEEE Transactions on Biomedical Engineering* **58** 2324–32

[8] Lago N, Yoshida K, Koch K P and Navarro X 2007 Assessment of biocompatibility of chronically implanted polyimide and platinum intrafascicular electrodes *IEEE Transactions on Biomedical Engineering* **54** 281–90

[9] Mathews K S, Wark H A C and Normann R A 2014 Assessment of rat sciatic nerve function following acute implantation of High Density Utah Slanted Electrode Array (25 electrodes/mm^ 2) based on neural recordings and evoked muscle activity *Muscle Nerve* **in press**

[10] Luís A L, Amado S, Geuna S, Rodrigues J M, Simões M J, Santos J D, Fregnan F, Raimondo S, Veloso A P, Ferreira A J A, Armada-da-Silva P A S, Varejão A S P and Maurício A C 2007 Long-term functional and morphological assessment

of a standardized rat sciatic nerve crush injury with a non-serrated clamp *Journal Neuroscience Methods* **163** 92–104

[11] Rodríguez F J, Valero-Cabré A and Navarro X 2004 Regeneration and functional recovery following peripheral nerve injury *Drug Discovery Today: Disease Models* **1** 177–85

[12] Moore A M, Borschel G H, Santosa K A, Flagg E R, Tong A Y, Kasukurthi R, Newton P, Yan Y, Hunter D A, Johnson P J and Mackinnon S E 2012 A transgenic rat expressing green fluorescent protein (GFP) in peripheral nerves provides a new hindlimb model for the study of nerve injury and regeneration *Journal Neuroscience Methods* **204** 19–27

[13] Hunter D A, Moradzadeh A, Whitlock E L, Brenner M J, Myckatyn T M, Wei C H, Tung T H H and Mackinnon S E 2007 Binary imaging analysis for comprehensive quantitative histomorphometry of peripheral nerve *Journal Neuroscience Methods* **166** 116–24

[14] Mackinnon S E, O'Brien J P, Dellon A L, McLean A R, Hudson A R and Hunter D A 1988 An assessment of the effects of internal neurolysis on a chronically compressed rat sciatic nerve *Plastic and Reconstructive Surgery* **81** 251–6

[15] Varejão A S P, Cabrita A M, Meek M F, Bulas-Cruz J, Melo-Pinto P, Raimondo S, Geuna S and Giacobini-Robecchi M G 2004 Functional and morphological assessment of a standardized rat sciatic nerve crush injury with a non-serrated clamp *Journal of Neurotrauma* **21** 1652–70

[16] Mackinnon S E, Hudson A R and Hunter D A 1985 Histologic assessment of nerve regeneration in the rat *Plastic and Reconstructive Surgery* **75** 384–8

[17] Koka R and Hadlock T A 2001 Quantification of functional recovery following rat sciatic nerve transection *Experimental Neurology* **168** 192–5

[18] Bervar M 2000 Video analysis of standing--an alternative footprint analysis to assess functional loss following injury to the rat sciatic nerve *Journal Neuroscience Methods* **102** 109–16

[19] Hu D, Hu R and Berde C B 1997 Neurologic evaluation of infant and adult rats before and after sciatic nerve blockade *Anesthesiology* **86** 957–65

[20] de Medinaceli L, Freed W J and Wyatt R J 1982 An index of the functional condition of rat sciatic nerve based on measurements made from walking tracks *Experimental Neurology* **77** 634–43

[21] Ferguson S A and Cada A M 2003 A longitudinal study of short- and long-term activity levels in male and female spontaneously hypertensive, Wistar-Kyoto, and Sprague-Dawley rats *Behavioral Neuroscience* **117** 271–82

[22] Rodnick K J, Reaven G M, Haskell W L, Sims C R and Mondon C E 1989 Variations in running activity and enzymatic adaptations in voluntary running rats *Journal Applied Physiology* **66** 1250–7

[23] Rousche P J and Normann R A 1992 A method for pneumatically inserting an array of penetrating electrodes into cortical tissue. *Annals of Biomedical Engineering* **20** 413–22

[24] Rennaker R L, Miller J, Tang H and Wilson D A 2007 Minocycline increases quality and longevity of chronic neural recordings *Journal of Neural Engineering* **4** L1–5

[25] Spataro L, Dilgen J, Retterer S, Spence A J, Isaacson M, Turner J N and Shain W 2005 Dexamethasone treatment reduces astroglia responses to inserted neuroprosthetic devices in rat neocortex *Experimental Neurology* **194** 289–300

[26] Cobianchi S, Casals-Diaz L, Jaramillo J and Navarro X 2013 Differential effects of activity dependent treatments on axonal regeneration and neuropathic pain after peripheral nerve injury *Experimental Neurology* **240** 157–67

[27] Normann R A, Dowden B R, Frankel M A, Wilder A M, Hiatt S D, Ledbetter N M, Warren D A and Clark G A 2012 Coordinated, multijoint, fatigue-resistant feline stance produced with intrafascicular hind limb nerve stimulation *Journal of Neural Engineering* **9** 6019

[28] Christensen M B 2011 *Doctoral Thesis: Evaluation of inflammation and morphometric parameters associated with neural device implantation in the sciatic nerve* (Salt Lake City: University of Utah)

[29] Kokkalis Z T, Pu C, Small G A, Weiser R W, Venouziou A I and Sotereanos D G 2011 Assessment of processed porcine extracellular matrix as a protective barrier in a rabbit nerve wrap model *Journal of Reconstructive Microsurgery* **27** 19–28

[30] McConnell G C, Rees H D, Levey A I, Gutekunst C-A, Gross R E and Bellamkonda R V 2009 Implanted neural electrodes cause chronic, local inflammation that is correlated with local neurodegeneration *Journal of Neural Engineering* **6** 056003

[31] Biran R, Martin D C and Tresco P A 2005 Neuronal cell loss accompanies the brain tissue response to chronically implanted silicon microelectrode arrays *Experimental Neurology* **195** 115–26

[32] Biran R, Martin D C and Tresco P A 2007 The brain tissue response to implanted silicon microelectrode arrays is increased when the device is tethered to the skull *Journal of Biomedical Materials Research Part A* **82** 169–78

[33] Polikov V S, Tresco P A and Reichert W M 2005 Response of brain tissue to

chronically implanted neural electrodes *Journal Neuroscience Methods* **148** 1–18

[34] Cogan S F 2008 Neural Stimulation and Recording Electrodes *Annual Review of Biomedical Engineering* **10** 275–309

[35] McCreery D B, Agnew W F, Yuen T G and Bullara L 1990 Charge density and charge per phase as cofactors in neural injury induced by electrical stimulation *IEEE Transactions on Bio-medical Engineering* **37** 996–1001

[36] Rushton W 1951 A theory of the effects of fibre size in medullated nerve *The Journal of Physiology* **115** 101–22

[37] Skousen J L, Merriam S M E, Srivannavit O, Perlin G, Wise K D and Tresco P A 2011 Reducing surface area while maintaining implant penetrating profile lowers the brain foreign body response to chronically implanted planar silicon microelectrode arrays *Progress in Brain Research* **194** 167–80

[38] Winslow B D, Christensen M B, Yang W-K, Solzbacher F and Tresco P A 2010 A comparison of the tissue response to chronically implanted Parylene-C-coated and uncoated planar silicon microelectrode arrays in rat cortex *Biomaterials* **31** 9163–72

[39] Donaldson H H and Hoke G W 1905 On the areas of the axis cylinder and medullary sheath as seen in cross sections of the spinal nerves of vertebrates *Journal Comparative Neurology Psychology* **15** 1–16

[40] Winslow B D and Tresco P A 2010 Quantitative analysis of the tissue response to chronically implanted microwire electrodes in rat cortex *Biomaterials* **31** 1558–67

[41] Tresco P A and Winslow B D 2011 The challenge of integrating devices into the central nervous system *Critical Reviews in Biomedical Engineering* **39** 29–44

[42] Brown B N, Ratner B D, Goodman S B, Amar S and Badylak S F 2012 Macrophage polarization: an opportunity for improved outcomes in biomaterials and regenerative medicine *Biomaterials* **33** 3792–802

[43] Shain W, Spataro L, Dilgen J, Haverstick K, Retterer S, Isaacson M, Saltzman M and Turner J N 2003 Controlling cellular reactive responses around neural prosthetic devices using peripheral and local intervention strategies *IEEE Transactions on Neural Systems and Rehabilitation Engineering* **11** 186–8

[44] Zhong Y and Bellamkonda R V 2007 Dexamethasone-coated neural probes elicit attenuated inflammatory response and neuronal loss compared to uncoated neural probes *Brain Research* **1148** 15–27

[45] Azemi E, Lagenaur C F and Cui X T 2011 The surface immobilization of the neural adhesion molecule L1 on neural probes and its effect on neuronal density and gliosis at the probe/tissue interface *Biomaterials* **32** 681–92

CHAPTER 4

SELECTIVE ACTIVATION OF THE MUSCLES OF MICTURITION USING INTRAFASCICULAR MICROELECTRODE STIMULATION OF THE PUDENDAL NERVE

Publication Reference:

Wark HAC, Dowden BR, Cartwright PC, Normann RA. IEEE Journal on Emerging and Selected Topics in Circuits and Systems. 2011. 1(4):631-636

Author contributions: design of and carrying out the experiments by HACW, BD, PC, RAN; data analysis by HACW; writing of the manuscript by HACW; editing of the manuscript by all authors.

4.1 Abstract

To investigate the hypothesis that intrafascicular stimulation of the Pudendal Nerve (PN) can be used to selectively activate the detrusor bladder muscle and the External Urethral Sphincter (EUS). Nine anesthetized male canines were used in this study. Muscle activations were measured via bladder catheter pressure transducers and EUS Electromyography (EMG) wires. The PNs were exposed via dissection of the ischioanal fossa and implanted with Utah Slanted Electrode Arrays (USEAs). USEAs consist of 100, 0.5-1.5 mm long microelectrodes that project out from a 4x4 mm substrate. Intrafascicular stimulation was delivered via individual USEA microelectrodes in order to map the ability of each electrode to selectively or nonselectively evoke detrusor and/or EUS contractions. We were able to selectively activate the detrusor using 33 Hz stimulation of PN axons with an average of 4.57 ± 3.82 (mean ± sd) USEA electrodes per animal tested. Electrically-evoked and distention-evoked bladder contractions had similar kinetics. Sustained bladder contractions were evoked via 60 s of intrafascicular stimulation. The EUS was activated using 33 Hz stimulation via an average of 26.14 ± 19.45 electrodes per animal tested. High frequency (>2 kHz) stimulation delivered via EUS selective electrodes produced nonselective block of PN axons. Examples of how this selective axonal access could be used to restore continence and activate micturition were demonstrated in two animals. We report herein the first study demonstrating selective detrusor and EUS activation via microelectrodes implanted intrafascicularly in the PN. Such selective activation enables new therapeutic possibilities for controlling the muscles of micturition.

4.2 Introduction

Bladder dysfunction—or neurogenic bladder—may include hesitancy, incontinence or urinary retention and can arise from neurological injuries, diseases, or disorders [1,2]. Current treatments for neurogenic bladder include catheterization, pharmaceuticals, urinary tract reconstruction, or electrical stimulation of sacral nerves [3,4]. Due to limitations and complications related to these therapies, new treatments for neurogenic bladder are warranted for refractory patients.

Functional electrical stimulation of various parts of the urogenital system is one approach that has been successful [3,5]. Recently, the pudendal nerve (PN) has been targeted for electrical stimulation therapy to restore urinary function [6-11] and fecal continence [12]. Electrical stimulation of the PN can either relax the detrusor to promote continence or excite the detrusor to promote micturition, depending on the frequency of stimulation [13]. Stimulation of PN afferent axons excites the pudendal-to-bladder reflexive micturition pathway [14]. Previous studies have evoked detrusor muscle contractions via low frequency PN stimulation (33 Hz) delivered using whole-nerve cuff electrodes [7,8]. In addition, High Frequency Alternating Current (HFAC) (>1 kHz) delivered to the PN using cuff electrodes has been shown to produce conduction block of orthodromic action potentials, resulting in relaxation of the external urethral sphincter (EUS) [15].

Intrafascicular stimulation can provide highly selective activation of axons in peripheral nerves. Utah Slanted Electrode Arrays (USEAs) implanted in feline sciatic nerves have been shown to selectively activate hind-limb muscles in acute [16,17] and chronic preparations [18]. Additionally, HFAC stimulation delivered intrafascicularly via

USEAs can selectively block activation of targeted hind-limb muscles [19]. To date, no study has investigated whether intrafascicular stimulation of the PN can selectively activate the efferent and afferent pathways involved in micturition. We report herein the first results of intrafascicular stimulation of the PN in nine anesthetized canines. This study demonstrates the capacity of USEAs to selectively evoke contractions of either the EUS or the detrusor. Additionally, we describe preliminary results of two applications of intrafascicular stimulation of the PN: restoration of continence in one animal and limited activation of micturition in another. These results show that the selectivity provided by intrafascicular microelectrodes may allow for more flexible control of targeted muscles involved in micturition.

4.3 Materials and methods

Nine adult male mongrel dogs (ranging from 17-31 kg) were used in these acute studies. All animal procedures were approved by the University of Utah Institutional Animal Care and Use Committee. Anesthesia was initiated with Telazol (9-12 mg/kg IM; Animal Health, Fort Dodge, Iowa) and general anesthesia was maintained by Isoflurane (1.0-2.5%) for surgical procedures. α-Chloralose (5-65 mg/kg IV; Sigma-Aldrich and Alpha-Aesar) was used during electrophysiological mapping and data collection as this anesthetic has been shown to maintain the spinal reflexes necessary to activate the pudendal-to-bladder reflex [7,8]. α-Chloralose solutions (1%) were prepared within 24 hrs of use by dissolving α-chloralose in sterile 0.9% w/v NaCl at 50-60 ºC and storing at 40 ºC [20]. Artificial respiration (10-15 breaths/min) and body temperature (39 ºC) were maintained while heart rate and end-tidal CO_2 were continuously monitored. Lactated

Ringer's solution was administered intravenously at 10 mL/kg/hr during surgical procedures, then at 2mL/kg/hr during experimental procedures to limit urine production. A warm water blanket maintained normal body temperature.

A ventral midline incision was made to expose the bladder and EUS. Catheters (7 Fr) were inserted directly into the bladder and secured with purse-string sutures. One catheter was used to fill the bladder with 0.9% w/v NaCl using a syringe pump (New Era Pump Systems, Inc., Model NE-1000). The other suprapubic catheter was filled with 0.9% w/v NaCl and connected to a pressure transducer (Deltran DPT-100, Utah Medical Products, Salt Lake City, UT) to record bladder pressure increases due to detrusor contractions. Bladders were filled at 2-15 mL/min. Electrical stimulation trials were carried out when the bladder volume was approximately 78% of the bladder capacity. The EUS was instrumented with 1-2 pairs of 0.051 cm bifilar electromyography (EMG) wires (California Fine Wire Co., Model #: M146240) in seven animals. Approximately 2 mm of insulation was removed from the end of each EMG wire and the tips of the wires were bent at a 45º angle for insertion into the muscle. The ventral midline preparation was sutured in layers.

The PN was exposed by dissection of the ischioanal fossa and a USEA was implanted proximal to any branching points using high-speed pneumatic insertion [21]. In some animals, bilateral PNs were exposed in order to assure the larger PN (if applicable) was chosen for USEA implantation.

The USEA is a 10x10 array of silicon microelectrodes that vary in length from 0.5 mm to 1.5 mm [22]. The median tip impedances for the four USEAs used in these studies were 13.5, 11.0, 23.8, and 100.0 kOhms. After implantation, each USEA microelectrode

was mapped to an evoked response—detrusor and/or EUS contractions. Electrodes were stimulated with cathodic monophasic stimulation at amplitudes of 0.8-9.0 V with 100-300 μs pulse-widths at 30-33 Hz for 5-10 s duration. After experiments were terminated, USEAs were cleaned in a stirring solution of ~1% Enzol Enzematic Detergent (Advanced Sterilization Products, division of Ethicon, Inc., USA), washed with distilled water, and electrodes were inspected for damage under a microscope. USEA impedances were verified between experiments using a custom-built impedance testing system [23]. Stimuli were delivered via voltage-controlled stimulators (Grass Technologies, SD9; West Warwick, Rhode Island, USA). HFAC waveforms were generated with a PC running a custom MATLAB (The MathWorks, Inc., Natick, MA) program and delivered to USEA microelectrodes by a National Instruments DAC card (NI6711) [19]. Animals were grounded using a 22-guage needle placed under the skin. Reflexive detrusor bladder muscle contractions were evoked by filling the bladder with saline [24], and here we refer to these contractions as 'distension evoked contractions.' Analog data from our stimulator, pressure transducers, and EMG wires were sampled at 10 kSamples/s and stored on a hard disk using a Cerebus data acquisition system (Blackrock Microsystems, Inc., Salt Lake City, UT). Voided urine weight was collected through urethral catheters and continuously monitored with a force transducer.

Data analysis was carried out using MATLAB. USEA electrodes that, upon stimulation, evoked only EUS or detrusor contractions were classified as 'selective.' Electrodes that evoked contractions in both muscles were classified as 'nonselective.' We interpreted any bladder pressure increases above baseline—excluding increases seen as a result of ventilation artifact—as evoked muscle activity (usually increases > 5-10 cm

H_2O). For EUS EMG activity, we also interpreted any increases above the normally recorded sphincter tone as electrical activation of efferent EUS fibers from USEA stimulation. In two animals, EMG of the EUS was not recorded, and therefore, these trials were classified as nonselective (Table 4.1; animals 1 and 2). The electrode counts from these animals were labeled as 'not applicable' (n/a) and were excluded from the statistical analysis. We determined the threshold voltages needed to evoke detrusor or EUS contractions in five animals by stimulating via individual electrodes with 33 Hz starting at 0 V and increasing in steps of 0.1 -0.5 V.

4.4 Results

Distention of the bladder from passive filling evoked reflexive detrusor contractions in all animals tested. During distention evoked detrusor contractions, voids ranged from 8-120 mL, bladder pressure increases ranged from 15-100 cm H_2O, and the mean bladder capacity was 125.17 ± 43.91 mL (range of 80-225 mL) for all nine animals. Distention evoked contractions were followed by a reflexive reconstriction of the urethral sphincter (measured by EMG).

In all nine animals, we were able to selectively and nonselectively activate the detrusor bladder muscle via brief (3-5 s) low frequency (33 Hz) stimulation of afferent PN axons with 4.57 ± 3.82 and 5.56 ± 8.00 (mean ± sd) electrodes per animal, respectively (Table 4.1). In three animals we measured threshold voltages of 4.10 ± 1.54 V (n = 15 electrodes) for selectively activating the detrusor using intrafascicular stimulation. Figure 4.1A shows five consecutive detrusor contractions evoked by intrafascicular stimulation delivered via electrode 92 using 5-8 V (bottom bars; $2V_{threshold}$,

100 μs pulse-width at 33 Hz). The kinetics and amplitudes of these increases in bladder pressure, evoked by selective stimulation of the PN, were similar to the kinetics and amplitude of distention evoked contractions. As with distention evoked contractions, intrafascicularly evoked contractions resulted in reconstriction of the urethral sphincter (Fig. 4.1A; top trace). We also observed that 1 min of 33 Hz stimulation produced a prolonged detrusor contraction that persisted as long as stimulation was delivered (Fig. 4.1B).

In the seven animals in which EUS EMG was measured, an average of 26.14 ± 19.45 and 2.43 ± 1.99 (mean ± sd) USEA microelectrodes evoked selective and nonselective contractions of the EUS, respectively (Table 4.1). In five animals the threshold voltage for selectively activating the EUS using USEAs was 3.61 ± 2.01 V (n = 40 electrodes). Nonselective electrodes (n =7) were found to have threshold activations of 5.00 ± 1.31 V for the detrusor and 6.85 ± 2.10 V for the EUS. For the arrays where threshold voltages were recorded, there was no apparent trend between threshold voltage and array impedance [Array 1, median tip = 100.00 kOhm, mean $V_{threshold}$ = 3.09; Array 2, median tip = 23.80 kOhm, mean $V_{threshold}$ = 5.06; Array 4, median tip = 23.00 kOhm, $V_{threshold}$ = 0.50]. Selective activation of the EUS by intrafascicular stimulation is shown in Figure 4.2, where stimulation delivered via two USEA electrodes evoked EUS contractions only. Figure 4.2 also shows a neighboring electrode that did not evoke a response in the EUS or detrusor.

The distributions of USEA electrodes that activated either the detrusor and/or the EUS suggested a functional organization of the PN. Electrodes that excited the EUS appeared to be spatially separated from those that excited the detrusor reflexive pathway.

The geometric centers of the electrodes that excited the detrusor and those that excited the EUS were determined for each animal. In the seven experiments where mapping was attempted for both detrusor and EUS, the average separation of the geometric centers was 1.11 ± 0.69 mm (mean ± sd).

We investigated the possibility of restoring continence using intrafascicular stimulation of EUS efferent axons. Stress urinary incontinence was modeled in one animal after unilateral PN crush (Fig. 4.3a). The detrusor could be filled to pressures between 20-30 cm H_2O before leaking occurred. The black bar indicates continued bladder filling, that began after the bladder was filled to just below the leak point pressure (20 cm H_2O). Episodes of urine leakage were free of detrusor contractions. Two periods of 35-40 s duration, 33 Hz stimuli were delivered via a USEA electrode that selectively activated the EUS. Urine leakage completely stopped during stimulation. During such stimulation periods the rate of urine flow went from 17.4 to 0 mL/min.

In a separate experiment, USEA microelectrodes that targeted the detrusor and EUS were used to deliver stimulation via two USEA electrodes simultaneously in order to activate voiding (Fig. 4.3b). Four consecutive trials were conducted in which low frequency stimulation (7 V with 200 μs pulse-width at 30 Hz) was delivered for 1 min via a detrusor selective electrode. Because the EUS was presumably constricted, this stimulus produced only a small transient flow of urine at the onset and offset of stimulation (0.2 mL/s; Fig. 4.3b). In three of the trials, we were able to transiently increase urine flow (0.7 mL/s) by also delivering an HFAC blocking stimulus (4 V peak-to-peak for 10 s duration at 1 kHz) via a EUS selective electrode (trials 1, 2 & 4; Fig. 4.3b). Trial 3 was used as a control and no HFAC stimulation was delivered during the 1

min of detrusor stimulation, and no transient increase in urine flow was observed. The HFAC stimulation appeared not only to produce a block of efferent axons, but HFAC also appeared to block afferent activity causing bladder pressure to fall to prestimulation levels (Fig. 4.3b; bottom trace). Upon cessation of HFAC, bladder pressure increased, due to the ongoing low frequency stimulation via the electrode activating the pudendal-to-detrusor reflexive pathway.

4.5 Discussion

The results described herein validate the hypothesis that microelectrode arrays, intrafascicularly implanted in the PN, can provide selective access to the afferent and efferent neural pathways involved in the control of micturition. In all nine animals, selective activation of both the detrusor and EUS was possible by stimulating via individual USEA electrodes. In all seven animals where both detrusor and EUS contractions were measured, we were able to evoke selective contractions of each muscle with different USEA electrodes. Because such selective access was achieved, we also investigated if targeted axonal stimulation could form the basis for new therapeutic approaches to problems of micturition. The two examples demonstrated in this work, restoration of continence and controlled, but limited micturition, were not intended as definitive studies, but only as indicators of research areas based upon intrafascicular stimulation that are likely to be fruitful when more focused work has been done.

Figure 4.1 and Table 4.1 illustrate that individual microelectrodes in an array of electrodes implanted intrafascicularly in the PN can be identified that selectively excite afferent axons mediating reflexive contraction of the bladder. Importantly, the kinetics

and amplitudes of the pressure waveforms evoked via these electrodes were virtually identical to the distension evoked contraction waveforms. Further, when prolonged low-frequency intrafascicular stimulation was used, bladder pressure increases persisted as long as the stimulation was delivered (Figs. 4.1b and 4.3b).

We were able to selectively evoke detrusor contractions using a small number of USEA electrodes (mean = 4.57) compared to the number of electrodes that selectively evoked EUS activity (mean = 26.14). This finding suggests that the canine PN may contain a smaller number of afferent fibers than efferent fibers. Another explanation would be potential differences in thresholds of activation between afferent and efferent fibers; however, no significant difference between threshold voltages was found for selective ($n = 55$; $p > 0.3$; two-tailed paired t-test) or nonselective ($n = 7$; $p > 0.09$; two-tailed paired t-test) electrodes. An additional explanation for this discrepancy may be due to effects of α-chloralose on the pudendal-to-bladder micturition reflex.

A similar functional PN organization was observed for the seven animals in which both detrusor and EUS contractions were monitored, suggesting that afferent and efferent axons in the PN may be localized to separate fascicles in the canine. Another possibility is that the canine PN, unlike the feline [25] or the human [26], contains one or a few larger fascicle(s). If the afferent detrusor and the efferent EUS fibers coursed through the same fascicle, the geometric centers of these subsets of electrodes would be expected to overlap. However, for the seven experiments where mapping was attempted, the geometric centers were separated by an average of 1.11 ± 0.69 mm (mean ± sd). This separation between geometric centers suggests that in the canine model the afferent fibers activating the reflexive detrusor pathway and the efferent fibers innervating the EUS may

course through separate fascicles or one large fascicle but be segregated spatially. Histological evaluation of the canine PN will help shed light on these questions.

Stimuli delivered using intrafascicularly implanted microelectrodes were able to selectively excite the EUS. This observation suggests an approach to restore continence in individuals who have lost this function due to loss of EUS tone or decreased innervation. In one animal, we were able to model stress urinary incontinence by unilateral crushing of the PN [27,28]. The crush injury was carried out on the PN contralateral to the USEA implant. Bladder pressure increases above 20-30 cm H_2O resulted in leaking. Low frequency stimulation via an electrode implanted in the PN that selectively excited the EUS was able to eliminate this leakage for the two 35-40 s periods that stimulation was delivered. Although this demonstration is encouraging, a major concern about the use of intrafascicular stimulation to restore continence is that stimulation must be provided for multiple hours, and such sustained prolonged stimulation could cause adverse effects on the tissues being stimulated or on the electrodes used for stimulation. One advantage of using multielectrode arrays to interface with the PN is that many electrodes excite axons that innervate the EUS (an average of 26.14/animal in this report). The overall stimulation amplitude delivered via each electrode may be reduced by interleaving stimulation among multiple USEA electrodes. Additionally, interleaved stimulation has been shown to result in more fatigue-resistant muscle activation [29], and such stimulation paradigms may result in fatigue-resistant contraction of the EUS for multiple hours of restored continence. Additional longitudinal studies will be required for this to be established conclusively.

In order to achieve controlled micturition, the detrusor muscle must contract while

the EUS simultaneously relaxes. Although the example of controlled voiding shown in Figure 4.3B is only from one experiment, these results have shown this hypothesis to be worth investigating in more focused studies. Future work will be aimed at optimizing stimulation parameters in order to investigate the extent to which intrafascicular stimulation of the PN using USEAs can produce controlled voiding. Additionally, HFAC stimulation delivered to an electrode that selectively activated the EUS at low frequencies of stimulation produced a nonselective block at high frequencies, which lead to relaxation of the detrusor. Such stimulation paradigms may also be used to inhibit the detrusor in patients with overactive bladder. Future work is needed to investigate to what extent HFAC stimulation can selectively block axons within a single fascicle or whether such stimulation produces only nonselective block of an entire fascicle.

We were able to elicit distention evoked detrusor contractions in all nine animals by methods previously reported for feline models [24]; however, we were unable to do so reproducibly over the course of each experiment. We hypothesize that α-chloralose may depress the pudendal-to-bladder micturition reflex in canines, as it has been shown to do in felines [7], [27]. Yoo et al. were able to demonstrate that electrical stimulation of the PN drives excitation of the pudendal-to-bladder reflex, which overcomes any inhibition caused by α-chloralose in the feline model [8]. Delivering stimulation via multiple USEA electrodes may improve selective detrusor activation electrode counts by increasing activity in the reflexive micturition pathway.

The studies reported herein were conducted in the large canine model in order to work with a PN that has a size more consistent with the human PN. However, in the canines studied, we saw varying side effects of α-chloralose including hyperthermia and

spontaneous muscle activity. There are several reports in the literature that indicate α-chloralose has: (1) dose-dependent effects on the nervous system [30], and (2) varying effects across different species [31]. The species-dependent effects of α-chloralose are still not well understood, and may account for the effects we observed during these studies. In future experiments, the USEA will be redesigned such that it will be custom-fit for the smaller size and fascicular organization [25] of the feline PN, as no side effects have been reported for felines anesthetized with α-chloralose.

4.6 Conclusion

We have demonstrated that intrafascicular stimulation of the PN can selectively activate the detrusor bladder muscle and EUS using individual microelectrodes in an implanted USEA. The two examples using selective afferent and efferent activation demonstrate that intrafascicular electrodes may allow for targeted control of the muscles mediating micturition.

4.7 Acknowledgments

This work was supported by the state of Utah USTAR Research Grant and the University of Utah MD-PhD Training Program

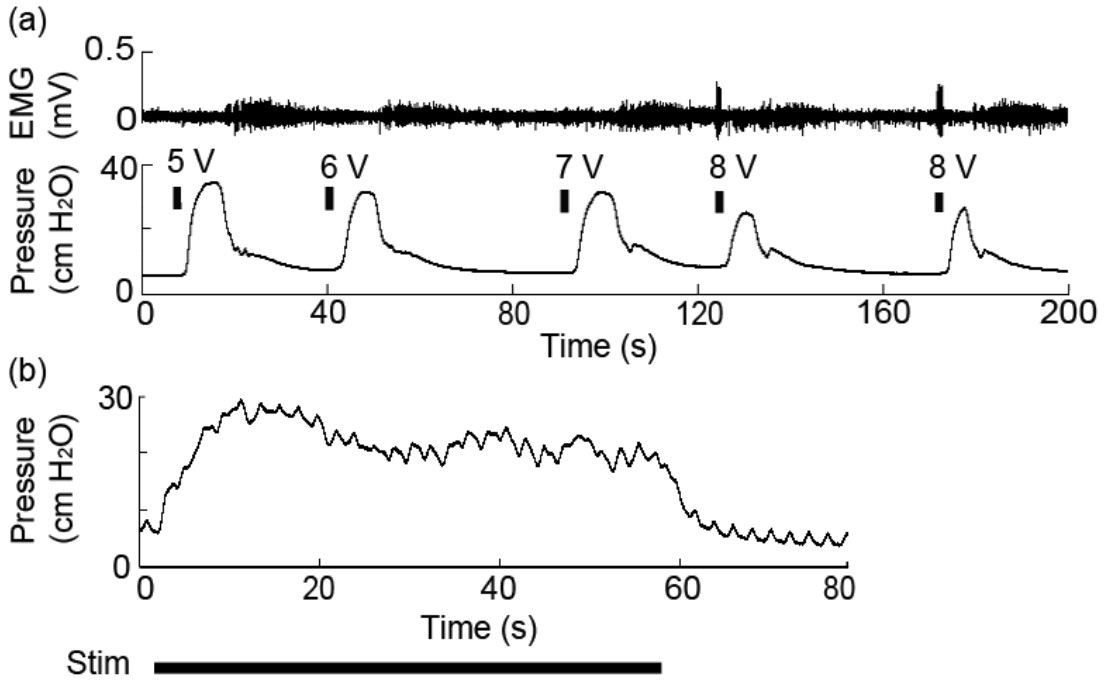

Figure 4.1: Selective activation of detrusor bladder muscle by intrafascicular stimulation. (A) Examples of 5 consecutive detrusor contractions (pressure trace) after stimulating USEA electrode 92 with 5-8 V, 100 μs pulse-width at 33 Hz (bottom bars). Each epoch is followed by sphincter reconstriction (top trace). At 8V stimulation, current began to spread to EUS efferent nerve fibers, which evoked EUS contractions. (B) Prolonged detrusor contraction was evoked by 1 min of stimulating a USEA electrode that selectively activated the detrusor with 4V, 100 μs pulse-width at 33 Hz (bottom bar). Oscillations seen in the pressure trace are due to mechanical ventilation.

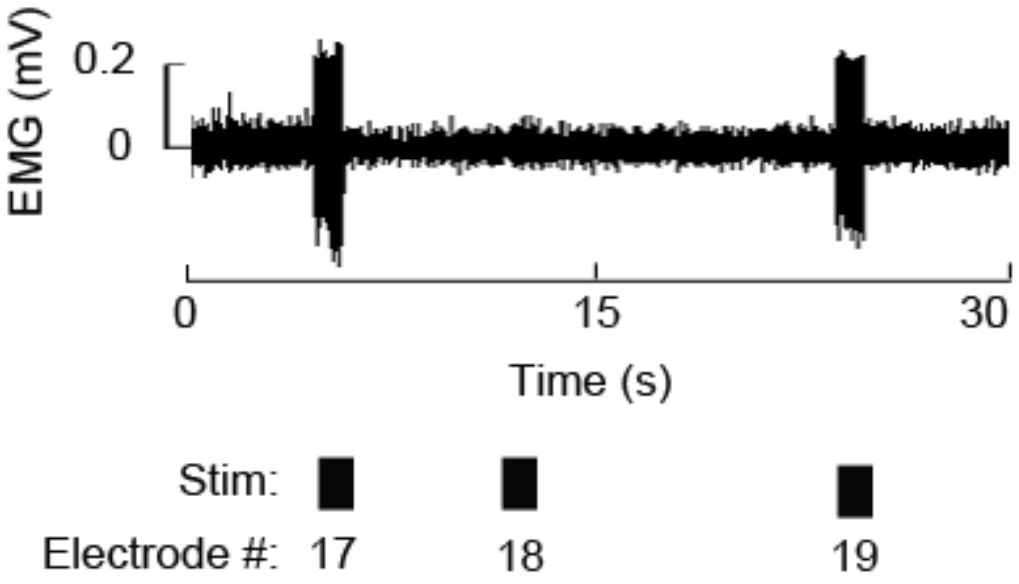

Figure 4.2. Selective activation of the EUS by intrafascicular stimulation. Suprathreshold stimulation (9V, 33 Hz; bottom bars) via three different USEA electrodes (electrode 17, 18, and then 19) in the same animal whose responses were shown in Figure 4.1A. USEA microelectrodes 17 and 19 evoked selective EUS contractions as measured by EMG, while electrode 18 did not evoke any muscle responses (bladder pressure did not increase and the trace was omitted for clarity).

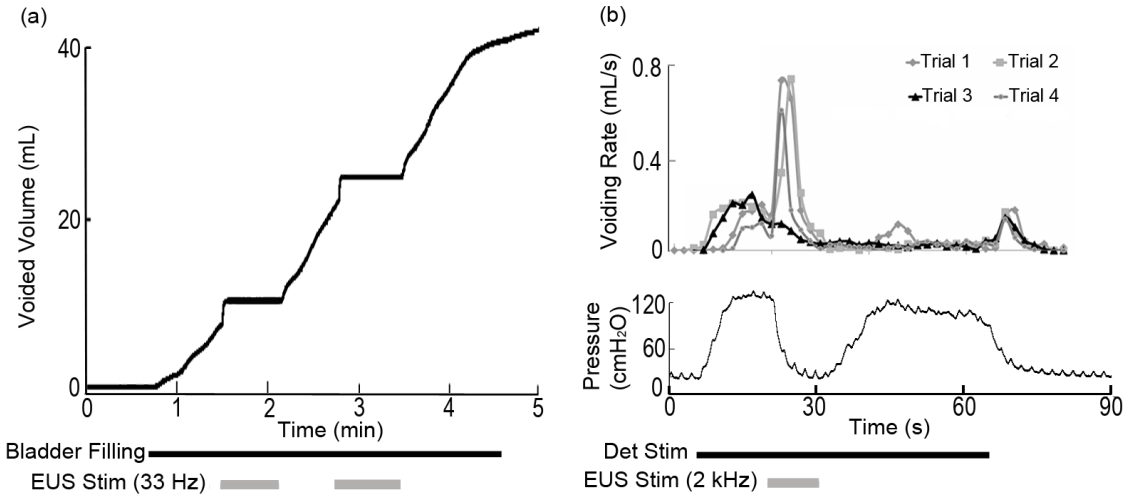

Figure 4.3. Applications of intrafascicular stimulation of the PN. (A) Restoration of continence. Trace shows voided urine volume in an animal made incontinent by unilateral PN crush injury. Gray bars show stimulation of the contralateral PN delivered via a single USEA electrode that selectively constricted the EUS. Continence was completely restored during stimulation. (B) Activation of micturition. Voiding was evoked (voiding rate; top traces) by 60 s of low frequency stimulation (33 Hz, black bar) via a detrusor-selective USEA electrode while a 10 s high frequency stimulation (2 kHz, gray bar) was delivered via another USEA electrode that was EUS-selective. In trial 3 (filled triangles, black line), a control was performed in which no HFAC was delivered and the voiding rate did not increase as in the other trials. Bottom trace shows detrusor pressure in response to one of the trials from Fig. 3B in which both low and high frequency stimulation was delivered. Oscillations seen in the pressure trace are due to mechanical ventilation.

Table 4.1: Number of USEA microelectrodes that evoked selective or nonselective muscle activity

	# USEA electrodes			
	Selective		Nonselective	
Animal	Det	EUS	Det	EUS
1	n/a	n/a	7	n/a
2	n/a	n/a	26	n/a
3	4	21	3	3
4	2	26	3	3
5	2	26	1	1
6	3	68	6	6
7	10	14	3	3
8	10	9	1	1
9	1	19	0	0
Mean	4.6	26.1	5.6	2.4
SD	3.8	19.5	8	2

4.8 References

1. Benevento BT and Sipski ML. "Neurogenic bladder, neurogenic bowel, and sexual dysfunction in people with spinal cord injury," *Phys Ther,* vol. 82, pp. 601-612, 2002.

2. Burks FN, Bui DT and Peters KM. "Neuromodulation and the neurogenic bladder," *Urol Clin North Am,* vol. 37, pp. 559-565, 2010.

3. van Balken MR, Vergunst H and Bemelmans BLH. "The use of electrical devices for the treatment of bladder dysfunction: a review of methods," *J Urol,* vol. 172, pp. 846-851, 2004.

4. Jamil F. "Towards a catheter free status in neurogenic bladder dysfunction: a review of bladder management options in spinal cord injury (SCI)," *Spinal Cord,* vol. 39, pp. 355-361, 2001.

5. Abdel-Gawad M, Boyer S, Sawan M et al. "Reduction of bladder outlet resistance by selective stimulation of the ventral sacral root using high frequency blockade: a chronic study in spinal cord transected dogs," *J Urol,* vol. 166, pp. 728-733, 2001.

6. Peters KM, Killinger KA, Boguslawski BM et al. "Chronic pudendal neuromodulation: expanding available treatment options for refractory urologic symptoms," *Neurourol Urodyn,* vol. 29, pp. 1267-1271, 2010.

7. Boggs JW, Wenzel BJ, Gustafson KJ et al. "Bladder emptying by intermittent electrical stimulation of the pudendal nerve," *J Neural Eng,* vol. 3, pp. 43-51, 2006.

8. Yoo PB, Woock JP and Grill WM. "Bladder activation by selective stimulation of pudendal nerve afferents in the cat," *Exp Neurol,* vol. 212, pp. 218-225, 2008.

9. Grill WM. "Electrical stimulation for control of bladder function," *Conf Proc IEEE Eng Med Biol Soc,* vol. 2009, pp. 2369-2370, 2009.

10. Spinelli M, Malaguti S, Giardiello G et al. "A new minimally invasive procedure for pudendal nerve stimulation to treat neurogenic bladder: description of the method and preliminary data," *Neurourol Urodyn,* vol. 24, pp. 305-309, 2005.

11. Tai C, Wang J, Wang X et al. "Voiding reflex in chronic spinal cord injured cats induced by stimulating and blocking pudendal nerves," *Neurourol Urodyn,* vol. 26, pp. 879-886, 2007.

12. Bock S, Folie P, Wolff K et al. "First experiences with pudendal nerve stimulation in fecal incontinence: a technical report," *Tech Coloproctol,* vol. 14, pp. 41-44, 2010.

13. Woock JP, Yoo PB and Grill WM. "Activation and inhibition of the micturition reflex by penile afferents in the cat," *Am J Physiol: Regul Integr Comp Physiol,* vol. 294, pp. R1880-1889, 2008.

14. Woock JP, Yoo PB and Grill WM. "Mechanisms of reflex bladder activation by pudendal afferents," *Am J Physiol: Regul Integr Comp Physiol,* vol. 300, pp. R398-407, 2011.

15. Bhadra N, Bhadra N, Kilgore K et al. "High frequency electrical conduction block of the pudendal nerve," *J Neural Eng,* vol. 3, pp. 180-187, 2006.

16. Branner A, Stein RB and Normann RA. "Selective stimulation of cat sciatic nerve using an array of varying-length microelectrodes," *J Neurophysiol,* vol. 85, pp. 1585-1594, 2001.

17. Dowden BR, Wilder AM, Hiatt SD et al. "Selective and graded recruitment of cat hamstring muscles with intrafascicular stimulation," *IEEE Trans Neural Syst Rehabil Eng,* vol. 17, pp. 545-552, 2009.

18. Branner A, Stein RB, Fernandez E et al. "Long-term stimulation and recording with a penetrating microelectrode array in cat sciatic nerve," *IEEE Trans Biomed Eng,* vol. 51, pp. 146-157, 2004.

19. Dowden BR, Wark HAC and Normann RA. "Muscle-selective block using intrafascicular high-frequency alternating current," *Muscle Nerve,* 42:339-347 2010.

20. Silverman J and Muir WW. "A review of laboratory animal anesthesia with chloral hydrate and chloralose," *Lab Anim Sci,* vol. 43, pp. 210-216, 1993.

21. Rousche PJ and Normann RA. "A method for pneumatically inserting an array of penetrating electrodes into cortical tissue," *Ann Biomed Eng,* vol. 20, pp. 413-422, 1992.

22. Branner A and Normann RA. "A multielectrode array for intrafascicular recording and stimulation in sciatic nerve of cats," *Brain Res Bull,* vol. 51, pp. 293-306, 2000.

23. Gunalan K, Warren DJ, Perry JD et al. "An automated system for measuring tip impedance and among-electrode shunting in high-electrode count microelectrode arrays," *J Neurosci Methods,* vol. 178, pp. 263-269, 2009.

24. Boggs JW, Wenzel BJ, Gustafson KJ et al. "Spinal micturition reflex mediated by afferents in the deep perineal nerve," *J Neurophysiol,* vol. 93, pp. 2688-2697, 2005.

25. Mariano TY, Boger AS and Gustafson KJ. "The feline dorsal nerve of the penis arises from the deep perineal nerve and not the sensory afferent branch," *Anat Histol Embryol,* vol. 37, pp. 166-168, 2008.

26. Gustafson KJ, Zelkovic PF, Feng AH et al. "Fascicular anatomy and surgical access of the human pudendal nerve," *World J Urol,* vol. 23, pp. 411-418, 2005.

27. Sajadi KP, Gill BC and Damaser MS. "Neurogenic aspects of stress urinary incontinence," *Curr Opin Obstet Gynecol,* vol. 22, pp. 425-429, 2010.

28. Chen S-C, Grill WM, Fan W-J et al. "Bilateral pudendal afferent stimulation improves bladder emptying in rats with urinary retention," *British J Urology Internat,* vol. Aug, pp. 1-8, 2011.

29. McDonnall D, Clark GA and Normann RA. "Interleaved, multisite electrical stimulation of cat sciatic nerve produces fatigue-resistant, ripple-free motor responses," *IEEE Trans Neural Syst Rehabil Eng*, vol. 12, pp. 208-215, 2004.

30. Balis GU and Monroe RR. "The pharmacology of chloralose," *Psychopharmacologia*, vol. 6, pp. 1-30, 1964.

31. Dripps RD and Dumke PR. "The effect of narcotics on the balance between central and chemoreceptor control of respiration," *J Pharm Experim Therap,* vol. 77, pp. 290-300, 1943.

CHAPTER 5

ACUTE MONITORING OF GENITOURINARY FUNCTION USING INTRAFASCICULAR ELECTRODES: SELECTIVE PUDENDAL NERVE ACTIVITY CORRESPONDING TO BLADDER FILLING, BLADDER FULLNESS, AND GENITAL STIMULATION

Reprinted with permission from the journal, Urology, and the co-authors

Publication Reference:

Mathews K*, Wark HAC*, Warren DJ, Christensen MB, Nolta NF, Cartwright PC, Normann RA. Urology. Accepted for publication May 2014. In press

*co-first authors

The co-authors of this chapter each made the following contributions: design of and carrying out the experiments by KM, HACW, DJW, PC, RAN; data analysis by KM, HACW; histology and graphics for figure 1 by BC, NFN; writing of the manuscript by HACW; preparation of the figures by KM; editing of the manuscript by all authors.

5.1 Abstract

To investigate the use of a microelectrode array with a high spatial density of penetrating intrafascicular electrodes for selective recording of pudendal nerve activity evoked by a variety of genitourinary stimuli. Felines were anesthetized with alpha-chloralose and High Density Utah Slanted Electrode Arrays (HD-USEAs; 48 microelectrodes; 200 μm spacing) were implanted into the pudendal nerve for acute experimentation. Neural activity was recorded during bladder filling, spontaneous reflexive Distention Evoked bladder Contractions (DECs), and tactile somatosensory stimulation. The intrafascicularly implanted pudendal nerve electrodes were able to selectively record neural activity that corresponded to various genitourinary stimuli. Across all seven experimental animals, a total of 10 microelectrodes recorded neural units that were selectively driven by bladder filling or DECs. Twenty-two electrodes were selectively driven by tactile stimulation. Microelectrode arrays implanted intrafascicularly into the pudendal nerve can be used to selectively record the neural responses that reflect bladder status and urogenital tactile stimulation. This work sets the stage for developing future implantable closed-loop neuroprosthetic devices for restoration of bladder function.

5.2 Introduction

The work described herein is focused on investigating a critical element in achieving closed-loop control of genitourinary function: the selective monitoring of urogenital status via pudendal nerve single-unit recordings. Previous research has shown that whole-nerve cuff electrodes can record pudendal nerve activity that corresponds to genital stimulation[1] or bladder contractions[2], but this method records the overall evoked nerve activity (not the selective activity from individual axons) and, thus, suffers from false-positive detection of bladder fullness produced by tactile stimulation. Therefore, a neural interface that can selectively detect and differentiate different genitourinary functions could improve the accuracy of bladder monitoring and the effectiveness of such a closed-loop system.

Here we investigated the use of penetrating microelectrode arrays implanted intrafascicularly into the pudendal nerve of anesthetized felines as a means for selectively monitoring various genitourinary states. The arrays[3] contained 48 wired microelectrodes of varying lengths and were used to record neuronal activity at multiple sites across the cross-section of the pudendal nerve evoked by bladder filling, Distension-Evoked bladder Contractions (DECs), and by tactile stimulation. Further, because the tips of the implanted electrodes sample neural activity at discrete loci across the cross section of the nerve, we also show that such recordings can be used to determine the distribution of afferent and efferent fibers within the pudendal nerve. This study demonstrates that an intrafascicularly-based pudendal neural interface could provide an important component of a closed-loop approach for accurately controlling genitourinary function.

5.3 Materials and methods

All acute (< 30 h) experimental procedures were approved by the University of Utah's Institutional Animal Care and Use Committee. Male felines (n = 7 animals; 3-5 kg; intact sexual organs) were induced with Telazol (9-12 mg/kg; IM) and surgical anesthesia was maintained with isoflurane (0.25-2.0% gas). Alpha-chloralose (10-65 mg/kg IV; as needed) anesthesia was used during experimental procedures. Vital signs were monitored every 15 min throughout the experimentation to ensure maintenance of a stable anesthetic plane.

A dual-lumen suprapubic catheter (12 French, Cook Medical, Inc., Bloomington, IN, USA) was purse-string sutured into the bladder for filling and measuring bladder pressure. A syringe infusion pump was used to fill the bladder at constant rates (0.5-8 ml/min). These rates have been used in previous bladder physiology studies[2,4,5] and are within the ranges induced by diuretics[6]. In two animals, the ureters were ligated, transected proximal to the ligation, and drained internally. DECs were stimulated by filling the bladder with room temperature sterile saline to resting pressures of 5-15 cm-H_2O (infusion volumes ranged from approximately 5-20 ml)[4,7]. Felines were positioned either prone or laterally.

The pudendal nerve was exposed by dissection of the ischioanal fossa and the pudendal nerve trunk was identified via anatomical branching patterns. The nerve trunk and branches were further verified via whole nerve stimulation while resulting muscle contractions were monitored visually (penile, anal or both). In most animals, the gluteal muscle groups were reflected in order to gain access to the pudendal nerve trunk for the implantation of High-Density Utah Slanted Electrode Arrays (HD-USEAs). A nerve

platform was placed under the nerve trunk and then an HD-USEA was implanted using a hand-held pneumatic insertion technique[8]. After implantation, the nerve and HD-USEA were wrapped in low-density polyethylene wrap to keep the nerve hydrated and to contain the implanted electrode array. To investigate the origin of the recorded responses, the pudendal nerve in one animal was crushed proximal to the implant site. The HD-USEAs had 48, 300-800 μm long, wired electrodes arranged in a 5×10 grid (200 μm spacing, with the four corner electrodes used as reference electrodes)[3]. The ~50 μm long deinsulated and metalized electrode tips formed the active surfaces. This architecture was chosen to custom-fit the anatomy of the feline pudendal nerve[9].

Recordings were taken from all wired electrodes while filling and emptying the bladder or brushing the skin near the anus, scrotum or penis. Neural units were detected using a threshold initially set at six times the Root Mean Squared (RMS) of the continuously recorded signal on each electrode and thresholds were further adjusted during the experiments. Units were then screened subjectively and categorized as either: 1) multimodal - defined as a unit that was driven by multiple forms of stimulation or a unit that fired spontaneously, or 2) selective – defined as units that were driven only by tactile stimulation, or by changes in bladder pressure produced either via filling or by bladder DECs. For units with activity that correlated with DECs, unit firing rates (calculated as the number of neuronal events in 100 ms bins) were smoothed with a 0.5 Hz fourth-order low-pass Butterworth filter. Recorded suprapubic pressure was regressed against the firing rates for one trial, and the regression coefficients were used in subsequent trials to predict the bladder pressure. Finally, the coefficient of determination (R^2) of the regression of the recorded and predicted bladder pressures and the Root Mean

Square Errors (RMSE) of the estimated bladder pressures were calculated with respect to the recorded pressures.

All data were collected using a Cerebus Data Acquisition System (Blackrock Microsystems, Salt Lake City, UT, USA). Neural data were bandpass filtered (750-7,500 Hz) and sampled at 30 kHz. Bladder pressure recordings were sampled either at 10 kHz or 30 kHz. Data analysis was performed using Offline Sorter (Plexon, Inc., Dallas, TX, USA), MATLAB (The MathWorks, Inc., Natick, MA, USA) and Microsoft Excel (Microsoft, Redmond, WA, USA).

After one animal was sacrificed, the exposed nerve containing the HD-USEA implant site was soaked in 4% paraformaldehyde phosphate buffer solution (PBS) for 30 min. The array was explanted and the nerve was excised and stored in 4% paraformaldehyde PBS for 24 h, then rinsed and stored in 1% PBS with 0.01% sodium azide. Tissue was then stained with 1-2% OsO_4 in a 0.1M sodium cacodylate buffer, dehydrated in graded concentrations of ethanol, cleared with propylene oxide, and embedded in Embed 812 (Epon, Electron Microscopy Science, Hatfield, PA, USA). Serial 0.5-0.6 μm semithin sections were stained and examined using a color CCD camera attached to a Nikon E600 microscope. Serial overlapping images were captured over the entire nerve (at 60x magnification) and then reconstructed to form a mosaic image (Adobe Photoshop CS, Adobe Systems Inc., San Jose, CA, USA).

5.4 Results

The mean electrode impedance of the four HD-USEAs used in this study was 130 ± 124 kΩ. Electrode impedances above 500 kΩ were considered nonfunctional and not

included in the mean impedance calculation. The mean number of functional electrodes was 45 $\pm$ 2 (mean $\pm$ standard deviation) in each of the seven experiments.

The drawings of Figures 5.1A and B illustrate that a 5×10 HD-USEA implanted into the feline pudendal nerve provides uniform electrical access across its cross-section. A cross-section of the feline pudendal nerve that was implanted with an HD-USEA for 10 h is shown in Figures 5.1C, D, and E. The base of the array was located at the top portion of the nerve and the tracks made by the extracted electrodes are evident. At the implant site shown in this figure, the feline pudendal nerve trunk is 39% neuronal tissue (Fig. 5.1D with fascicular areas filled in) and 61% nonneuronal tissue (connective, vascular, adipose, etc).

In the 7 feline experiments performed, 48 of the 336 wired electrodes recorded single unit activity. In 2 of the experiments, an average of 23% of the implanted electrodes recorded single unit activity. Table 5.1 summarizes the stimuli that evoked selective and nonselective neuronal activity for each animal. In 4 of the 7 preparations, we recorded at least one neuronal unit that selectively responded only to bladder pressure changes due to bladder filling or DECs. In 2 of these 4 preparations, we additionally recorded at least one additional neuronal unit that selectively responded to tactile stimulation only. In each animal, there was at least one neuronal unit recorded that was exclusively driven by tactile stimulation, by bladder filling, or by DECs. In two animals, nonselective, multimodal units were recorded (1 unit/animal) that were driven by both tactile stimulation and bladder filling. In 3 animals, we recorded spontaneous neural activity that could not be associated with either tactile stimulation or any bladder states. Across all preparations, 22 electrodes recorded single unit activity that was driven by

genital tactile stimulation alone and 10 electrodes recorded single unit activity that was driven by changing the bladder pressure due to filling or due to DECs. The temporal profiles of the action potentials of these 10 units varied: bladder filling produced a monotonic increase in firing over the duration of filling, while DECs produced bursts of firing.

Figures 5.2A and B show examples of single unit waveforms that were evoked in one animal by stroking the scrotum. A raster of spiking events recorded by each electrode evoked by periodic tactile stimulation was plotted (Fig. 5.2C), and 12 electrodes recorded neural activity driven by the stimulus (scrotal stroking). The map of electrodes that recorded single unit activity (Fig. 5.2D) indicates that the afferent fibers responding to scrotal stimulation were distributed across the entire cross-section of the nerve.

Figure 5.3 shows an example of bladder filling along with the spiking data recorded on two HD-USEA electrodes. These electrodes recorded increases in the firing rates of nearby axons as the bladder began to fill. For example, in 10-second windows before and after filling, the number of spikes recorded by electrode 39 increased from 5 to 47 spikes. These firing rates either remained with constant volume (20 mL) in the bladder or decreased upon emptying of the bladder. The neural activity map (Fig. 5.3B) suggests that the afferent fibers encoding tactile or bladder fullness may be somewhat segregated in the pudendal nerve. The two electrodes that recorded activity correlated with bladder fullness were located to one side of the nerve and the seven electrodes recording activity that correlated with tactile stimulation were localized on the opposite side of the nerve.

Filling the bladder to 5-15 cm-H_2O resting pressure evoked reflexive DECs (Fig.

5.4A, top trace). This figure also shows the spiking data from four electrodes during this experiment. Electrodes 6-8 recorded transiently increased firing from neurons in response to bladder contractions, while electrode 5 recorded only spontaneous activity. The histogram (Fig. 5.4A, bottom trace) shows the summed spiking events recorded across electrodes 6-8 and these events were correlated with bladder contractions (R^2 = 0.60; normalized RMSE = 0.42 cm-H_2O). The neural activity from these four electrodes was also recorded during 10 periods of tactile genital stimulation (Fig. 5.4B, upper trace). Neural activity recorded on electrode 5 was driven by genital stimulation (the binned spiking events on electrode 5 are shown in the bottom histogram), but the neural activity recorded on electrodes 6-8 was not driven by such stimuli. In order to identify if this recorded activity arose from afferent or efferent pathways, the pudendal nerve of this animal was crushed proximal to the implanted HD-USEA, resulting in the loss of activity selectively driven by bladder filling and DECs. The neural activity map (Fig. 5.4C) supports the fiber segregation seen in Figure 5.3B, but in this experiment the fibers with activity that correlated with bladder fullness were localized to the upper region of the nerve, and the electrodes responding to tactile stimulation were localized to one side of the nerve.

5.5 Discussion

Neurogenic bladder can result from many different central or peripheral nerve injuries or diseases, such as spinal cord injury or spina bifida. Patients for whom pharmacological or surgical interventions are not effective are being considered for various implantable neuroprosthetic interventions[10]. The pudendal nerve is one of the

locations that is being investigated for the development of a neuromodulation system to restore genitourinary function in people with problems such as neurogenic bladder[11]. Animal studies have shown that whole-nerve (cuff electrode) stimulation of pudendal afferent fibers can be used to drive the micturition reflex (20-40 Hz) or inhibit bladder contractions (10-20 Hz)[12,13], while very high frequency stimulation (1-20 kHz)[14] can be used to block efferent EUS motor fibers and produce sphincter relaxation.

A pudendal nerve closed-loop control system would presumably achieve improved control of urogenital function. However, such an approach would require the monitoring of detrusor muscle status (via reflexive circuitry reflecting different bladder states) and the use of this information to provide electrical stimulation to subsets of nerve fibers that modulate detrusor and/or external urethral sphincter activity. Whole-nerve cuff electrodes have been used to record pudendal nerve activity corresponding to genital stimulation[1,2] or bladder contractions[2]; however, such recordings are unable to differentiate activity evoked by these different stimuli. Thus, a closed-loop neuroprosthetic device based on whole-nerve cuff electrodes for the treatment of bladder dysfunction would likely suffer from false-positive detection of bladder fullness due to unrelated genital tactile stimulation[2].

Intrafascicular penetrating peripheral nerve electrodes have been developed for large (3-4 mm)[15] and small (≤1 mm)[3] diameter neuronal structures. Using the nonslanted version of these microelectrode arrays, Bruns et al. have achieved selective detection of bladder-driven units by recording neurons in sacral dorsal root ganglia, another potential site for a closed-loop neuroprosthesis for bladder control[4]. We previously demonstrated that USEAs can be implanted into the canine pudendal nerve to electrically stimulate

small subsets of nerve fibers, allowing for the selective activation of the detrusor and EUS muscles[16]. Here we have expanded upon that work and investigated whether recording of pudendal nerve neural activity could be used to selectively detect various genitourinary stimuli, and thus, provide an important component in the future development of a single implant site for a closed-loop neuroprosthetic device for the control of human urinary function.

HD-USEAs have a slanted architecture, allowing the tips of the electrodes to penetrate into various depths of the nerve, thereby providing access to nerve fibers in different regions of most of the nerve fascicles. However, as shown in the pudendal nerve cross-section (Figs. 5.1D), much of the nerve is nonfascicular tissue (61%), causing many electrodes to reside in nonneural regions of the nerve. However, many of these electrodes could be used for stimulation of the nerve fibers, but with less selectivity than electrodes located within fascicles. We have also used HD-USEAs to investigate the distribution of afferent fibers within this small diameter nerve (electrode activity maps of Figs. 5.2, 5.3 and 5.4). Despite observed differences, likely due to variations in nerve orientation, these activity maps support previously published histology work describing the fascicular organization of the pudendal nerve in felines[9].

Bladder filling, reflexive DECs and tactile stimulation evoked neural activity that was selectively and nonselectively recorded via different HD-USEA microelectrodes. Of all successfully recording electrodes across all animals, only two electrodes were found to record multimodal activity that could not distinguish between tactile stimulation and different bladder states. Thus, microelectrode arrays may be expected to have few electrodes, if any, that provide false-positive detection of bladder contractions during

tactile stimulation.

The temporal profile of firing evoked by bladder filling or DECs differed; contractions evoked transient activity and filling evoked monotonic increases in firing. Therefore, a closed-loop system for monitoring bladder status will likely need to incorporate an algorithm that detects different bladder states based on the temporal signature of neuronal firing. Additionally, these studies were carried out using bladder infusion rates within ranges induced by diuretics (0.5-8 mL/min)[6] and future studies need to investigate whether pudendal nerve activity differs during lower urine flow rates (0.5-1.4 mL/hr). In one animal, the pudendal nerve was crushed proximally to the implanted HD-USEA in order to investigate whether signals in the pudendal nerve corresponding to bladder filling/DECs were being recorded from afferent or efferent pudendal fibers. The loss of all neural signals postneuronal crushing suggests that these units were reflexively activated, and therefore, a pudendal neural interface for detection of bladder status may necessitate intact reflexive arcs.

Over the course of an experiment, many of the electrodes drifted in and out of their ability to record neural activity. This may be a result of micromovements at the device-nerve interface causing the electrode tips to move in and out of the listening radius of individual nerve fibers, a problem that may be mitigated in chronically implanted HD-USEAs where tissue encapsulation would tend to stabilize the electrodenerve interface. It is likely that implantation of the HD-USEA also causes minor nerve damage that leads to a loss in neuronal signals over time. However, previous research has shown that these devices can be implanted without major nerve damage for acute electrophysiology studies[3,17]. Additionally, if nerve damage were causing the loss of these signals, we

would not expect to have regained the ability to record the signals that were lost at earlier times. Future chronic studies in feline pudendal nerves are warranted to investigate the long-term recording capabilities and anatomical consequences of HD-USEA implantations, and various containment systems that may better serve to decrease possible movement at the device-nerve interface.

The experiments described in this report were performed in the small diameter feline pudendal nerve, and it is expected that this approach may be more effective in the larger human pudendal nerve[18] where implantation of larger electrode arrays with more electrodes could allow even greater numbers of single unit recordings of neural activity that correlate with bladder fullness. Further, pairs of electrode arrays could be implanted bilaterally in both pudendal nerves, enabling even greater selective monitoring of bladder status.

5.6 Conclusion

In order to develop a clinically useful neuroprosthesis for the restoration of genitourinary functions—such as inhibition of overactive bladder or the restoration of controlled micturition—a fully implantable system must be able to both detect various genitourinary states and then send the appropriate electrical stimulation to drive the desired physiological response (e.g., control the states of the external urethral sphincter and the detrusor muscle). The results presented herein provide evidence that an array of microelectrodes inserted intrafascicularly into the pudendal nerve could be used as a neural interface for the selective monitoring of various genitourinary stimuli, such as bladder filling, DECs and tactile stimulation of the genital region. Such a neural interface

could form the basis for an implantable system that provides closed-loop control of genitourinary functions without suffering from false-positive detection of different bladder states due to unrelated genital tactile stimulation.

5.7 Acknowledgments

This work was funded by the National Science Foundation (CBET-1134545).

Table 5.1: Number of electrodes that recorded neural activity for various stimuli

Animal	Nonselective		Selective	
	Multimodal	Spontaneous	Tactile	Bladder
1	-	3	-	1
2	-	-	1	-
3	-	-	12	-
4	1	-	7	2
5	1	-	1	6
6	-	4	1	-
7	-	7	-	1
Totals	2	14	22	10

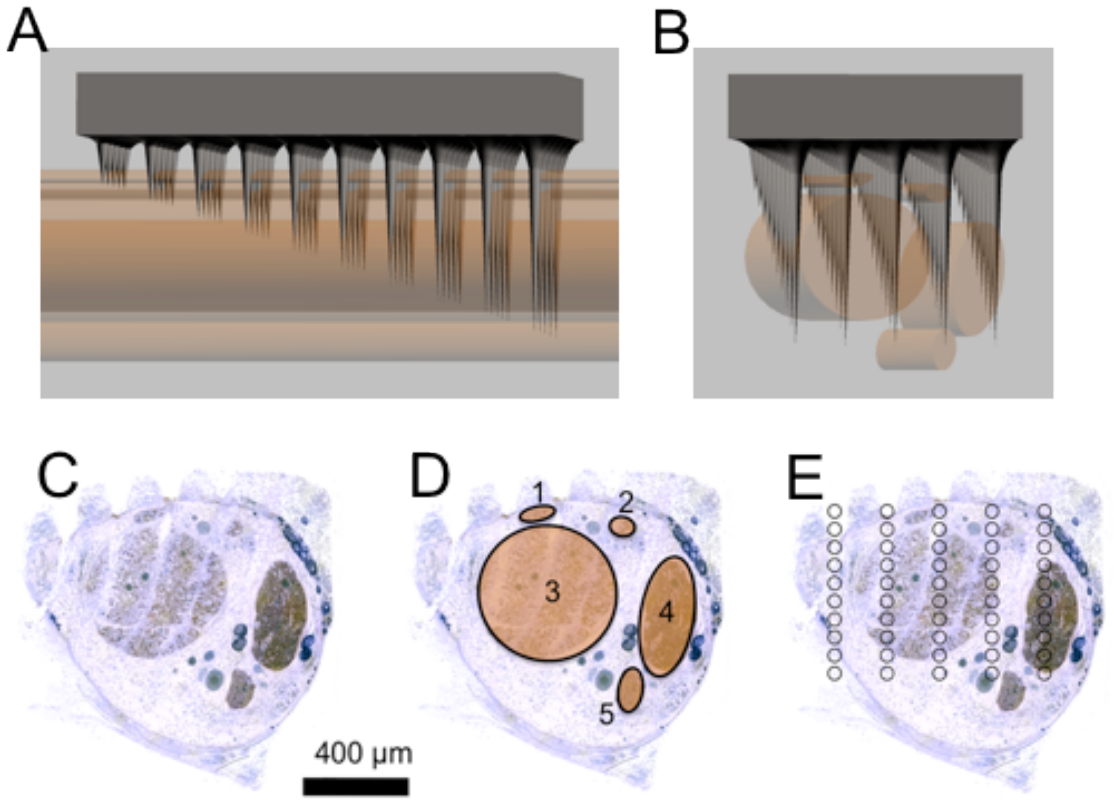

Figure 5.1. Side and end-on perspective diagrams of a High-Density Utah Slanted Electrode Array (HD-USEA) implanted into the feline pudendal nerve (fascicles indicated with shaded cylinders). (A-B) The 200 µm spacing of the HD-USEA electrodes was based upon feline pudendal nerve dimensions. The location and sizes of the pudendal nerve fascicles were estimated from the cross-sectional image shown in C. The diagrams show the tips of electrodes accessing fibers distributed throughout the nerve. C. Cross-section of the pudendal nerve after an acute (10 h) HD-USEA implantation. The base of the array was located on the top surface of the imaged nerve and evidence of the electrode tracks penetrating into the nerve can be seen (histological processing produced curvature in the electrode tracts in this image). D. Same cross-section as in C but with the fascicles outlined and numbered. At the site of this implantation, the fascicular area made up 39% of the total cross sectional area of the pudendal nerve. E. Distribution of electrode tips (represented as circles) throughout cross section of nerve. In this image, the electrode tips of 18-24 of the 48 implanted electrodes appear to be located within fascicles #1-4, such that the axons inside these fascicles are within ≈ 100 µm of an electrode tip. Scale bar is for (C-E).

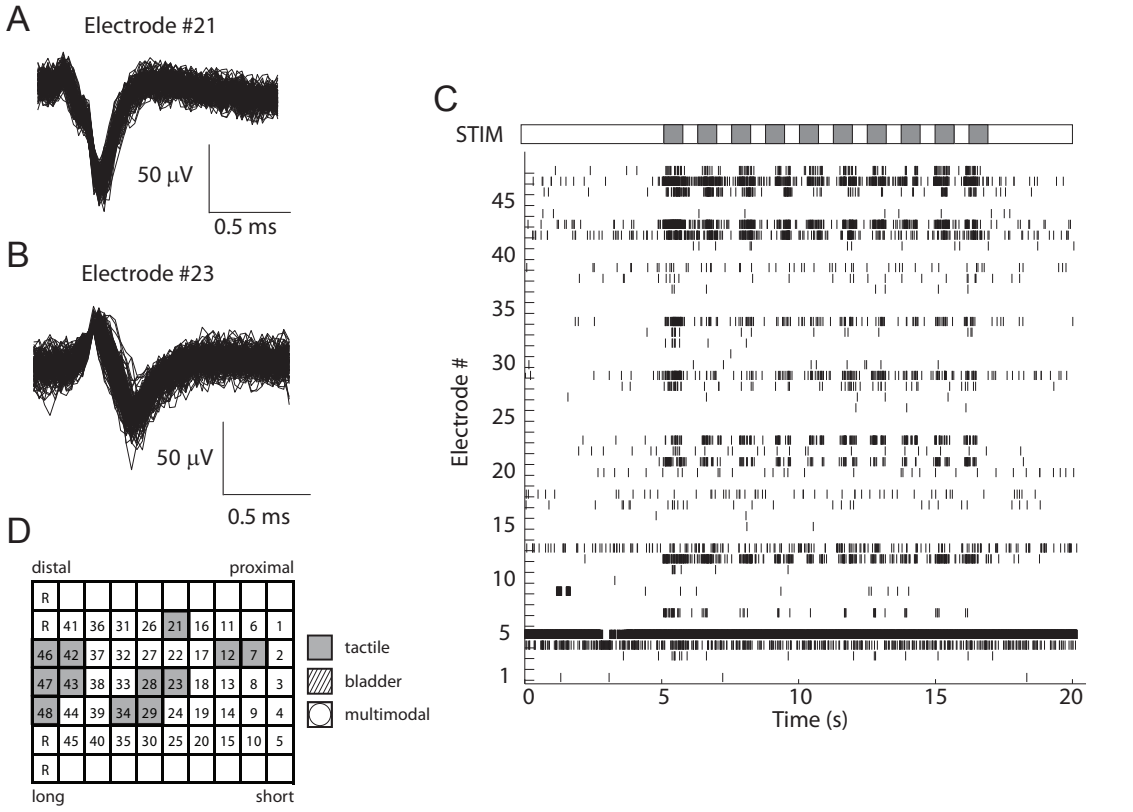

Figure 5.2. Selective detection of genital tactile stimulation. Tactile stimulation evoked neural activity that could be recorded via individual microelectrodes on an HD-USEA implanted into the feline pudendal nerve. Neural activity was evoked during stroking of the scrotum and various neural units could be recorded from different electrodes, such as electrode 21 (A) and electrode 23 (B). C. A raster plot of the spikes recorded on each microelectrode were plotted during ten scrotal stroking events (top bar, marked 'STIM') and only the electrodes that were within the listening radius of fibers associated with the tactile stimulation showed increased firing during each event. D. Electrode array activity map showing the location and identifying numbers of electrodes in the implanted HD-USEA. Electrodes that recorded increased neural activity when the scrotum was stroked are indicated with filled tiles. Data shown were recorded from cat #3.

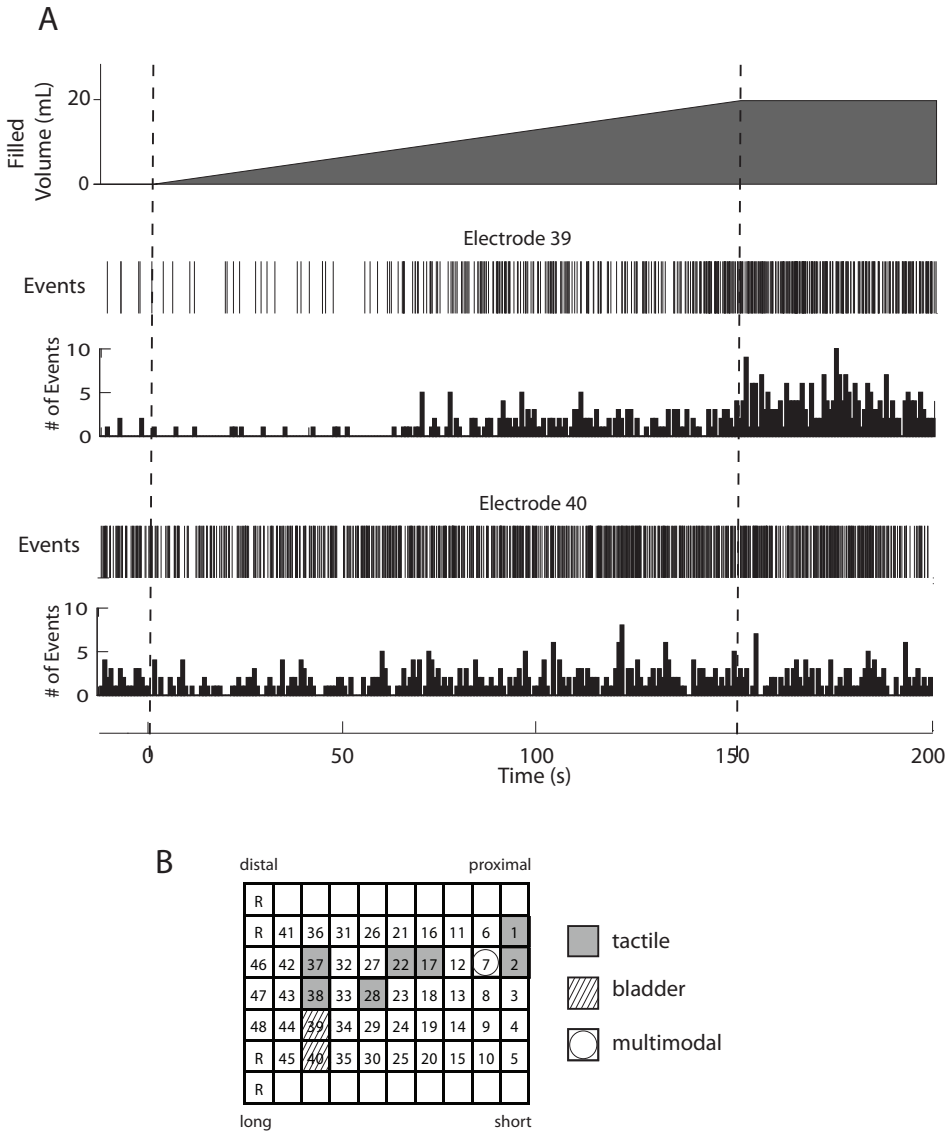

Figure 5.3. Selective detection of bladder fullness. A. The top trace shows the volume of saline infused into the bladder (20 mL) over 150 seconds. The dashed lines mark the beginning and end of the filling episode. The bottom four traces show raster plots and firing rates (100 ms bins) of the neurons recorded with two different electrodes during this filling epoch. Note the constant increase in spike firing for each unit over the course of filling. B. Electrode array map showing the location and identifying numbers of electrodes in the implanted HD-USEA. Electrodes that recorded increased neural activity during the filling epoch are identified with cross-hatched tiles, suggesting that these afferent fibers were distributed along on one side and deep within the nerve. Data shown were collected from cat #4.

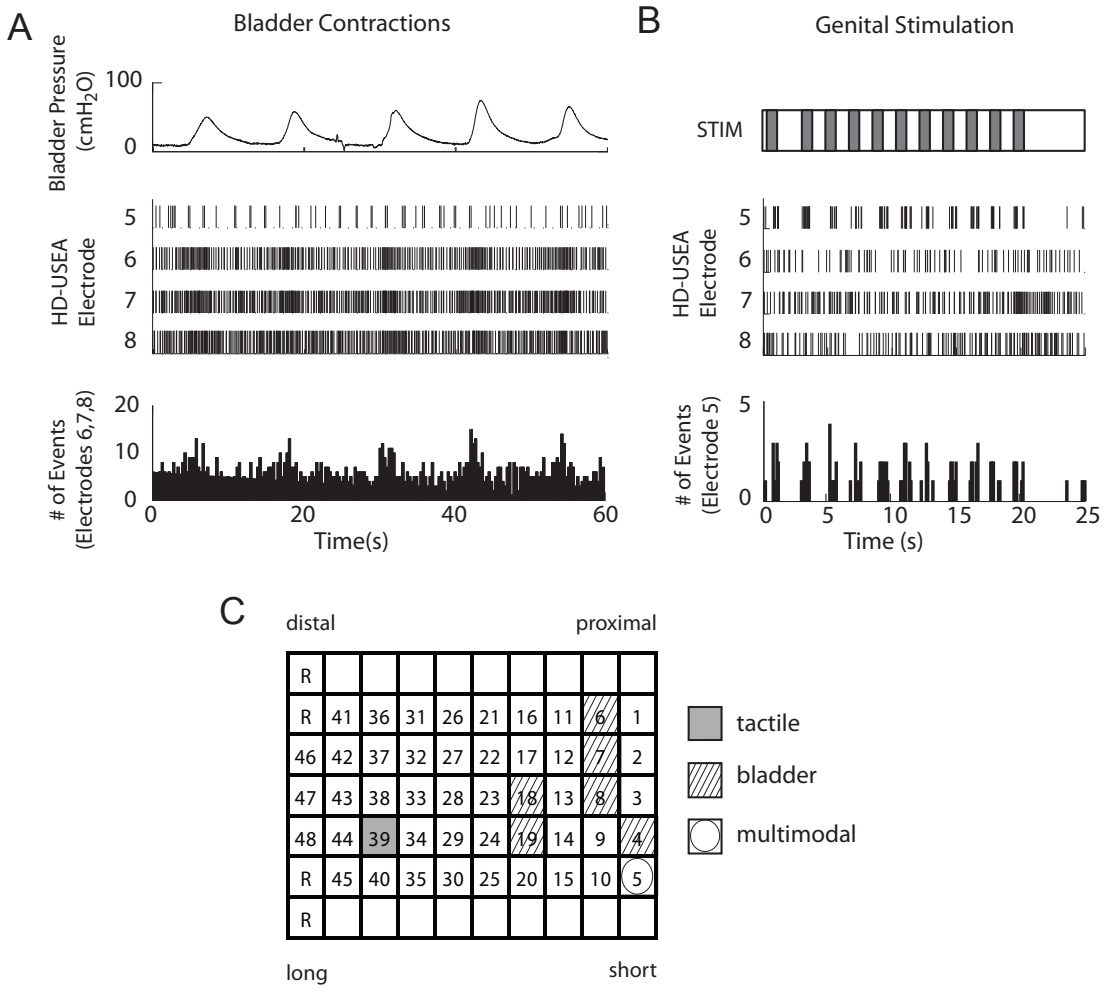

Figure 5.4. Selective discrimination of various urogenital stimulation-associated nerve activity. A. The bladder was filled to 5 mL, a volume that evoked reflexive DECs (top trace). Spike data recorded with four HD-USEA microelectrodes are shown in the middle traces. Electrodes 6-8 showed increased neural activity during DECs while electrode 5 showed no consistent change in neural activity. The bottom trace shows the combined firing rate (100 ms bins) for spike events recorded on electrodes 6-8. Increased neural activity in electrodes 6-8 correlated with bladder contractions. B. Neural activity recorded from the same four electrodes shown in A. have different patterns of evoked activity during periodic genital stimulation (top bar, marked 'STIM'). Electrode 5 was specifically driven by tactile stimulation (the firing rate, 100 ms bins are plotted the on bottom), whereas electrodes 6-8 were not modulated by tactile stimulation. C. Electrode array map showing the location and identifying numbers of electrodes in the implanted HD-USEA. The map indicates that these bladder activated afferent fibers were located along the top portion of the nerve. Data shown were collected from cat #5.

5.8 References

1 Pastelín CF, Zempoalteca R, Pacheco P, et al. Sensory and somatomotor components of the "sensory branch" of the pudendal nerve in the male rat. Brain Research 2008; 1222: 149–155.

2 Wenzel BJ, Boggs JW, Gustafson KJ, et al. Detecting the onset of hyper-reflexive bladder contractions from the electrical activity of the pudendal nerve. IEEE Trans Neural Sys Rehab Eng: 2005; 13: 428–435.

3 Wark HAC, Sharma R, Mathews KS, et al. A new high-density (25 electrodes/mm^2) penetrating microelectrode array for recording and stimulating submillimeter neuroanatomical structures. J Neural Eng 2013; 10: 5003.

4 Bruns TM, Gaunt RA, Weber DJ. Multielectrode array recordings of bladder and perineal primary afferent activity from the sacral dorsal root ganglia. J Neural Eng 2011; 8: 056010 (8pp).

5 Wenzel BJ, Boggs JW, Gustafson KJ, et al. Closed loop electrical control of urinary continence. J Urol 2006; 175: 1559–1563.

6 Upsdell SM, Leeson SM, Brooman PJ, et al. Diuretic-induced urinary flow rates at varying clearances and their relevance to the performance and interpretation of diuresis renography. Br J Urol 1988; 61: 14–18.

7 Yoo PB, Klein SM, Grafstein NH, et al. Pudendal nerve stimulation evokes reflex bladder contractions in persons with chronic spinal cord injury. Neurourol Urodyn 2007; 26: 1020–1023.

8 Rousche PJ, Normann RA. A method for pneumatically inserting an array of penetrating electrodes into cortical tissue. Ann Biomed Eng 1992; 20: 413–422.

9 Mariano TY, Boger AS, Gustafson KJ. The feline dorsal nerve of the penis arises from the deep perineal nerve and not the sensory afferent branch. Anat Histol Embryol 2008; 37: 166–168.

10 Burks FN, Bui DT, Peters KM. Neuromodulation and the neurogenic bladder. Urol Clin North Am 2010; 37: 559–565.

11 Peters KM, Killinger KA, Boguslawski BM, et al. Chronic pudendal neuromodulation: expanding available treatment options for refractory urologic symptoms. Neurourol Urodyn 2010; 29: 1267–1271.

12 Boggs JW, Wenzel BJ, Gustafson KJ, et al. Frequency-dependent selection of reflexes by pudendal afferents in the cat. J Phys 2006; 577: 115–126.

13 Tai C, Chen M, Shen B, et al. Plasticity of urinary bladder reflexes evoked by stimulation of pudendal afferent nerves after chronic spinal cord injury in cats. Exp Neurol 2011; 228: 109–117.

14 Bhadra N, Bhadra N, Kilgore K, et al. High frequency electrical conduction block of the pudendal nerve. J Neural Eng 2006; 3: 180–187.

15 Branner A, Stein RB, Normann RA. Selective stimulation of cat sciatic nerve using an array of varying-length microelectrodes. J Neurophys 2001; 85: 1585–1594.

16 Wark HAC, Dowden BR, Cartwright PC, et al. Selective activation of the muscles of micturition using intrafascicular stimulation of the pudendal nerve. IEEE Emerg Sel Topics Cir Sys 2011; 1: 631–636.

17 Mathews KS, Wark HAC, Normann RA. Assessment of rat sciatic nerve function following acute implantation of High Density Utah Slanted Electrode Array (25 electrodes/mm^2) based on neural recordings and evoked muscle activity. Muscle Nerve 2014; *in press*, published online: doi:10.1002/mus.24171.

18 Gustafson KJ, Zelkovic PF, Feng AH, et al. Fascicular anatomy and surgical access of the human pudendal nerve. World J Urol 2005; 23: 411–418.

CHAPTER 6

RESTORATION OF URINARY FUNCTION USING UTAH ELECTRODE ARRAYS IMPLANTED INTO THE FELINE PUDENDAL NERVE

In review May 2014

Contributing Authors:

HAC Wark, S Black, KS Mathews, P Cartwright, K Gustafson, RA Normann

Author contributions: HACW, SB, KM, PC, KG, RAN designed and carried out the experiments; data analysis by HACW; writing of the manuscript by HACW; editing of the manuscript by all authors.

6.1 Abstract

To investigate intrafascicular pudendal nerve stimulation in felines as a means to restore urinary function in acute models of urinary incontinence, and in overactive and underactive bladder states. Felines were anesthetized and high-electrode count (48 electrodes; 25 electrodes/mm^2) intrafascicular electrode arrays were implanted into the pudendal nerve trunk. Electrodes were mapped for their ability to selectively or nonselectively excite the external anal sphincter, external urethral sphincter and the detrusor bladder muscle. Multielectrode arrays implanted into the pudendal nerve trunk were able to selectively and nonselectively excite genitourinary muscles. After inducing urinary incontinence with bilateral pudendal nerve transections (proximal to the implants), electrical stimulation delivered using HD-USEA electrodes was able to eliminate leaking. Electrical stimulation on detrusor selective electrodes was able to inhibit overactive detrusor states or excite contractions, depending on the stimulation frequency. Multielectrode arrays implanted intrafascicularly into the pudendal nerve trunk may provide a promising new clinical neuromodulation therapy for the restoration of urinary function.

6.2 Introduction

Many urinary complications can arise from nervous system injury or disease, and may include a variety of changes in the activity of the External Urethral Sphincter (EUS) and/or the detrusor bladder muscle. Neuromodulation of the Pudendal Nerve (PN) is emerging as a potential therapeutic option for the restoration of urinary control[1]. To date, the neural interfaces that have been used to investigate neuromodulation of the PN in

humans have included extraneurally placed electrodes[1-3], intraurethral electrodes[4] or surface electrodes[5,6].

Because there are multiple nerve pathways in the PN—including those that mediate reflex micturition[4,7], defecation[8], and erection[9]—a multipurpose PN stimulator would be able to selectively activate these different nerve pathways, depending on clinical needs. Computer modeling studies have shown that whole-nerve cuff electrodes could be designed and electrical stimulation delivered such that selective access to the different fascicles within the PN may be possible[10]. In addition, the frequency of electrical stimulation delivered to different PN branches can also differentially activate or inhibit neural pathways[7,11].

Intrafascicularly implanted microelectrode arrays have emerged as a neural interface that can provide high degrees of information transfer to and from the nervous system using a high-count (48-96) number of microelectrodes[12-14]. Utah Slanted Electrode Arrays (USEAs, with 6.25electrodes/mm^2) have been implanted Intrafascicularly into the canine PN and were used to selectively activate the muscles of micturition[15].

Here we extend those results by investigating whether intrafascicular electrode arrays could be used to deliver electrical stimulation to restore urinary function in three different clinical conditions: 1) to restore continence in an acute model of urinary incontinence, 2) to inhibit overactive detrusor contractions and 3) to excite detrusor contractions in underactive states. The results presented herein provide evidence that an intrafascicular PN neuroprosthesis could be used for the restoration of detrusor or EUS function in either hyporeflexive or hyperreflexive pathological states.

6.3 Materials and methods

All experiments were approved by the Institutional Animal Care and Use Committee of the University of Utah. Adult male felines (13 animals; 3-5kg) were anesthetized with Telazol (9-12mg/kg; IM) and anesthesia was maintained with isoflurane (0.25-2.0%) and alpha-chloralose (5-30mg/kg IV; every 1.5 h or as needed) during surgical and experimental procedures, respectively. Two animals (cat #s: 11 & 12) were used to investigate effects of Telazol on reflex bladder contractions the induction of anesthesia was done with isoflurane (2-4%). Alpha-chloralose solutions (1% solutions) were prepared as needed on the day of the experiment by dissolving alpha-chloralose (Alpha-Aesar) in sterile 0.9% w/v NaCl at 40-55ºC stirring on a hot plate. Solutions were maintained at 40-55ºC[18]. Lactated Ringer's solution was administered intravenously at ≤2mL/hr to hydrate the animal but to minimize urine production. Ureters were ligated near the bladder, transected proximally and allowed to drain internally in cat #s 7-9. Vital signs were monitored throughout the experiment.

A dual-lumen suprapubic catheter (12Fr, Cook Medical, Inc., Bloomington, IN, USA) was purse-string sutured into the bladder for filling and measuring bladder pressure. A syringe infusion pump (Yale Apparatus, Wantagh, NY, USA) was used to fill the bladder at constant rates (2-8ml/min). An intraurethral catheter (3.5Fr, Utah Medical Products, Midvale, UT, USA) was used to measure urethral pressure at the location of the EUS (located by performing a urethral pressure profile). Both the intraurethral and bladder pressures were measured using pressure transducers (Deltran-DPT-100, Utah Medical Products, Midvale, UT, USA) that were calibrated on each experimental day. External anal sphincter contractions were measured using EMG wires (California Fine

Wire, Model #: M146240) or by visual inspection.

Nerve trunks were exposed through dissection of the ischioanal fossa and reflection of the gluteal muscles[15]. A nerve platform was placed under the nerve and then a High electrode Density USEA (HD-USEA; 25 electrodes/mm^2: 48 electrodes in a 5×10 grid with 200 μm spacing; 300 to 800μm lengths)[12] was pneumatically implanted[19]. After implantation, the nerve and HD-USEA were wrapped in low-density polyethylene plastic wrap to keep the nerve exposure hydrated and assist in containment of the implanted electrode array[20].

Reflexive voiding was investigated in eight animals and measurements were taken of the volumes voided (V) and retained (R) in the bladder in order to calculate the voiding efficiency (VE = [V/(R+V)]*100). Periods of voiding were recorded with a foot switch. Three to five voiding trials were completed with 10min rest intervals between trials for each group: control, unilateral and bilateral nerve transection.

After implantation, each HD-USEA microelectrode was mapped to an evoked muscle response: detrusor bladder, EUS and/or external anal sphincter (EAS) contractions. Electrodes were stimulated with cathodic monophasic stimulation at amplitudes of 0.1-4.0V (steps of 0.25 – 0.5V) with 200μs pulse-widths at 30-33Hz for 5-30s durations. Stimuli were delivered via voltage-controlled stimulators (SD9, Grass Technologies, West Warwick, Rhode Island, USA). The mean electrode tip impedance was 73±54 (median = 36; n = 7 HD-USEAs; impedances >1000kOhms were considered nonworking electrodes and were excluded from the analysis). All data were collected at a 30kHz or 10kHz sampling frequency (Cerebus, Blackrock Microsystems, UT, USA), and analyzed using MATLAB (MathWorks, Inc., MA, USA) and Microsoft Excel (Microsoft,

WA, USA).

6.4 Results

6.4.1 Somatotopic and musculotopic maps of the feline pudendal nerve

Figure 6.1 shows two example maps that were generated by delivering electrical stimulation (monopolar cathodic, 30Hz, 100-200μs pulse-widths, mapped to thresholds between 0.1-2V) via individual electrodes on the HD-USEAs. The numbers of selective and nonselective electrodes were different for each implant. In one animal, selective activation of the EUS and EAS muscles could be achieved with individual electrodes (Fig.6.1A, cat #8), while the electrodes that were able to drive bladder contractions simultaneously evoked EUS and/or EAS contractions. In a different preparation (Fig.6.1B, cat #12), electrodes were found that when used to deliver stimulation could selectively activate all three of the muscles studied herein. Each implantation was done with the row of long electrodes located proximally along the nerve. Reference electrodes were wired to two of the electrodes for recording purposes not investigated in this study, and instead, an extraneural reference wire was used as the current return path for monopolar and some multipolar electrode configurations.

6.4.2 Reflexive detrusor contractions

Reflexive detrusor contractions (defined as >10cm-H_2O in amplitude) were evoked in six animals (Table 6.1; cat #s marked with 'y') by infusing saline into the bladder at 2mL/min and contractions were observed at 5-15cm-H_2O above resting pressure (Fig. 6.2A). In the other seven animals, no reflexive contractions were evoked

using any of the following strategies: constant fill rates 0.5-8mL/min; 1-3mL bolus/min; and at different time periods prior to or following alpha-chloralose dosing.

6.4.3 Reflexive voiding

Reflexive voiding was investigated in eight of the preparations (#'s: 6-13) by measuring the voiding patterns and volumes evoked by filling the bladder (2mL/min) with saline. When bilateral PNs were intact, voiding was observed in an intermittent pattern following the initial leak point, indicative of normal reflexive voiding patterns (Fig. 6.2A; cat #7). Five of the eight animal preparations (see Table 6.1) had evoked reflexive voiding during filling, and in these animals, the average leak point pressure was 14±14 cm-H_2O (mean ± std; range 3-45cm-H_2O) and the VE was 47 ± 24% (range 9-79%).

Unilateral PN transection did not result in a significant change to urinary function compared to controls (VE $p = 0.94$; leak point pressure $p = 0.82$; two-tailed heteroscedastic t-test). Following unilateral PN transection, average leak point pressure was 12±20cm-H_2O (range 4-57cm-H_2O) and average VE was 46 ± 29% (range 6-76%). Bilateral PN transection, however, resulted in constant leaking following the initial leak point in 5 of 8 cats (Table 6.1). Note that the three cats (#s 9-11) that did not have incontinence induced after bilateral nerve transections were the same three that did not have reflexive detrusor contractions or voiding. Figure 6.2B shows an example of constant leaking after the initial leak point in cat #7 after bilateral nerve transections. The average leak point pressure during filling trials for the five cats with induced incontinence was not significantly different from control ($p = 0.48$; 10±11cm-H_2O; range

3-33cm-H_2O), while the average VE was significantly increased ($p = 0.01$; 69±20%; range 41-87%).

6.4.4 Restoration of continence

Following induction of incontinence in bilaterally transected animals, electrical stimulation was delivered via HD-USEA electrodes that either selectively or nonselectively evoked contractions of the EUS. When no stimulation was applied (Fig. 6.2B), a constant voiding pattern (grey bar) occurred after the leak point and until filling stopped (right arrowhead). However, voiding stopped and continence was restored during the periods when stimulation was being delivered intrafascicularly to the PN (solid bars in Fig. 6.2C and 6.D). When stimulation was delivered over multiple 30s periods during voiding, the VE significantly decreased ($p = 0.008$; 46±18%) compared to no stimulation. Stimulation delivered via electrodes that selectively activated the bladder or the EAS were unable to eliminate leaking.

6.4.5 Inhibition of overactive bladder

In two animals (cat #s: 8 & 12) we investigated whether low frequency stimulation (10 Hz) could inhibit pudendal-to-bladder reflexes and lead to inhibition of reflexive detrusor contractions evoked after filling. Bladders were filled to threshold volumes needed to evoke the overactive bladder model, but under volumes that would evoke reflexive voiding. In each experiment, 10Hz stimulation (200μs pulse-widths, 0.4-2V, single or multielectrode stimulation via detrusor selective electrodes) was able to inhibit detrusor contractions (Figs. 6.3A and B). Inhibition lasted for at least the duration

of stimulation. Some of the trials showed longer lasting inhibition that continued after the stimulation was turned off (Fig. 6.3B). In cat #8, stimulation delivered via one electrode (electrode #20; 10Hz, 1V, 200μs pulse-widths) was able to inhibit reflexive detrusor contractions. In cat #12, inhibition was achieved by delivering stimulation via two electrodes simultaneously (electrodes 38 & 42, 10Hz, 2V, 200μs pulse-widths), while stimulation via each electrode individually did not result in detrusor inhibition. These were neighboring electrodes separated by a row and a column (≈203μm tip-to-tip separation; compare electrode locations in Fig.6.1B).

6.4.6 Excitation of underactive bladder

Robust and sustained bladder contractions (defined as >10cm-H_2O for >10s) were electrically evoked using intrafascicular PN stimulation (n = 5 successful preparations; Table 6.1). During these stimulation trials, bladders were filled to 5-15 cm-H_2O above resting pressure and below reflexive voiding volumes. Monopolar cathodic stimulation delivered via single microelectrodes resulted in robust contractions of the detrusor in cat #7 and #12 (Fig. 6.4A; cat #12; 30Hz, 1V, 200μs pulse-widths). In two preparations where reflexive detrusor contractions were unable to be evoked by filling, electrical stimulation was able to drive detrusor contractions (Figs. 6.4B-E). In three felines (#s: 1, 5 & 8), long duration (5-30s) monopolar cathodic stimulation delivered via detrusor-selective electrodes evoked only small amplitude and transient detrusor contractions (Figs. 6.4C and E; <15cm-H_2O for <5s). Increasing the amplitude of the monopolar stimulation did not increase the amplitude of the contractions. In cat #8, no robust bladder contractions could be evoked using different electrode configurations; however, this was

achieved in the other two cats using multipolar (Fig. 6.4B) or bipolar (Figs. 6.4D) electrode configurations. For multielectrode stimulation, each electrode was used to deliver cathodic stimulation with the return electrode placed extraneurally. For this experiment, each of the four electrodes was stimulated individually, then in groups of two, three or four for approximately 20s durations. Increasing the number of electrodes used to deliver the stimulation resulted in an increase in the amplitude of the evoked bladder contractions for each trial (compare Figs. 6.4B and 6.C). The amplitudes of the bladder contractions were significantly ($p<0.001$; student t-test; heteroscedastic) higher when evoked by four electrodes (19±4cm-H_2O; mean ± std; n = 19 trials) than by just one electrode (8±1cm-H_2O; n = 12 trials).

For bipolar electrode configuration trials, electrodes on the HD-USEA were used to deliver cathodic stimulation and as the return of anodic current. Figure 6.4D shows an example of a detrusor contraction evoked by a bipolar electrode configuration with the cathodic (electrode #18) and anodic (electrode #23) electrodes aligned in parallel with the nerve. Figure 6.4C shows the transient detrusor responses evoked by monopolar stimulation alone (electrode #18 as the cathode). Stimulation parameters were fixed for all electrode configurations (4V, 30Hz, 100μs pulse-width, for 15-20s durations; a suprathreshold voltage was used). Controlling longitudinal current distribution along axons using bipolar electrode configurations resulted in mean pressure increases of 25cm-H_2O for 16s durations (n = 3 different bipolar configurations used). Point source current delivered via monopolar electrodes produced mean bladder pressure increases of 8cm-H_2O for 4 s durations (n = 10 electrodes).

6.5 Discussion

6.5.1 Using HD-USEAs to map neural pathways

Somatotopic and musculotopic mapping of the PN implants showed that many different electrodes could be used to stimulate different genitourinary muscles, either selectively or nonselectively. No two implants produced maps that were the same, which was expected considering the orientation of nerve fibers and fascicles change along and between nerves[21,23]. Using different single or multielectrode configurations, different subsets of nerve fibers could be activated. Future studies are warranted to assess the ability of multielectrode arrays to also provide modulation of reflexive defecation and erection pathways.

6.5.2 Intrafascicular stimulation to restore continence

PN injury has been used as a model for urinary incontinence in female rats[24] and cats[25]. To our knowledge, this is the first study that evaluated PN transection as an acute model of incontinence in male felines. Bilateral transection resulted in significantly increased voiding efficiencies following the initial leak point. Clinical applications for pudendal neuromodulation may also include the restoration from urinary incontinence via selective stimulation of the motor fibers innervating the EUS; however, future experiments are needed to test the success of intrafascicular stimulation for the restoration of continence in chronic PN or spinal cord injured animals.

6.5.3 Intrafascicular stimulation to control overactive or underactive bladder

Whole-nerve stimulation of the PN at different frequencies can excite or inhibit the pudendal-to-bladder reflexes[7,11]. Here for the first time we have shown that intrafascicularly implanted electrodes can also activate or inhibit pudendal-to-bladder reflexes in a frequency dependent manner. Using multielectrode arrays, it was possible to use different electrodes or subsets of electrodes to drive these pathways independently.

We hypothesized that varying the current distribution along axons or subsets of axons within a fascicule using multipolar configurations may activate PN pathways differentially. Such current steering techniques presumptively increased the likelihood that adjacent Nodes of Ranvier on nearby axons experienced the voltage gradients needed to initiate action potentials[26]. Interestingly, detrusor contractions evoked by longitudinal current fields had activation latencies approximately 3sec longer than those evoked by monopolar stimulation. This may suggest that different underlying nerve pathways are involved with monopolar and bipolar electrode stimulation of pudendal-to-bladder reflexes.

6.5.4 Effects of anesthetics

In order to activate the bladder by stimulation of pudendal afferents in anesthetized animal models, alpha-chloralose is commonly used as the anesthetic agent[7,17]. However, alpha-chloralose has been shown to alter autonomic functions of the urinary system, including decreasing VE compared to decerebrate felines[27]. Despite these results, researchers have indicated this is a useful agent for studying electrical stimulation of the PN, as voiding efficiencies increase with pudendal stimulation[17]. In line with these

previous findings, we observed 46% success rates for evoking reflex detrusor contractions via filling. However, we observed lower success rates for evoking detrusor contractions via electrical stimulation (38%). These results suggest alpha-chloralose anesthetized, spinal intact animals may be an appropriate model for investigating pudendal-to-bladder reflexes as driven by electrical stimulation, but the success rates can be variable.

Telazol is a combination of a dissociative agent (tiletamine HCl) that should leave spinal reflexes intact and a muscle relaxant agent (zolazepam HCl). It may be possible that the detrusor muscle remains impacted by this agent and thus, inhibition of bladder contractile states may occur. However, the effects of this agent usually wear off < 1hr and the experiments performed herein lasted for up to 30hrs. In the two animals induced without Telazol, reflexive detrusor contractions were observed, but we were unable to electrically excite the detrusor in one animal. The small numbers of animals that did not receive Telazol are insufficient to draw conclusions on the effects of this drug on pudendal-to-bladder and/or detrusor states, and future studies are warranted. Chronic implantation of HD-USEAs into the PNs of spinalized felines may help shed light on this issue as trials could be carried out in awake animals without the potentially confounding effects of alpha-chloralose and/or Telazol.

6.5.6 Effects of HD-USEA implantation

Other factors that may contribute to our low success rate for electrically driving detrusor contractions may include damage to the nerve fibers following HD-USEA implantation. In acute studies, Mathews et al. have shown that there is a 38% average

decrease in nerve compound action potentials following implantation of HD-USEAs into rat sciatic nerve, with a 12% chance in the loss of entire signals[20]. Thus, this nerve damage may be a factor when using HD-USEAs to investigate intrafascicular stimulation of the PN in acute studies. In chronic studies, HD-USEAs have been shown to cause transient sensorimotor deficits in rats implanted for 8 weeks; however, viable neurons (normal & presumptive regenerating) were found within proximities of the electrode tips that would be needed for stimulation and recording[28].

6.5.7 Potential for translational use

The access to the human PN has been well characterized and the branching patterns are indicative of a common PN trunk found near the level of the sacrotuberuous ligament[23]. Therefore, it should be possible to implant intrafascicular microelectrode arrays with longer electrodes[14] into the human PN trunk. In recent work, we were able to show that HD-USEAs were able to selectively detect different genitourinary stimuli, such as bladder fullness, bladder contractions, and tactile stimulation[29]. Future multielectrode PN devices should be able to combine the ability to selectively detect different states, and then activate different stimulation paradigms to excite or inhibit different genitourinary muscles. Such a closed-loop device[30] may be a promising addition to clinical PN neuromodulation therapies.

6.6 Conclusion

The results of this study demonstrate that intrafascicular electrode arrays implanted into the PN trunk provide effective neuromodulation of the urinary muscles in

acute models of incontinence, overactive bladder and underactive bladder.

6.7 Acknowledgments

This work was supported by the National Science Foundation (CBET -1134545) and the University of Utah Undergraduate Research Opportunity.

Table 6.1: Summary of feline experimental results

Feline#	Reflexive Detrusor Contractions	Electrical Detrusor Contractions	Reflexive Voiding
1	n	y	-
2	y	n	-
3	y	n	-
4	n	n	-
5	n	y	-
6	n	n	y
7	y	y	y
8	y	y	y
9	n	n	n
10	n	n	n
11	n	n	n
12	y	y	y
13	y	n	y
Result Totals:	6	5	5
Percent Success:	46	38	63

y = yes, experiments succesfull in evoking given response

n = no, experiments not succesful in evoking given response

- = not investigated

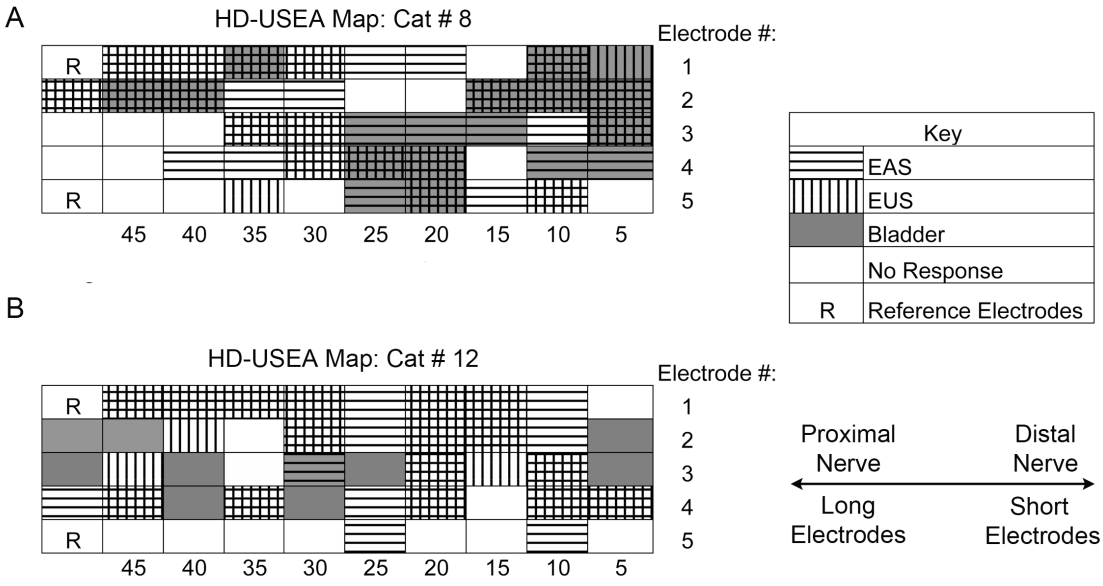

Figure 6.1. Intrafascicular microelectrodes selectively and nonselectively activated direct and reflexive nerve pathways in the PN trunk. After implantation of an HD-USEA into a PN, electrical stimulation was delivered via individual electrodes in order to map the genitourinary response(s) evoked by each electrode. Example maps are shown for two different implants (A- cat #8; B- cat #12) that evoked selective and nonselective muscle contractions including: the external anal sphincter (EAS, horizontal lines), external urethral sphincter (EUS, vertical lines) or detrusor bladder (grey boxes). Arrays were implanted such that the longest electrodes were located proximally along the nerve. The wire bundle came off of the array substrate parallel to the nerve and on the short electrode end. Electrode number configurations were the same across all devices.

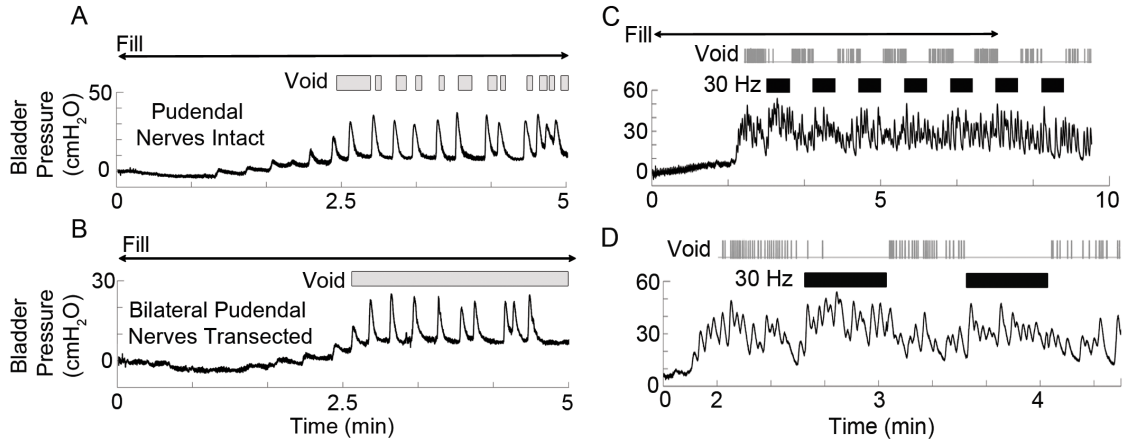

Figure 6.2. Modeling of incontinence and restoration of continence due to overactive bladder. (A) Infusion of saline (2 mL/min) into the bladder (black arrow labeled 'Fill') evoked reflexive contractions of the bladder once a threshold volume was reached (data from cat #7; leak point volume = 4.8 mL). In five animal preparations, these contractions caused leaking of the bladder (grey rectangles labeled 'Void') and this state was used as a model of incontinence due to overactive bladder. The mean VE across all animals with intact PNs was 47 ± 24%. (B) After bilateral PN transection, the voiding pattern changed from intermittent leaking to constant leaking (data from cat #7). Across all animals, the VE significantly increased ($p = 0.011$; mean = 69±20%) compared to animals with bilateral nerves intact. (C) Delivery of electrical stimulation to motor fibers in the PN (black bars; 30 Hz, 3V, 200 μs pulse-width durations) via a nonselective HD-USEA electrode (#9) resulted in contraction of the EUS and eliminated voiding for the duration of stimulation (data from cat #12). (D) Magnification of the first two stimulation periods from (C).

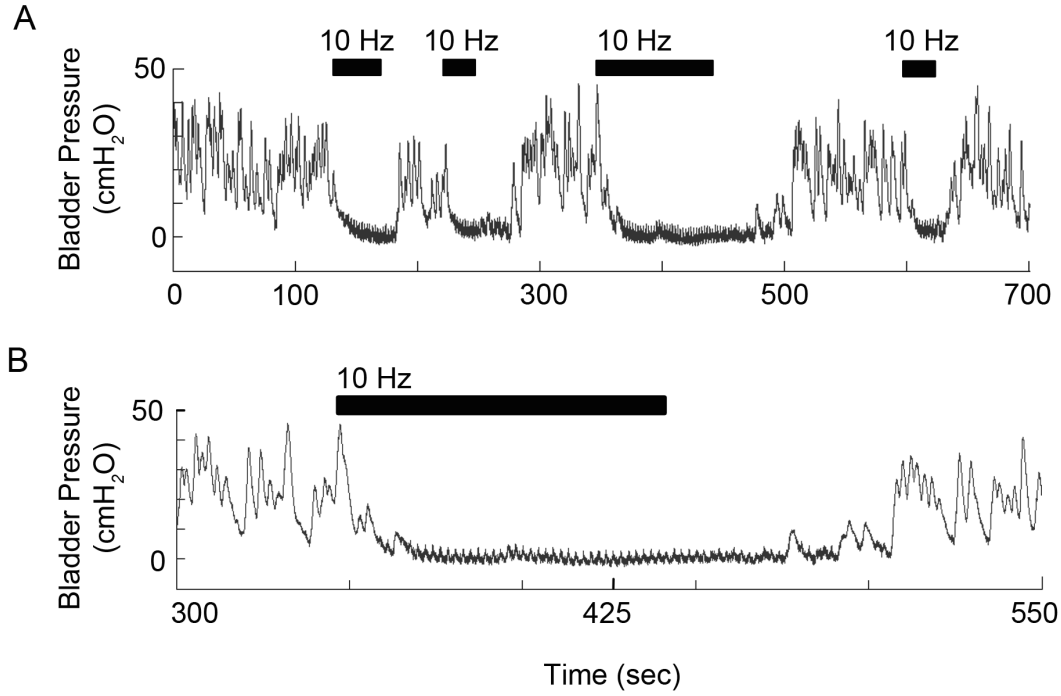

Figure 6.3. Selective inhibition of detrusor contractions in a model of overactive bladder. (A) Lower frequency stimulation (10 Hz, 1V, 200 μs pulse-width cathodic; black bars) delivered via two HD-USEA electrodes simultaneously (electrode #'s 38 & 42) during distension-evoked bladder contractions was able to inhibit contractions for the duration of stimulation and for varying periods after stimulation was turned off. (B) Magnification of the third stimulation period shown in (A). Oscillations in the pressure trace when no detrusor contractions were occurring (during stimulation) were due to mechanical ventilation of the animal. Data from cat #12

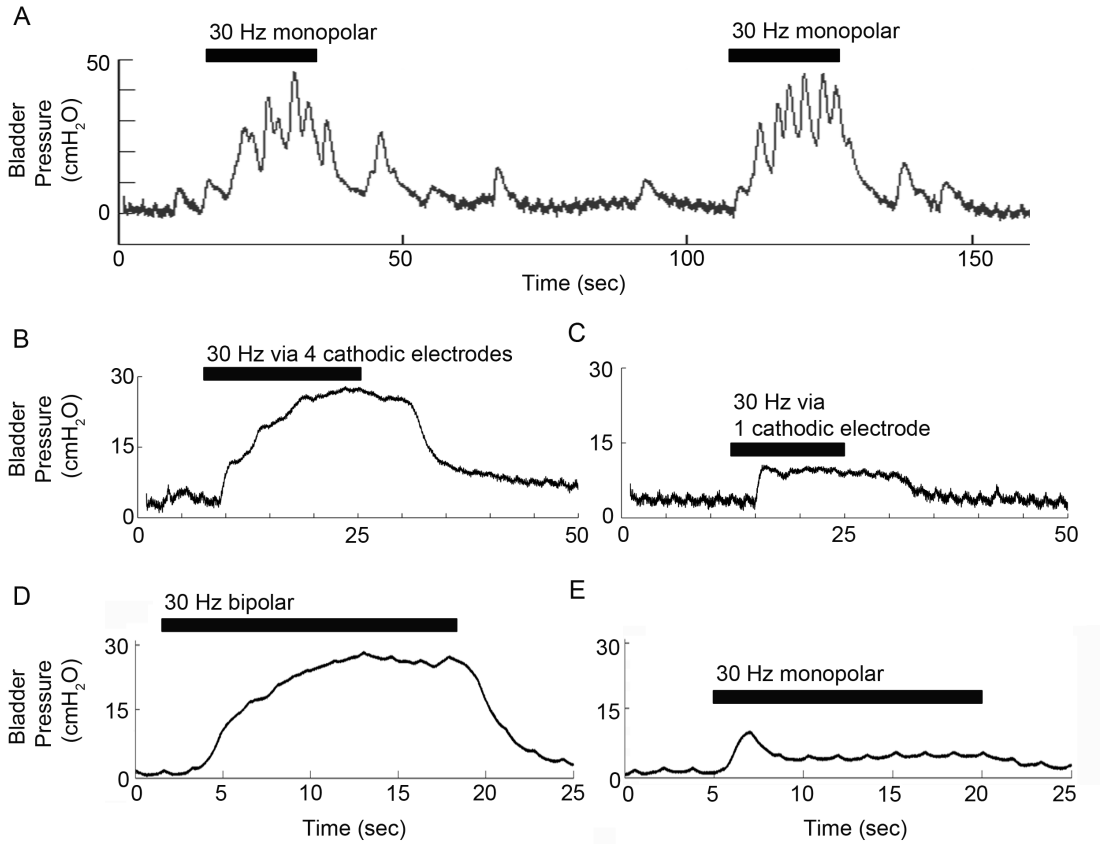

Figure 6.4. Selective excitation of the detrusor during underactive bladder states. Electrical stimulation (30 Hz) was able to drive detrusor contractions depending on the frequency of stimulation and the type of current delivered to the nerves. The electrode configuration needed to evoke more robust bladder contractions (>15 cm-H_2O) changed for different implants. (A) Monopolar stimulation (1 V with 200 μs pulse-widths) was able to evoke detrusor contractions for the duration of stimulation (cat #12). (B) Stimulation (3.5 V with 200 μs pulse-widths) delivered simultaneously using four HD-USEA electrodes (#'s: 6, 7, 12, 13) was able to evoke robust contractions for the duration of stimulation (cat #5). (C) However, when those same electrodes were stimulated in groups of three, two or single electrodes, the amplitude of the evoked detrusor contraction was decreased. Increasing the amplitude of stimulation on a single electrode did not drive robust bladder contractions that were comparable to multielectrode stimulation (cat #5). (D) Bipolar electrode configurations were used to deliver stimulation that evoked detrusor contraction. (cat #1). (E) However, in this same preparation monopolar stimulation (4V with 100 μs pulse-widths) was unable to evoke detrusor contractions for the duration of stimulation or that were as robust in amplitude. Stimulation train durations are marked with black bars. Oscillations in the pressure trace are due to mechanical ventilation of the animal. Before stimulation was delivered, bladders where filled with saline to 5-10 cm-H_2O above resting pressure or before any robust reflexive detrusor contractions were evoked.

6.8 References

1 Peters KM, Killinger KA, Boguslawski BM, et al. Chronic pudendal neuromodulation: expanding available treatment options for refractory urologic symptoms. Neurourol Urodyn 2010;29:1267–1271.

2 Yoo PB, Klein SM, Grafstein NH, et al. PN stimulation evokes reflex bladder contractions in persons with chronic spinal cord injury. Neurourol Urodyn 2007;26:1020–1023.

3 Spinelli M, Malaguti S, Giardiello G, et al. A new minimally invasive procedure for PN stimulation to treat neurogenic bladder: description of the method and preliminary data. Neurourol Urodyn 2005;24:305–309.

4 Gustafson KJ, Creasey GH, Grill WM. A urethral afferent mediated excitatory bladder reflex exists in humans. Neurosci Lett 2004;360:9–12.

5 Opisso E, Borau A, Rodríguez A, et al. Patient controlled versus automatic stimulation of PN afferents to treat neurogenic detrusor overactivity. J Urol 2008;180:1403–1408.

6 Vodusek DB, Light JK, Libby JM. Detrusor inhibition induced by stimulation of PN afferents. Neurourol Urodyn 1986;5:381–389.

7 Boggs JW, Wenzel BJ, Gustafson KJ, et al. Frequency-dependent selection of reflexes by pudendal afferents in the cat. J Phys 2006;577:115–126.

8 Bock S, Folie P, Wolff K, et al. First experiences with PN stimulation in fecal incontinence: a technical report. Tech Coloproctol 2010;14:41–44.

9 Pescatori ES, Calabro A, Artibani W, et al. Electrical stimulation of the dorsal nerve of the penis evokes reflex tonic erections of the penile body and reflex ejaculatory responses in the spinal rat. J Urol 1993;149:627–632.

10 Kent AR, Grill WM. Model-based analysis and design of nerve cuff electrodes for restoring bladder function by selective stimulation of the PN. J Neural Eng 2013;10:6010.

11 Tai C, Smerin SE, de Groat WC, et al. Pudendal-to-bladder reflex in chronic spinal-cord-injured cats. Exp Neurol 2006;:1–10.

12 Wark HAC, Sharma R, Mathews KS, et al. A new high-density (25 electrodes/mm^2) penetrating microelectrode array for recording and stimulating submillimeter neuroanatomical structures. J Neural Eng 2013;10:5003.

13 Rousche PJ, Normann RA. Chronic recording capability of the Utah Intracortical Electrode Array in cat sensory cortex. J Neurosci Methods 1998;82:1–15.

14 Branner A, Stein RB, Normann RA. Selective stimulation of cat sciatic nerve using an array of varying-length microelectrodes. J Neurophys 2001;85:1585–1594.

15 Wark HAC, Dowden BR, Cartwright PC, et al. Selective activation of the muscles of micturition using intrafascicular stimulation of the PN. IEEE Emerg Selected Topics Circuits Syst 2011;1:631–636.

16 Boggs JW. Spinal micturition reflex mediated by afferents in the deep perineal nerve. J Neurophys 2005;93:2688–2697.

17 Yoo PB, Woock JP, Grill WM. Bladder activation by selective stimulation of PN afferents in the cat. Exp Neurol 2008;212:218–225.

18 Silverman J, Muir WW. A review of laboratory animal anesthesia with chloral hydrate and chloralose. Lab Anim Sci 1993;43:210–216.

19 Rousche PJ, Normann RA. A method for pneumatically inserting an array of penetrating electrodes into cortical tissue. Ann Biomed Eng 1992;20:413–422.

20 Mathews KS, Wark HAC, Normann RA. Assessment of rat sciatic nerve function following acute implantation of High Density Utah Slanted Electrode Array (25 electrodes/mm 2) based on neural recordings and evoked muscle activity. Muscle Nerve 2014;*in press*. published online: doi:10.1002/mus.24171.

21 Mariano TY, Boger AS, Gustafson KJ. The feline dorsal nerve of the penis arises from the deep perineal nerve and not the sensory afferent branch. Anat Histol Embryol 2008;37:166–168.

22 Gunalan K, Warren DJ, Perry JD, et al. An automated system for measuring tip impedance and among-electrode shunting in high-electrode count microelectrode arrays. J Neurosci Methods 2009;178:263–269.

23 Gustafson KJ, Zelkovic PF, Feng AH, et al. Fascicular anatomy and surgical access of the human PN. World J Urol 2005;23:411–418.

24 Peng C-W, Chen J-JJ, Chang H-Y, et al. External urethral sphincter activity in a rat model of PN injury. Neurourol Urodyn 2006;25:388–396.

25 Bernabé J, Julia-Guilloteau V, Denys P, et al. Peripheral neural lesion-induced stress urinary incontinence in anaesthetized female cats. BJU Int 2008;102:1162–1167.

26 Rattay F. Analysis of models for extracellular fiber stimulation. IEEE Trans Biomed Eng 1989;36:676–682.

27 Rudy DC, Downie JW, McAndrew JD. Alpha-chloralose alters autonomic reflex function of the lower urinary tract. Amer J Phys: Reg Integ Comp Phys 1991;261:R1560–R1567.

28 Wark H, Mathews KS, Normann RA, et al. Behavioral and cellular consequences of high-electrode count Utah Arrays chronically implanted in rat sciatic nerve. *In revision* J Neural Eng Apr 2014.

29 Mathews KS, Wark H, Warren DJ, et al. Acute monitoring of genitourinary function

using intrafascicular electrodes: selective PN activity corresponding to bladder filling, bladder fullness, and genital stimulation. *In press* Urology Apr 2014.

30 Wenzel BJ, Boggs JW, Gustafson KJ, et al. Closed loop electrical control of urinary continence. J Urol 2006;175:1559–1563.

CHAPTER 7

USING A HIGH ELECTRODE COUNT INTRAFASCICULAR PERIPHERAL NERVE INTERFACE TO RESTORE MOTOR CONTROL AND SENSORY FEEDBACK IN HUMANS WITH TRANSRADIAL AMPUTATIONS

In review with Journal of Neuralengineering April 2014

Contributing Authors:

Wark HAC*, Davis T*, Hutchinson DT, Warren DJ, O'Neill K, Scheinblum T,

Clark GA, Normann RA, Greger B

*co-first authors

Author contributions: implantation of electrodes by DTH; design of and carrying out the experiments by HACW, TD, RAN, GC, BG; data analysis by HACW, TD, DJW, KO, TS; writing of the manuscript by HACW; preparation of figures by TD; editing of the manuscript by all authors.

7.1 Abstract

Modern prosthetic arms/hands have been developed, which are capable of greater than 20 Degree Of Freedom (DOF) movements. An important goal of neuroprosthetic research is to establish bidirectional communication between the user and high-DOF prosthetic limbs. Having intuitive neural control of, and sensory feedback from, high-DOF prosthetic limbs is critical to their effective utilization. One strategy for achieving this goal is to interface the prosthetic limb directly with efferent and afferent fibres in the peripheral nervous system using an array of intrafascicular microelectrodes. A high electrode count microelectrode array may provide the large number of sufficiently independent neural signals needed to control a high-DOF prosthetic limb. A high electrode count microelectrode array may also enable the selective stimulation of afferent fibres needed to evoke discrete sensory percepts across the phantom-limb. Here we report the initial results of the first one-month implantations of microelectrode arrays into the median or ulnar nerves in two subjects that had undergone transradial amputations thirty-one and one-and-a-half years prior to the study, respectively. Using a Kalman filter to decode neural activity recorded by the microelectrode arrays that was correlated with volitional phantom finger movements, the subjects were able to proportionally control the fingers of a virtual robotic hand. Furthermore, when electrical microstimulation was

delivered via individual electrodes, sensory percepts of varying sizes and qualities were perceived as originating from loci distributed over the phantom hand. Modulating the stimulation parameters altered the quality of the percepts, and simple patterns of percepts could be evoked when electrical stimulation was simultaneously delivered via multiple electrodes. This study demonstrated that a high-count intrafascicular microelectrode array can be subchronically implanted into the human peripheral nervous system and provide intuitive and dexterous control of an artificial limb with sensory feedback.

7.2 Introduction

The volitional control of movement involves a complex hierarchy of motor and sensory neural systems. Our understanding of these complex systems has been facilitated with arrays of microelectrodes that have been implanted at various levels in this hierarchy to record the spatiotemporal patterns of neural activity that correlate with motor behaviours. Early efforts to obtain volitional control signals from the cortex were conducted in nonhuman primates, where the control of external devices has been achieved by decoding neural activity patterns recorded with microelectrodes implanted in the motor cortex of nonhuman primates [1-6]. Researchers have begun translating these efforts to human subjects, and electrode arrays implanted into the motor cortex of people with paralysis have provided the unidirectional communication needed for the volitional control of external devices such as the two-dimensional movements of computer cursors [7-9] and the manipulation of objects in three-dimensional space with robotics [10]. Although the central nervous system is an effective implantation site for people with paralysis, alternative strategies are warranted for people with amputations, such as

peripheral nerve targeted reinnervation [11, 12] or peripheral nerve electrode implantation [13-19].

The current gold standard for people with upper-limb amputations are mechanically or myoelectrically controlled prosthetic arms with few DOF that do not provide sensory feedback [20]. Next generation prosthetic arms are being developed with upwards of 26 DOF [21, 22] and with embedded sensors capable of providing sensory feedback to the user [13, 19, 23]. Several strategies are being investigated for providing sensory feedback from these new prosthetic limbs including surface vibrators [23], and extraneural [17, 18, 24, 25] or intraneural [19, 26-29] electrodes. Motor intent has been decoded online and offline [13, 19, 30] with achievement of up to three DOF of control [13], and sensory feedback has been provided via electrical stimulation [13, 14, 16, 19, 23] with the evocation of up to nine different percepts [19]. To date, neural interfaces have successfully used one electrode [13, 16], six electrodes [30], sixteen electrodes [19], and twenty electrodes [28] to established bidirectional communication with a subject's peripheral nervous system. In order to provide intuitive dexterous control of modern high-DOF prosthetic arms and hands it is likely that a high number of electrodes (i.e., more electrodes than the DOF being controlled) capable of conveying sufficiently independent control and feedback signals will be required.

We report herein an approach for the control of prosthetic limbs using a high-electrode count intrafascicular array, the Utah Slanted Electrode Array (USEA) [27]. This work was conducted in two subjects who had previously undergone transradial amputations. The subjects each had a microelectrode array implanted in either their median (Subject 1) or ulnar (Subject 2) nerve in order to selectively access individual or

small groups of motor and sensory fibres within the distal end of their transected peripheral nerve. Selective spatiotemporal neural activity patterns were recorded when subjects were asked to make volitional movements of their phantom fingers. Closed-loop neural control of multiple cursors or virtual robotic fingers was achieved in each subject with two DOF control achieved online for both subjects, and up to 13 DOF control achieved offline using the data from Subject 2. Electrical stimulation delivered via individual electrodes evoked distinct sensory percepts that were distributed over the subjects' phantom hands. The subjective quality of these sensory percepts could be altered through modulation of the parameters of electrical stimulation. This work demonstrated that an array of microelectrodes implanted into residual nerves of patients with a forearm amputation allows for selective access of both sensory and motor nerve fibres. These results further suggest that intuitive and dexterous control of prosthetic fingers and sensory feedback for future bidirectional prosthetic limbs can be provided using a high-electrode count intrafascicular array of microelectrodes.

7.3 Materials and methods

This study was approved by the University of Utah Institutional Review Board and the Salt Lake City Veterans Affairs Hospital Research and Development Service Center.

7.3.1 Prestudy enrolment period

Potential volunteers were evaluated for the extent by which they perceived that they were able to make specific movements with their phantom fingers. Any baseline

phantom limb sensations, including pain, were documented with the duration, frequency, and intensity (scale of 1-10, 10 being most intense phantom sensation ever perceived). Such documentation continued for the duration of the study and again at a 3-month postexplantation follow-up. Multiple movements mediated by median and ulnar nerve activity were evaluated in each volunteer and the extent of their ability to move their fingers was noted from their descriptions (e.g., Subject 1 had 'a very fluid hand' but Subject 2's phantom fingers were often 'clenched tight'). Volunteers were then given a mirror box and specific exercises to perform in order to strengthen their perceived ability to move the digits on their phantom hands. Study personnel contacted the volunteers to document any changes in the perceived control of their phantom hand, and if any decreased control or unpleasant sensation was experienced, the volunteers would have been asked to discontinue use of the mirror box. Prior to enrolment, volunteers underwent a psychosocial evaluation in order to determine if any underlying psychological disorders were present which would have excluded them from the study.

7.3.2 Nerve electrode arrays

The USEA (Blackrock Microsystems, Salt Lake City, UT, USA) has been described elsewhere [27] and consists of ninety-six electrodes with lengths ranging from 0.5 to 1.5 mm that project out from a 4 x 4 x 0.3 mm substrate. Lead wire lengths from the connector (ZIF Clip Connector, Tucker Davis Technologies, Inc., Alachua, FL) to the array were configured for implantation into the upper limb nerves at a transradial location and included 1) 96 electrode lead wires to the 96 electrodes used for recording (9 cm long), 2) four electrode lead wires to four electrodes tied to one reference channel, which

were available as backup references but were not used for amplification 3) two low impedance platinum reference wires tied to one reference channel, which were used for amplification (≈8.5 cm long) and 4) two low-impedance platinum ground wires tied to the same ground (≈7.5 cm long). Approximately 10 mm of the distal ends of the reference and ground wires were twisted, looped back, the ends were secured onto the proximal reference or ground wires with silicone (MED-4211, NuSil Technology LLC, Carpinteria, CA, USA), and then the loops were deinsulated to make them low-impedance. The length of the reference and ground wires was measured from the base of the connector to the end of the distal loop. The reference and ground wires were placed inside the nerve wrap (see section 2.3 surgical procedures) near the electrode array. Before implantation, the electrodes on each device had an average (mean ± std) impedance of 75 ± 57 kΩ (Subject 1, median nerve) and 90 ± 28 kΩ (Subject 2, ulnar nerve).

7.3.3 Surgical procedures

The two volunteers with previous transradial amputations underwent implantation for one month with a USEA into their median (Subject 1, 31 yrs postamputation) and ulnar (Subject 2, 1.5 yrs postamputation) nerves. The distal nerve end was exposed and the implant site was selected such that it was distal to any branching points and proximal to the transitional zone adjacent to the neuroma (approximately 5-10 mm from the neuroma). The USEA was then passed transcutaneously via a trocar (7-8 mm diameter) down to the exposed implantation site. A metal platform was placed underneath the nerve, along with a high visibility background and a reconstituted organic nerve wrap

(AxoGuard Nerve Wrap, AxoGen Inc., Alachua, FL). The lead wires were then sutured (8-0 nylon) to the epineurium (≈5 mm from the base of the electrode array) and then the USEAs were inserted with a pneumatic insertion device [31] hand-held by the surgeon. The implanted USEA, reference wires, ground wires, and nerve were contained within the organic nerve wrap, which was closed snuggly around the implant site with titanium vascular clips (Figure 7.1(a-b)). The organic nerve wrap was sutured (8-0 nylon) to the epineurium proximal and distal to the array site to prevent movement of the wrap along the nerve.

The percutaneous site was dressed with an antibacterial patch (1" diameter Biopatch, clorohexadine, Ethicon Inc., Johnson & Johnson). In Subject 2, the connector was sutured down to the skin to prevent stress on the lead wires due to movement of the connector. The entire percutaneous site was layered with gauze and covered with a breathable and waterproof transparent dressing (Tegaderm, 3M Healthcare). The gauze and film dressing was changed during each experimental session and antibacterial patches were replaced every 7-10 days. To decrease the inflammatory process and potentially assist in enhanced signal quality over time, subjects were given dexamethasone (0.1 mg/kg IV, intraoperatively after removal of the tourniquet) and minocycline (100 mg BID, 2 days prior and for 5 days after surgery) [31, 32].

Both subjects underwent explantation of the USEAs under general anesthesia at the end of one month. The percutaneous connector was cut at the level of the skin and the entire limb was then prepared for surgery. Implant sites were exposed, the lead, reference and ground wires were cut just prior to their entry into the organic nerve wrap containment system, and all wires were removed. The entire implant site and neuroma

was excised and placed in 4% Paraformaldehyde for subsequent histological analysis. The new nerve end was then sutured deep in the surrounding musculature according to standard surgical procedures for neuroma excisions.

7.3.4 Data acquisition and analysis

Two-hour experimental sessions were performed on an average of three times a week. The time was limited by the availability of the subjects or their willingness to continue testing (Subject 1 underwent 12 total experimental sessions: 6 electrophysiological recording sessions and 8 microstimulation sessions; Subject 2 underwent 14 total experimental sessions: 13 electrophysiological recording sessions and 8 microstimulation sessions). All experimental sessions were recorded by video camera, which was time-stamped to the neural recording or stimulation data. Neural signals were amplified and recorded using active head-stage cables (ZIF-Clip 96 channels, Tucker Davis Technologies, Inc., Alachua, FL) that connected to a custom-built board used to interface the TDT-connector with a Neuroport data acquisition system (Blackrock Microsystems, Salt Lake City, UT, USA). Data were collected using Cerebus Software (Blackrock Microsystems, Salt Lake City, UT, USA). The continuous neural signals were band-pass filtered with cutoff frequencies of 0.3 Hz (1^{st} order high-pass Butterworth filter) and 7500 Hz (3^{rd} order low-pass Butterworth filter) and sampled at 30 kHz. Online multiunit activity was extracted from high-pass filtered data (250 Hz 4^{th} order Butterworth filter) by setting a threshold using the auto threshold setting in the Cerebus data acquisition software (multiplier = 3, threshold = multiplier × noise estimate of the signal). Multiunit neural firing rates were calculated using unsorted spikes and a moving

box-car average of 300 ms with an update period of 33 ms. Offline action potentials were isolated from the high-pass filtered data using commercially available software (Offline Sorter version 3, Plexon Inc., Texas, USA). Signal-to-noise ratios (SNR) were calculated by dividing the peak-to-peak action potential amplitude by two times the standard deviation of the noise.

7.3.5 Neural decodes

A standard Kalman filter was implemented to perform the continuous neural decodes [33]. This algorithm assumes a linear relationship between the kinematics (finger movements) and the neural data. For this study, it was used to provide continuous estimates of finger position based on the firing rates of multiple neurons. Sessions began by cueing the subjects to perform multiple flexions, extensions or abductions of their individual phantom fingers. A total of 4 movements were performed for Subject 1 (Thumb-Flex, Index-Flex, Middle-Flex, and Ring-Flex) and 13 movements for Subject 2 (Thumb-Flex, Thumb-Extend, Index-Flex, Index-Extend, Index-Abduct, Middle-Flex, Middle-Extend, Ring-Flex, Ring-Extend, Ring-Abduct, Little-Flex, Little-Extend, Little-Abduct). These movements are given acronyms based on the first one or two letters of each word, which are used in subsequent figures (e.g., Thumb-Flex = TF). The subjects were instructed to make finger movements by either a computer controlled display of indicators (Subject 1) or by movement of virtual robotic fingers [34] (Subject 2). Subject 1 held a small manipulandum consisting of individual, movable pads that could be depressed by each finger with his intact hand. He was asked to mirror the movements made with his phantom fingers by pressing on the manipulandum pads with his intact

fingers. The instructed finger position (instruction variable) for Subject 1 was measured as the continuous analogue voltage signal from pressure sensors on the pads of the manipulandum. Subject 2 was instructed to duplicate the movements of the virtual prosthetic hand using her phantom hand. The instructed finger position (instruction variable) for Subject 2 was taken as the software generated position of the virtual prosthetic finger. The positions of the virtual prosthetic fingers were generated using a cosine function, which was normalized from -1 (full extension/adduction) to +1 (full flexion/abduction). Multiunit firing rates from selected electrodes and the movement instruction variables were then used to train and test the decode algorithm for both online and offline control.

For online decoding, electrodes were selected based on their ability to record movement correlated action potentials. This selection process was made using two methods: 1) the experimenters viewed a map of correlation coefficients between the instruction variables and the firing rates on each electrode and 2) the experimenters' subjective observations of the high-pass filtered neural data on each electrode during the cued movements. Following electrode selection, the decode algorithm was trained on a set of 10 trials for each movement type. For testing, subjects were asked to control a computer display of indicators (Subject 1) or virtual prosthetic fingers (Subject 2) and acquire targets in a trial-based format. During these testing trials, subjects were presented with a target of varying size and distance from a starting point. Subjects began a trial by moving the fingers of their phantom hand to a neutral at rest position, which moved the indicators or virtual prosthetic fingers to a start position. Once all fingers were at the start position for a specified hold period, subjects would be shown the target(s) to which they

were to move their finger(s). In order to correctly complete a trial, the subjects had to acquire and hold the target(s) while maintaining the fingers that were not being instructed to move at the start position. Start and target hold periods varied from 300 to 5000 msec. This task format assessed the ability of subjects to move the virtual fingers/cursors independently. Targets were placed at various distances to assess the ability of the subjects to proportionally control the indicators or virtual fingers.

For offline decoding, an average of 22 (13-37) trials of each movement type recorded during a typical experimental session were analyzed. Electrodes were chosen based on the results of a Wilcoxon signed-rank test. First, a 'baseline period' was defined as 2 sec prior to the onset of the movement cue, while a 'movement period' was defined as the 2 sec after the onset of the cue. Then, the difference in median firing rates was calculated between the 'movement period' and the 'baseline period' for all movement types recorded on each electrode. This was repeated for all movement trials across all electrodes. The null hypothesis was that the data came from a continuous, symmetric distribution with a median equal to zero (i.e., no electrode recorded increased firing rates in the movement period compared to the baseline period). All electrodes for which the null hypothesis was rejected ($p<0.001$) with a positive median difference from baseline were kept. These electrodes were then sorted in order of increasing median difference and the top 90% of electrodes were used in the offline decode. After electrode selection, the decode algorithm was trained on the first 10 trials for each movement and tested on the remaining trials. A Pearson's correlation coefficient between the instruction variable and the Kalman filter estimate was used to quantify decode performance.

7.3.6 Neural stimulation, percept mapping, and analysis

Current-controlled, biphasic, cathodic-first (without anodic bias) stimulation [35] (IZ2, 128-Channel Tucker-Davis Technologies Stimulator, Inc., Alachua, FL) was delivered to individual or subsets of electrodes using custom LabVIEW software (National Instruments Corp., Austin, TX). The stimulator battery had a compliance voltage of ± 15V (LZ48-400, Tucker-Davis Technologies Stimulator, Inc., Alachua, FL). Maximum stimulation was limited by either: 1) the comfort level of the subject, 2) a perceived change in the quality of the percept or 3) if the maximum safety limit for delivering electricity to tissue was reached [36]. The safety limit for injecting charge into the tissue was determined by measuring the maximum cathodic voltage excursion (with a limit of -0.6V) across the electrode and ground during stimulation [37-39]. Stimulation parameters varied depending on the objective of the experimental session. Pulse amplitude, frequency, and train duration ranged from 1-100 μA, 1-320 Hz, and 0.2-60 sec, respectively. Pulse width and interphase interval were held fixed at 200 μs and 100 μs.

In Subject 1, stimulation experiments were focused on a subset of electrodes to investigate the subject's ability to detect and discriminate single and multiple sensory percepts and the effects of modulating stimulation frequency on sensory percepts. Using a custom-built software interface, Subject 1 was allowed to control the amplitude, i.e., the level of current per pulse (1-100 μA in steps of 1 μA), to determine the threshold or minimum level needed for detection using a frequency of 200 Hz and train duration of 0.2 sec (sessions 1-8, postimplant days 5-26). Additionally, Subject 1 was allowed to control the frequency of the microstimulation pulses (1-320 Hz in steps of 1 Hz) by

pressing down on a pressure sensor mounted on the manipulandum with a finger from the intact hand (sessions 4-8, postimplant days 14-26). The amplitudes for these sessions were set at the previously determined 200 Hz threshold level, and pulses were delivered continuously for up to 60 sec.

In Subject 2, the first six stimulation sessions (postimplant days 6-25) were focused on investigating the thresholds and percepts evoked by delivering stimulation to individual electrodes across the entire array at a constant frequency of 200 Hz and train duration of 0.2 sec. The last two sessions (postimplant days 26 and 27) were focused on investigating the threshold and percepts evoked by lower frequency stimulation (20 Hz) using a train duration of 2 sec. Subject 2 was allowed to control when stimulation was delivered, but the experimenter controlled the amplitude (1-100 μA in steps of 1-5 μA) and pulse train duration (0.2 or 2 sec).

Both subjects indicated the location, size, and quality of the percept on anterior and posterior images of a hand. The subjects could choose the quality of the percept from a list (tingle, pressure, vibration, hot, cold) or they could define the quality using their own words. Subject 1 made these indications by marking on a sheet of paper, while subject 2 marked digitally using a mouse. When a percept was faint or the subject was unsure of the sensation, they could repeat stimulation until they were sure the percept was electrically evoked (as opposed to a phantom limb sensation).

In order to investigate to what extent the percepts remained stable over consecutive stimulation sessions, all of the electrodes that evoked a percept during each stimulation session when the entire array was stimulated at 200 Hz were analysed (postimplant days 10-25; Subject 2). A percept was considered stable if it remained in a

localized anatomical region of the phantom hand, defined as one of the following: anterior or posterior of a particular finger, the palm, or the back of the hand. If a portion of an evoked percept was located on the border differentiating two anatomical locations (e.g., over the metacarpophalangeal joint), the percept was considered within the location where the majority of the sensation occurred; however, if the size of the percept spread beyond the border then the percept was not considered stable.

7.4 Results

7.4.1 Device performance

For Subject 1, the mean *in vivo* impedance for working electrodes (measured at 1 kHz) over the 29-day implant was 222 ± 133 kΩ (mean ± std, n=7 sessions). Likely due to mechanical failure of the lead wires, the number of working electrodes (defined as electrodes with impedance < 500 kΩ) dropped from 96 to 20 by the end of week two, and then to four by the end of week four. In Subject 2, the percutaneous connector was sutured to the skin to minimize strain applied to the wires. The mean electrode impedance for working electrodes over the 31-day implant for this subject was 143 ± 76 kΩ (mean ± std, n=13 sessions), and the number of working electrodes was 87 ± 5 (mean ± std).

7.4.2 Neural recordings and decoding phantom finger movements

Neural recordings were made while the subjects were asked to make volitional flexion, extension or abduction movements of their phantom fingers. Several electrodes recorded action potentials over the course of the study (Figure 7.1(c-d)). In Subject 1, an average of 7 ± 9 electrodes recorded action potentials for the 6 recording sessions with a

maximum of 20 electrodes recording action potentials on postimplant day three (Figure 7.1(e). In Subject 2, an average of 22 ± 7 electrodes recorded action potentials for the 13 recording sessions with a maximum of 40 electrodes recording action potentials on postimplant day seven (Figure 7.1(f)). The mean SNR of these action potentials for all sessions was 5 ± 2 (Figure 7.1(e)) and 5 ± 3 (Figure 7.1(f)).

Subjects were cued to make the movements by a computer cursor or by movement of virtual robotic fingers (Figure 7.2(a-b)). The intent to flex or extend individual phantom digits produced spatiotemporal neural firing patterns that were visible in the high-pass filtered data (Figure 7.2(c-d)). The patterns of neural activity varied across electrodes and movement types. Some electrodes recorded action potentials that were correlated with a single movement type (Figure 7.2(c), flexion, electrode 44) or movement of a single digit (Figure 7.2(d), thumb, electrode 88), whereas other electrodes recorded action potentials that correlated with multiple different fingers and movement types (Figure 7.2(d), electrodes 13 & 44).

7.4.2.1 Multiple DOF movements could be decoded offline. Predicted finger positions showed high correlations (R = 0.9) with the instruction variables for the best 2 DOF in Subject 1 and best 4 DOF in Subject 2 (Figure 7.2(e-f)). Prediction accuracy decreased as the number of predicted movements or DOF increased (Figure 7.2(g-h)), but trended toward an asymptote of R≈0.5 at 13 DOF for Subject 2 (Figure 7.2(h)). To validate the decode results, the electrode order was randomly shuffled between the training and testing sets, and the firing rate data was decoded again. Using this shuffled data, the prediction accuracy dropped to R=0.14 for 13 DOF (Subject 2). For Subject 2, the median decode performance for seven sessions spanning 23 days for eight different

movements (8 DOF) was R=0.62 ± 0.07 (the five finger extension movements were added on postimplantation day 13 and could not be included in this analysis). Decoding data overtime for Subject 1 were not analyzed as impedances on most electrodes went out of specification and the electrophysiological recordings were lost on postimplant day 10.

7.4.2.2 Multiple DOF movements could be decoded online. Data recorded from the median nerve were decoded online for middle and index phantom finger flexion and the subject was able to move the cursor to targets specific to each finger individually with a median time to trial completion of 9 ± 6 sec (16 trials; 5 electrodes). Data recorded from the ulnar nerve were decoded online for thumb and little phantom finger flexions, and the subject was able to independently and proportionally control each of the virtual robotic fingers with a median time to trial completion of 2 ± 5 sec (79 trials, 4 electrodes). For both subjects, online decodes were successful in obtaining 2 DOF control (Figure 7.2(i-j)).

7.4.3 Evoked sensory percepts Subject 1: median nerve stimulation

Over the course of the study, microstimulation on 17 electrodes evoked sensory percepts approximately located in an expected median nerve distribution (Figure 7.3(a)). The mean threshold across all microstimulation sessions for evoking sensory percepts was 27 ± 20 μA (mean ± std) (Figure 3(e)).

In addition to the standard threshold detection experiments, stimulation sessions were performed where the subject was cued that a trial began, but did not know whether stimulation was delivered via either of two electrodes, both electrodes simultaneously, or no-stimulation was delivered. Such blinded-trial data were collected during three

different experimental sessions on postimplantation days 13, 19, and 26. Electrodes with different interelectrode distances were chosen, and suprathreshold stimulation amplitudes were used (Day 13: electrodes 16 and 19, 1200 μm distance, 19 μA and 25 μA thresholds; Day 19: electrodes 19 and 20, 400 μm distance, 47 μA and 18 μA thresholds; Day 26: electrodes 20 and 46, 1442 μm distance, 18 μA and 10 μA thresholds). For each trial, the subject had to record the size, location and intensity of the evoked percept. If no percept was evoked, the subject reported that he felt nothing. Across all three experimental sessions, Subject 1 correctly detected any-stimulation (stimulation on either electrode individually or both electrodes simultaneously) versus no-stimulation with 98% accuracy (58 out of 59 total trials; day 13 = 19 out of 19 trials, day 19 = 20 out of 20 trials, and day 26 = 19 out of 20 trials). Across all three experimental sessions, Subject 1 correctly discriminated between spatially distinct percepts evoked by microstimulation on the two electrodes individually (n = 5 for each electrode per session) with 87% accuracy (26 out of 30 total trials; day 13 = 9 out of 10 trials, day 19 = 8 out of 10 trials, and day 26 = 9 out of 10 trials). Spatial discrimination was accurately reported with electrodes only separated by 400 μm (day 19) (Figure 7.3(c)). Subject 1 was also able to discriminate between simple patterns of stimulation, i.e., stimulation via either electrode individually versus simultaneous stimulation via both electrodes, with 84% accuracy (38 out of 45 total trials; day 13 = 11 out of 14 trials, day 19 = 13 out of 15 trials, and day 26 = 14 out of 16 trials).

The quality of the evoked percept depended on stimulation parameters. High frequencies (100 – 320 Hz) evoked an ‘electric shock’ like quality for this volunteer, and lower frequencies (1 – 25 Hz) and longer stimulation times (up to 60 sec) could evoke

more physiological percepts (e.g., pressure) some of the time. Subject 1 was allowed to self-modulate the stimulation frequency from 1 – 100 Hz by pushing down on the manipulandum pressure sensor with his intact hand with stimulation being delivered via two electrodes at 30 μA (postimplant day 14). He noted:

(1) "As I'm pressing that down there [on the manipulandum pressure sensor] on that intensity and moving the finger a little bit…this [the sensory percept] stayed on that finger as I was moving it."
(2) "As they speed up [the stimulation frequency increasing from 1 to 100 Hz] I can feel more of the finger. … It applies pressure on the index and this finger [the tip of the ring finger on his intact hand]."
(3) Question from the experimenter: "Could you use this stimulation to recreate touch?"
Answer from Subject 1: "Definitely…The more you press it [subject pressed on manipulandum pressure sensor changing the frequency from 1 to 100 Hz] you can sense it [the phantom finger] more. … And you'll get the sense of touch, 'cause that's what you did for me."

7.4.4 Evoked sensory percepts Subject 2: ulnar nerve stimulation

Single electrode stimulation over the course of the study evoked sensory percepts approximately located in the normal ulnar nerve distribution with a mean of 81 electrodes that evoked percepts when all 96 electrodes were stimulated in Subject 2 (Figure 7.3(b)). Five of the total eight stimulation sessions (postimplant days 10-25) resulted in a complete mapping across the array at fixed parameters of 200 Hz, 0.2 ms durations, 200 μs pulse widths, and amplitudes that varied from 1-100 μA. The first stimulation session (postimplant day 6) resulted in an incomplete mapping of the array where maximum stimulation was not delivered to all 96 electrodes. The last two sessions (postimplant days 26 and 27) were mapped using a different frequency (20 Hz). These three stimulation sessions were not included in the spatial stability analysis. A total of 61 electrodes

evoked percepts across all five sessions. Out of these 61 electrodes, 18 electrodes produced percepts that were considered stable within a defined region of the phantom hand for two consecutive sessions (separated by 1-3 days). A total of eight electrodes evoked stable percepts for three consecutive sessions, four electrodes evoked stable percepts for four consecutive sessions, and three electrodes evoked stable percepts across all five stimulation sessions. Figure 7.3(d) shows examples of percepts evoked by two different electrodes over time. One of the electrodes (electrode 63) evoked a stable percept across all five sessions. The other electrode (electrode 88) was stable for two consecutive sessions. The quality of stimulation-evoked percepts in this subject combined across all five sessions included: 76 'tingle' percepts; 7 'pressure' percepts; and 216 'vibration' percepts. For the last two stimulation sessions where the array was mapped at 20 Hz, a total of 76 electrodes evoked percepts on both days, with 17 electrodes evoking stable percepts. The percept quality evoked during these sessions included: 21 'tingle' percepts; 19 'pressure' or 'hair brush' percepts; 17 'vibration' percepts; and 96 'cold' or 'air brush' percepts. The subject noted that the 'tingle' and 'vibration' percepts evoked during each session were of a 'painful' quality. Across all stimulation sessions, the mean threshold for evoking a sensory percept was 12 ± 11 μA (mean ± std) (Figure 7.3(f)).

7.4.5 Poststimulation evoked phantom limb sensations

Subjects each differentiated between phantom limb sensations (the normal feelings from their phantom hand) and phantom limb pains (percepts that were considered uncomfortable). Subjects reported an increase in the occurrence of phantom limb sensations that took on the characteristics of the sensory percepts evoked by

electrical stimulation. At times, the poststimulation sensations included percepts such as ‘pressure’ or ‘hair brushing on the skin.’ Subject 2 noted the feeling of the nonpainful poststimulation percepts in her phantom limb sensation diary:

> “I’ve had the kind of fluttering or breath-on-the-skin-or-hair-pressure that I had often in the lab session today. (Located in the web area between my PIF [phantom index finger] and PMF [phantom middle finger].) It’s as if now that the sensation has been awakened, it keeps registering, regardless of context …”

At other times, the subjects reported an increased occurrence of poststimulation evoked phantom limb sensations that were painful, and the quality of such percepts included: ‘electric shock,’ ‘stinging,’ or ‘tingling.’ For each subject, percepts (duration ≈1-2 sec) began after the first day of stimulation, and had peak occurrences of 10/hr for subject 1 and 2-9/hr for Subject 2. By 30 days postexplantation of the electrode array, both subjects no longer reported phantom sensations with the quality of stimulation-evoked percepts.

7.5 Discussion

In 2003, a human volunteer had a high-electrode count microelectrode array implanted in his median nerve for 96 days [28, 40]. The array implanted in the 2003 study had the microelectrodes arranged in a flat plane parallel to the base of the array, limiting the cross-sectional access to the nerve, and only 20 of the electrodes were wired for electrophysiological use. Therefore the full potential of a 96-electrode array could not be investigated. Furthermore, no containment system was used to protect the implanted array. Most importantly, this study was performed in a subject with an intact arm, so that the question of how much information would be available to and from a subject with an

amputation using a bidirectional neural interface for controlling an artificial limb could not be addressed.

7.5.1 Device performance

The impedances of all working electrodes remained stable for the duration of the study. In Subject 1, the impedances for the majority of the electrodes went out of specification at the end of the first week; however, four electrodes remained viable for the duration of the implant. Suturing the percutaneous connector to the skin may have reduced the chance of wire breakage in Subject 2. However, a robust percutaneous connector or a telemetry system will be needed before applications using high electrode count arrays achieve clinical utility. Work is underway to develop wireless versions of the electrode arrays described in this report [41]. The generation of microelectrode arrays used in this study have maximum electrode shank lengths of 1.5 mm, which limits the cross-sectional access to the outer region of the relatively large human peripheral nerves that are greater than 3 mm in diameter. Longer electrodes and/or multiple arrays are needed to expand electrophysiological access across the entire diameter of the nerves. A more robust containment system, an anchoring system, or a more compliant microelectrode array design may be required to achieve the very long functional lifetimes necessary for clinical applications. Additionally, not addressed in this study is the technological challenge of performing near simultaneous electrophysiological recordings and microstimulations via the same electrode or proximate electrodes.

7.5.2 Neural recordings and decoding independent and proportional phantom finger movements

The number of electrodes that recorded action potentials over time was relatively stable for Subject 2, providing evidence that the devices remained intrafascicularly implanted for the duration of the study. Both subjects were given dexamethasone and minocycline doses in order to potentially increase the quality of action potential recordings over time [31, 32]. Additional control studies are needed to investigate whether administration of these drugs can improve neural signal longevity. Previously published studies have used the rodent model.

An important aspect of any decoded signal that could be used to control a prosthetic hand is that the signals can mediate proportional control. This was investigated in two ways: using the trajectory tracking described above, and by challenging the subject to move their phantom finger to various end positions between full extension and full flexion. For both subjects, the decoded neural activity patterns provided proportional control of finger position and importantly, such control was achieved during the first recording session with each subject.

The relationship between the central representation of motor control and the kinematics of movement is complex, with activity in single neural units correlated with the movements of multiple finger muscles [42, 43]. The central and peripheral nervous systems are set up to control the synergistic biomechanics of the human hand [44], while current high-DOF prosthetic hands do not implement mechanical synergies [21, 22]. Future work needs to develop efficient mapping of these synergistic neural signals onto the nonsynergistic mechanics of high-DOF prosthetic hands.

7.5.3 Stimulation-evoked sensory percepts

The sensory feedback provided by the sensors distributed throughout the fingers and hand allow for the manipulation of complex objects in 3-D space. In this study, we explored the ability to evoke sensory percepts by injecting currents into the peripheral nerves via many of the electrodes in the implanted arrays. Translations of evoked percepts into more physiological percepts was achieved by varying the frequency and the duration of stimulation, i.e., the percept changed from an 'electric shock-like tingle' to pressure. The stability of the stimulation-evoked percepts was assessed, and the results indicate that implantations of microelectrode arrays into the peripheral nerves of amputees could provide the sensory feedback that would enable dexterous manipulation of complex objects with future generations of prosthetic hands. Future studies are warranted to investigate the stimulation parameters that evoke other sensations, such as proprioception, as well as, long duration stimulation to evoke long-lasting sensations.

7.5.4 Poststimulation evoked sensory percepts

The subjects experienced poststimulation percepts that occasionally had the uncomfortable or painful qualities of the percepts evoked by some electrical stimulation. Importantly, neither of the subjects experienced these quality of percepts prior to participating in the study. Future work may focus on optimizing stimulation parameters to produce only physiologically relevant and comfortable sensory percepts, and needs to address plasticity in the central motor and sensory neural representations [45-49].

7.6 Conclusion

Here we describe the first implantation of high-count microelectrode arrays into human peripheral nerves in subjects with forearm amputations. Electrodes recorded neural activity patterns from the residual nerves that were volitionally generated by the intention to flex, extend or abduct individual digits in the subject's missing hand. Up to thirteen movement types could be decoded and proportional control of all digits on a virtual prosthetic hand was achieved. Stimulation of up to 96 electrodes, either one-at-a-time or simultaneously, evoked multiple percepts that were widely spatially distributed across the phantom hands. The relatively large number of channels of motor and sensory information provided by the microelectrode arrays indicate that such arrays can serve as a neural interface for controlling high-DOF prosthetic limbs. Patients outfitted with a highly dexterous prosthetic limb controlled through a bidirectional peripheral nerve interface might begin to think of the prosthesis not as a piece of hardware attached to their amputated arm, but rather, as an integral extension of themselves.

7.7 Acknowledgments

Research reported in this publication was supported by (1) the National Center for Advancing Translational Sciences of the National Institutes of Health (award number 1ULTR001067 administered by the University of Utah Center for Clinical and Translational Science) and (2) the DARPA (contract number N66001-12-C-4042). The authors wish to thank the staff at their respective hospitals for their assistance in conducting this study, and most importantly the patients who selflessly participated in this research.

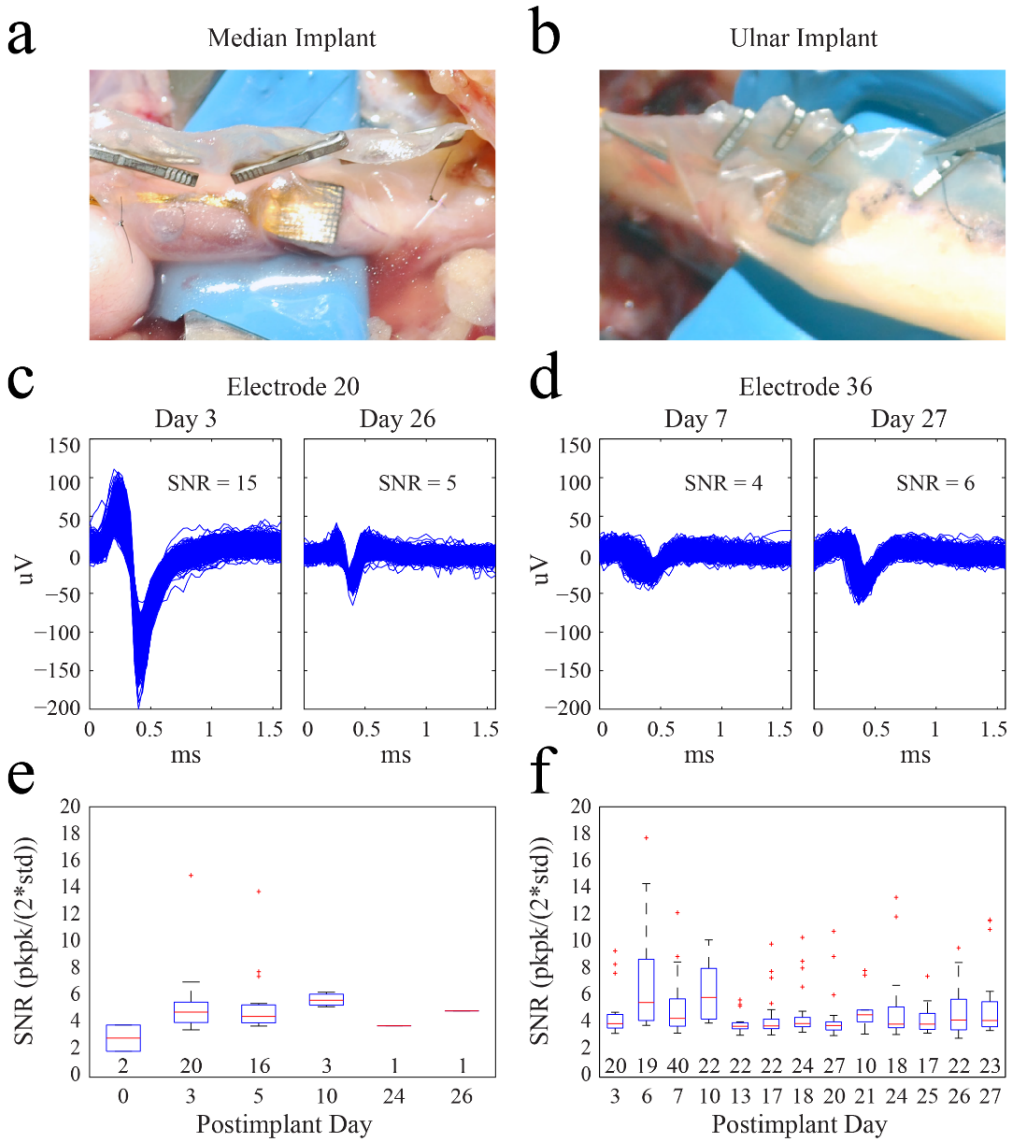

Figure 7.1. Neural signals recorded using USEAs implanted into human median and ulnar nerves. Panels (a), (c) and (e) show data from Subject 1; and panels (b), (d), and (f) show data from Subject 2. (a-b) Photographs of intrafascicular USEA implantation into the median and ulnar peripheral nerves. The device-nerve interfaces were contained within an organic nerve wrap (clear material surrounding the implant) and secured with vascular clips (3-5 clips are seen in each photo) to minimize movement of the device and allow containment of the reference wires proximal to the arrays. (c-d) Action potentials (APs) were recorded on individual electrodes for the duration of the study in both subjects, providing electrophysiological validation that the devices remained intrafascicular throughout the study. (e-f) Median signal-to-noise (SNR) for all APs recorded on all electrodes across the duration of the study. The number below each boxplot is the number of APs recorded during the experimental session.

Figure 7.2. Decoding volitional phantom finger movements from peripheral nerve action potentials. Panels (a), (c), (e), (g) and (i) show data from Subject 1; and (b), (d), (f), (h) and (j) show data from Subject 2. (a-b) Experimental setup showing each subject volitionally controlling either a computer controlled display (Subject 1) or the digit of a virtual hand (Subject 2). During the examples shown, the neural information corresponding to the phantom movement was decoded in real-time and used to control the virtual movement. (c-d) High-pass filtered, common-average referenced neural recordings (solid blue line) made by three electrodes during phantom finger movements for Subject 1 (Postimplant day 3) and Subject 2 (Postimplant day 24). Superimposed is the instructed finger movement (dashed black line). APs can be seen in the high-pass filtered data extending above and below the noise floor during the instruction period. Sorted AP waveforms are shown on the far right for each electrode. (e-f) Kalman filter predictions for the best two DOF for Subject 1 and the best four DOF for Subject 2. Prediction accuracies of 0.9 were achieved using multiunit firing rates calculated from unsorted spike events on 55 electrodes and 18 electrodes, respectively. (g-h) Kalman filter performance for all combinations of available DOF using the same electrodes as in (e-f). Red horizontal lines and blue boxes represent the median and interquartile ranges, respectively. (i-j) Kalman filter performance during real-time decode sessions for each subject. Boxes represent trial-by-trial target locations and the traces represent the Kalman filter predictions for the intended finger movement. To complete a trial, predicted movements must enter the same color box for a specified hold duration (3000 (i) and 300 (j) ms). Only a subset of trials for each subject are shown. Asterisks highlight verbally-stated volitional movements made by the subject in the absence of a target.

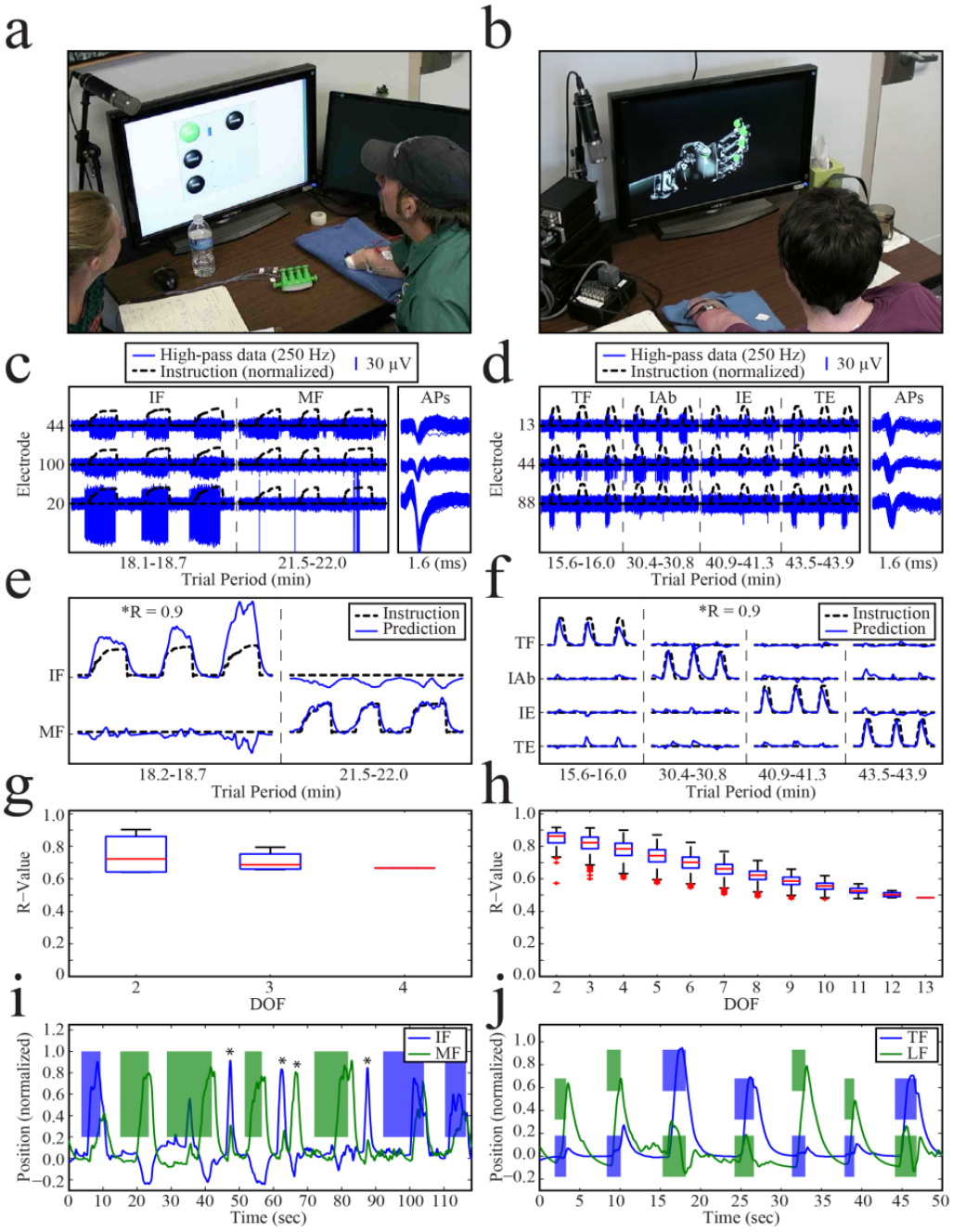
a
b
c
High-pass data (250 Hz)
Instruction (normalized)
30 µV
IF
MF
APs
Electrode
44
100
20
18.1-18.7
21.5-22.0
1.6 (ms)
Trial Period (min)
d
High-pass data (250 Hz)
Instruction (normalized)
30 µV
TF
IAb
IE
TE
APs
Electrode
13
44
88
15.6-16.0
30.4-30.8
40.9-41.3
43.5-43.9
1.6 (ms)
Trial Period (min)
e
*R = 0.9
Instruction
Prediction
IF
MF
18.2-18.7
21.5-22.0
Trial Period (min)
f
*R = 0.9
Instruction
Prediction
TF
IAb
IE
TE
15.6-16.0
30.4-30.8
40.9-41.3
43.5-43.9
Trial Period (min)
g
R-Value
DOF
h
R-Value
DOF
i
IF
MF
Position (normalized)
Time (sec)
j
TF
LF
Position (normalized)
Time (sec)

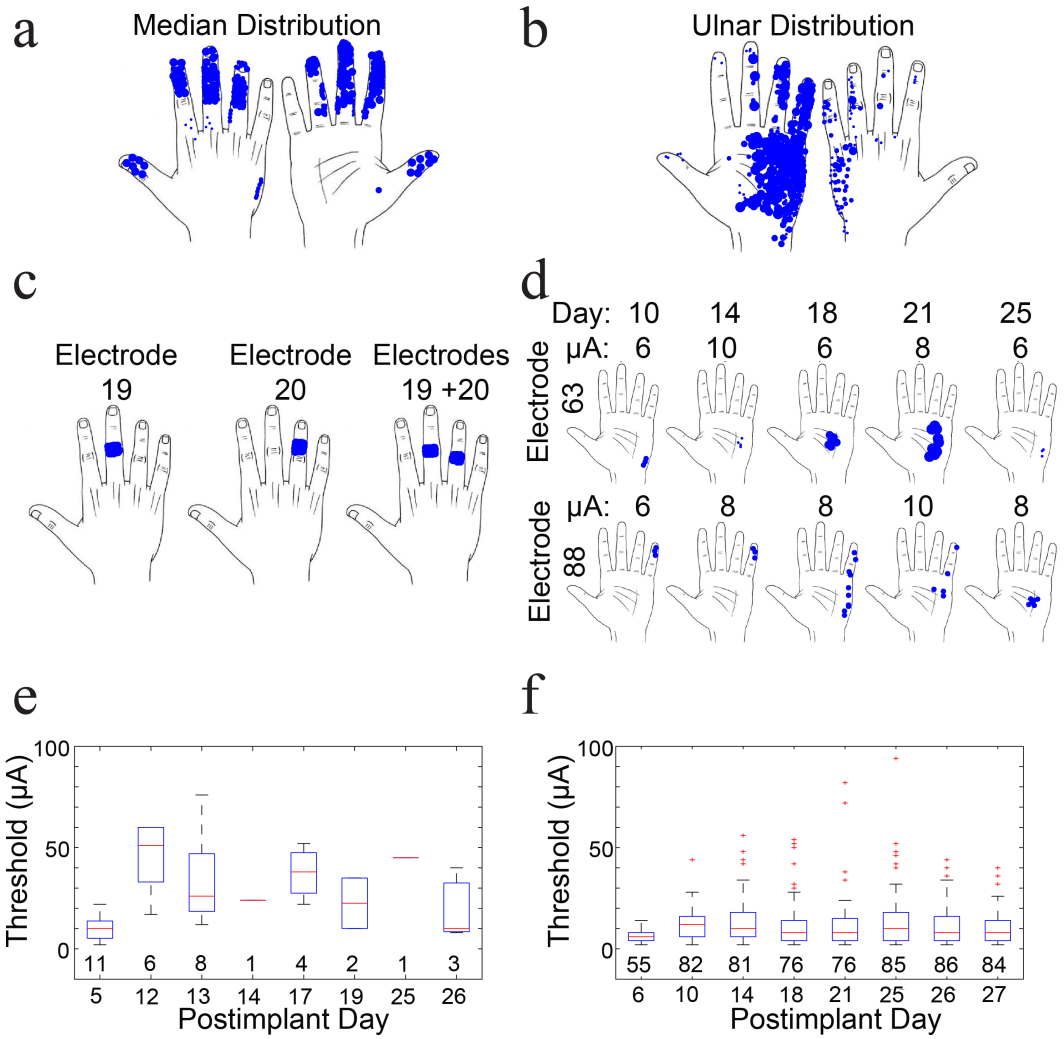

Figure 7.3. Electrical stimulation evokes spatially distinct and stable sensory percepts. Panels (a), (c) and (e) show data from Subject 1; and (b), (d), and (f) show data from Subject 2. (a-b) Results from intrafascicular stimulation of human median and ulnar nerves show evoked sensations in the phantom hand that follow the expected spatial distributions for each nerve. The percepts evoked outside of the expected distributions did not repeat location on subsequent stimulations and may have been phantom sensations occurring at the same time as stimulation. (c) Single electrode stimulation (electrode 19 at 47μA; electrode 20 at 15μA) produced discrete sensory percepts, and when the same electrodes were stimulated simultaneously the two discrete percepts could be perceived simultaneously (Subject 1, median implant). The interelectrode distance in this example was 400 μm. (d) Examples of percepts that were evoked by two different electrodes with one percept that was considered stable across all five sessions (electrode 63; top row of hands) and another that was stable for two consecutive sessions (electrode 88; bottom row of hands). Marked locations were felt simultaneously (Subject 2). (e-f) Sensory percept thresholds over the duration of the experimental period for both subjects. For subject 1, only a subset of electrodes were stimulated each session. For subject 2, except on postimplant day 6, all 96 electrodes were stimulated each session. The number below each boxplot is the number of electrodes that evoked a sensory percept.

7.8 References

[1] J. M. Carmena, M. A. Lebedev, R. E. Crist, J. E. O'Doherty, D. M. Santucci, D. F. Dimitrov, P. G. Patil, C. S. Henriquez, and M. A. L. Nicolelis, "Learning to control a brain-machine interface for reaching and grasping by primates," *PLoS Biology,* vol. 1 (2), p. E42, 2003.

[2] C. Kemere, G. Santhanam, B. M. Yu, A. Afshar, S. I. Ryu, T. H. Meng, and K. V. Shenoy, "Detecting neural-state transitions using hidden markov models for motor cortical prostheses," *J Neurophysiol,* vol. 100 (4), pp. 2441-52, 2008.

[3] S. Musallam, B. D. Corneil, B. Greger, H. Scherberger, and R. A. Andersen, "Cognitive control signals for neural prosthetics," *Science,* vol. 305 (5681), pp. 258-62, 2004.

[4] S. Suner, M. R. Fellows, C. Vargas-Irwin, G. K. Nakata, and J. P. Donoghue, "Reliability of signals from a chronically implanted, silicon-based electrode array in non-human primate primary motor cortex," *IEEE Transac Neural Sys Rehab Eng* vol. 13 (4), pp. 524-541, 2005.

[5] D. Sussillo, P. Nuyujukian, J. M. Fan, J. C. Kao, S. D. Stavisky, S. Ryu, and K. Shenoy, "A recurrent neural network for closed-loop intracortical brain-machine interface decoders," *J Neural Eng,* vol. 9 (2), p. 026027, 2012.

[6] M. Velliste, S. Perel, M. C. Spalding, A. S. Whitford, and A. B. Schwartz, "Cortical control of a prosthetic arm for self-feeding," *Nature,* vol. 453 (7198), pp. 1098-1101, 2008.

[7] L. R. Hochberg, M. D. Serruya, G. M. Friehs, J. A. Mukand, M. Saleh, A. H. Caplan, A. Branner, D. Chen, R. D. Penn, and J. P. Donoghue, "Neuronal ensemble control of prosthetic devices by a human with tetraplegia," *Nature,* vol. 442 (7099), pp. 164-171, 2006.

[8] J. Simeral, L. Hochberg, J. Donoghue, G. Friehs, and M. Black, "Point-and-click cursor control with an intracortical neural interface system in humans with tetraplegia," *IEEE Transac Neural Sys Rehab Eng,* 2011.

[9] J. D. Simeral, S.-P. Kim, M. J. Black, J. P. Donoghue, and L. R. Hochber, "Neural control of cursor trajectory and click by a human with tetraplegia 1000 days after implantation of an intracortical microelectrode array," *J Neural Eng,* vol. 8 2011.

[10] L. R. Hochberg, D. Bacher, B. Jarosiewicz, N. Y. Masse, J. D. Simeral, J. Vogel, S. Haddadin, J. Liu, S. S. Cash, P. van der Smagt, and J. P. Donoghue, "Reach and grasp by people with tetraplegia using a neurally controlled robotic arm," *Nature,* vol. 485 (7398), pp. 372-375, 2012.

[11] L. J. Hargrove, A. M. Simon, A. J. Young, R. D. Lipschutz, S. B. Finucane, D. G. Smith, and T. A. Kuiken, "Robotic leg control with emg decoding in an amputee with nerve transfers," *New England J Med,* vol. 369 (13), pp. 1237-42, 2013.

[12] T. A. Kuiken, G. Li, B. A. Lock, R. D. Lipschutz, L. A. Miller, K. A. Stubblefield, and K. B. Englehart, "Targeted muscle reinnervation for real-time myoelectric control of multifunction artificial arms," *J Amer Med Assoc,* vol. 301

(6), pp. 619-28, 2009.

[13] G. S. Dhillon and K. W. Horch, "Direct neural sensory feedback and control of a prosthetic arm," *IEEE Transac Neural Sys Rehab Eng,* vol. 13 (4), pp. 468-472, 2005.

[14] G. S. Dhillon, S. M. Lawrence, D. T. Hutchinson, and K. W. Horch, "Residual function in peripheral nerve stumps of amputees: Implications for neural control of artificial limbs," *J Hand Surg,* vol. 29 (4), pp. 605-15; discussion 616-8, 2004.

[15] K. Garde, E. Keefer, B. Botterman, P. Galvan, and M. I. Romero, "Early interfaced neural activity from chronic amputated nerves," *Frontiers Neuroeng,* vol. 2 p. 5, 2009.

[16] K. Horch, S. Meek, T. G. Taylor, and D. T. Hutchinson, "Object discrimination with an artificial hand using electrical stimulation of peripheral tactile and proprioceptive pathways with intrafascicular electrodes," *IEEE Transac Neural Sys Rehab Eng,* vol. 19 (5), pp. 483-489, 2011.

[17] K. H. Polasek, H. A. Hoyen, M. W. Keith, R. F. Kirsch, and D. J. Tyler, "Stimulation stability and selectivity of chronically implanted multicontact nerve cuff electrodes in the human upper extremity," *IEEE Transac Neural Sys Rehab Eng,* vol. 17 (5), pp. 428-437, 2009.

[18] K. H. Polasek, H. A. Hoyen, M. W. Keith, and D. J. Tyler, "Human nerve stimulation thresholds and selectivity using a multicontact nerve cuff electrode," *IEEE Transac Neural Sys Rehab Eng,* vol. 15 (1), pp. 76-82, 2007.

[19] P. M. Rossini, S. Micera, A. Benvenuto, J. Carpaneto, G. Cavallo, L. Citi, C. Cipriani, L. Denaro, V. Denaro, G. Di Pino, F. Ferreri, E. Guglielmelli, K.-P. Hoffmann, S. Raspopovic, J. Rigosa, L. Rossini, M. Tombini, and P. Dario, "Double nerve intraneural interface implant on a human amputee for robotic hand control," *Clinical Neurophys,* vol. 121 (5), pp. 777-783, 2010.

[20] D. A. Zlotolow and S. H. Kozin, "Advances in upper extremity prosthetics," *Hand clinics,* vol. 28 (4), pp. 587-593, 2012.

[21] J. M. Burck, J. D. Bigelow, and S. D. Harshbarger, "Revolutionizing prosthetics: Systems engineering challenges and opportunities," *Johns Hopkins APL Technical Digest,* vol. 30 2011.

[22] L. Resnik, S. L. Klinger, and K. Etter, "The deka arm: Its features, functionality, and evolution during the veterans affairs study to optimize the deka arm," *Prosthetics Orthotics Internat,* 2013.

[23] A. E. Schultz, P. D. Marasco, and T. A. Kuiken, "Vibrotactile detection thresholds for chest skin of amputees following targeted reinnervation surgery," *Brain Research,* vol. 1251 pp. 121-129, 2009.

[24] K. H. Polasek, M. A. Schiefer, G. C. Pinault, R. J. Triolo, and D. J. Tyler, "Intraoperative evaluation of the spiral nerve cuff electrode on the femoral nerve trunk," *J Neural Eng,* vol. 6 (6), p. 066005, 2009.

[25] M. A. Schiefer, K. H. Polasek, R. J. Triolo, G. C. Pinault, and D. J. Tyler,

"Selective stimulation of the human femoral nerve with a flat interface nerve electrode," *J Neural Eng,* vol. 7 (2), p. 26006, 2010.

[26] T. Boretius, J. Badia, A. Pascual-Font, M. Schuettler, X. Navarro, K. Yoshida, and T. Stieglitz, "A transverse intrafascicular multichannel electrode (time) to interface with the peripheral nerve," *Biosensors Bioelectronics,* vol. 26 (1), pp. 62-69, 2010.

[27] A. Branner, R. B. Stein, and R. A. Normann, "Selective stimulation of cat sciatic nerve using an array of varying-length microelectrodes," *J Neurophys,* vol. 85 (4), pp. 1585-1594, 2001.

[28] M. Gasson, B. Hutt, and I. Goodhew, "Invasive neural prosthesis for neural signal detection and nerve stimulation," *Internat J Control Signal Process*, vol 19, pp365-375, 2005.

[29] K. Yoshida and K. Horch, "Selective stimulation of peripheral nerve fibers using dual intrafascicular electrodes," *IEEE Transactions Biomed Eng,* vol. 40 (5), pp. 492-494, 1993.

[30] X. Jia, M. A. Koenig, X. Zhang, J. Zhang, T. Chen, and Z. Chen, "Residual motor signal in long-term human severed peripheral nerves and feasibility of neural signal-controlled artificial limb," *J Hand Surg,* vol. 32 (5), pp. 657-666, 2007.

[31] R. L. Rennaker, J. Miller, H. Tang, and D. A. Wilson, "Minocycline increases quality and longevity of chronic neural recordings," *J Neural Eng,* vol. 4 (2), pp. L1-5, 2007.

[32] L. Spataro, J. Dilgen, S. Retterer, A. J. Spence, M. Isaacson, J. N. Turner, and W. Shain, "Dexamethasone treatment reduces astroglia responses to inserted neuroprosthetic devices in rat neocortex," *Exp Neurol,* vol. 194 (2), pp. 289-300, 2005.

[33] W. Wu, Y. Gao, E. Bienenstock, J. P. Donoghue, and M. J. Black, "Bayesian population decoding of motor cortical activity using a kalman filter," *Neural Computation,* vol. 18 pp. 80-118, 2006.

[34] R. Davoodi and G. E. Loeb, "Real-time animation software for customized training to use motor prosthetic systems," *IEEE Trans Neural Syst Rehabil Eng,* vol. 20 (2), pp. 134-42, 2012.

[35] J. C. Lilly, J. R. Hughes, E. C. Alvord, Jr., and T. W. Galkin, "Brief, noninjurious electric waveform for stimulation of the brain," *Science,* vol. 121 (3144), pp. 468-9, 1955.

[36] D. B. McCreery, W. F. Agnew, T. G. Yuen, and L. Bullara, "Charge density and charge per phase as cofactors in neural injury induced by electrical stimulation," *IEEE Transac Biomed Eng,* vol. 37 (10), pp. 996-1001, 1990.

[37] S. F. Cogan, "Neural stimulation and recording electrodes," *Ann Rev Biomed Eng,* vol. 10 (1), pp. 275-309, 2008.

[38] T. S. Davis, R. A. Parker, P. A. House, E. Bagley, S. Wendelken, R. A. Normann, and B. Greger, "Spatial and temporal characteristics of v1 microstimulation

during chronic implantation of a microelectrode array in a behaving macaque," *J Neural Eng,* vol. 9 (6), p. 065003, 2012.

[39] P. R. Troyk, D. E. Detlefsen, S. F. Cogan, J. Ehrlich, M. Bak, D. B. McCreery, L. Bullara, and E. Schmidt, "Safe" charge-injection waveforms for iridium oxide (AIROF) microelectrodes, *Conference Proceedings: Ann Internat Conference IEEE Eng Med Biology,* vol. 6 pp. 4141-4144, 2004.

[40] K. Warwick, M. Gasson, B. Hutt, and I. Goodhew, "The application of implant technology for cybernetic systems," *Archives Neurology,* vol. 60 pp. 1369-1373, 2003.

[41] A. Sharma, L. Rieth, P. Tathireddy, R. Harrison, and F. Solzbacher, "Long term in vitro stability of fully integrated wireless neural interfaces based on utah slant electrode array," *Applied Physics Letters,* vol. 96 (7), p. 73702, 2010.

[42] J. Egan, J. Baker, P. A. House, and B. Greger, "Decoding dexterous finger movements in a neural prosthesis model approaching real-world conditions," *IEEE Trans Neural Syst Rehabil Eng,* vol. 20 (6), pp. 836-44, 2012.

[43] M. H. Schieber and L. S. Hibbard, "How somatotopic is the motor cortex hand area?," *Science,* vol. 261 (5120), pp. 489-92, 1993.

[44] B. Poston, A. Danna-Dos Santos, M. Jesunathadas, T. M. Hamm, and M. Santello, "Force-independent distribution of correlated neural inputs to hand muscles during three-digit grasping," *J Neurophysiol,* vol. 104 (2), pp. 1141-54, 2010.

[45] T. Allard, S. A. Clark, W. M. Jenkins, and M. M. Merzenich, "Reorganization of somatosensory area 3b representations in adult owl monkeys after digital syndactyly," *J Neurophysiol,* vol. 66 (3), pp. 1048-58, 1991.

[46] J. H. Kaas, M. M. Merzenich, and H. P. Killackey, "The reorganization of somatosensory cortex following peripheral nerve damage in adult and developing mammals," *Annual Review Neurosci,* vol. 6 pp. 325-56, 1983.

[47] M. M. Merzenich, J. H. Kaas, J. Wall, R. J. Nelson, M. Sur, and D. Felleman, "Topographic reorganization of somatosensory cortical areas 3b and 1 in adult monkeys following restricted deafferentation," *Neuroscience,* vol. 8 (1), pp. 33-55, 1983.

[48] M. M. Merzenich, J. H. Kaas, J. T. Wall, M. Sur, R. J. Nelson, and D. J. Felleman, "Progression of change following median nerve section in the cortical representation of the hand in areas 3b and 1 in adult owl and squirrel monkeys," *Neuroscience,* vol. 10 (3), pp. 639-65, 1983.

[49] C. Xerri, M. M. Merzenich, W. Jenkins, and S. Santucci, "Representational plasticity in cortical area 3b paralleling tactual-motor skill acquisition in adult monkeys," *Cerebral Cortex,* vol. 9 (3), pp. 264-76, 1999.

CHAPTER 8

CONCLUSIONS AND FUTURE DIRECTIONS

8.1 Neuromodulation

As neuromodulation goals grow in complexity, restoration of voluntary and autonomic functions will require multifaceted devices that can record and decode neural activity then send a corresponding electrical stimulation to evoke the desired physiological outcome(s). Such devices will likely be more complicated that the devices commonly used in the clinic today. For example, deep brain stimulators deliver constant electrical stimulation via large electrodes (> 1 mm) to the patient, achieving one clinical goal at all times.

As we continue to strive to restore normal physiological function using neural electrodes, we must aim to recapitulate what our nervous system does so well: send and receive signals to and from different neural pathways in a selective manner to achieve higher degrees of functionality. Taking these ideas one step further, we can begin to design devices that can detect multiple different neural signals associated with different stimuli, and then such devices can simultaneously drive excitation or inhibition of these different pathways. An example that demonstrates this idea would be a spinal cord injured person with a Utah Array-based pudendal neuroprosthesis that could detect and control all three different pathways in this nerve: urination, defecation and reflex erection.

Another branch of research in neuromodulation is the regrowth of injured nerves. In models of nerve growth today, such as injured peripheral nerves, this type of growth takes time. We also know from fundamental neurophysiology studies those neurons that ‘fire together wire together,’ meaning that neural activity drives the formation and strengthening of neural connections.[1,2] Therefore, we can begin to postulate that combinations of neural growth factors and nerve/muscle stimulators could work together

to achieve restoration of injured neural connections. Indeed, researchers are working on methods to promote axonal regeneration[3] and even combinations of nerve growth factors and electrical stimulation.[4] However, one confound for neural regeneration methods is targeting the regenerating fibers to appropriate targets, a problem that has yet to be resolved.

Neuromodulation may also act as a temporary therapy to increase functional recovery following nerve injury. New research is uncovering better functional recovery following spinal cord or peripheral nerve injury when neuromodulation is used immediately following nerve injury. In these cases, the neuromodulation methods may include the delivery of surface stimulation[5,6] and/or spinal cord stimulation[7] for acute periods of rehabilitation time following nerve injury.

The future of neuromodulation is here and exciting new research is demonstrating improved functionality in patients with nerve injury or disease. As mentioned in the preface, it will be essential for neural engineers and physicians to continue to bridge the gap and strengthen the relationship between research and clinical medicine, especially as we embark on the development of highly sophisticated neural modulation devices.

8.2 Neural electrodes

In this section, we first discuss the future of Utah Array technologies and three major topics are addressed: wireless arrays, arrays for larger peripheral nerves, and longer duration peripheral nerve implant studies. The end of this section then discusses the future of neural electrodes and the emerging techniques in neural stimulation, including magnetic, infrared, and optical stimulation.

In order to unfold the potential of multielectrode neural interfaces, these devices must become wireless: fully packaged and hermetically sealed. There can be no question that one of the current limitations of high electrode count devices stems from the requirement of a percutaneous connector. This is especially true once these devices are implanted into the peripheral nervous system, where the convenience of the skull as an attachment site, free from joint movements, is no longer an option. The human studies we carried out in amputees were limited by one-month duration implants, due to having the required percutaneous connector attached to the skin, which negated their ability to use an elbow-joint prosthesis. In order to fully uncover the potential of USEA devices, they must be implanted and electrophysiologically monitored for years in human studies. It is our hope that the initial studies we carried out in amputees helps to motivate neural engineers to push their ongoing efforts in developing wireless technologies,[8] for without this feature, the clinical usefulness of high-electrode count devices will be limited.

Devices that can be implanted in larger peripheral nerves will also dictate the future of Utah Array technologies. The studies carried out in Chapter 7 utilized USEAs with electrode lengths from 0.5 to 1.0 mm. However, the human ulnar and median nerves are > 1 mm diameter (4-6 mm diameters were observed during our preliminary dissections in human cadavers), and thus, we were only able to achieve intrafascicular implantation into the portion of the nerve adjacent to the array. As we developed higher electrode density devices with shorter length electrodes for smaller neuronal structures, future work is needed to develop arrays with longer electrodes for larger neuronal structures.

Although the UEA has been implanted in the CNS for > 5 years,[9] published data

for chronic USEA implants extends to only 7 months.[10] In order to translate USEA applications to human studies, more data are needed to assess the effects of these devices after years of implantation. The importance of conducting these studies in animals will be to investigate whether the current devices are sufficient for such long durations, so that modifications can be made to these devices before their long-term implantation into humans (see biocompatibility section below). Therefore, the next steps for peripheral nerve Utah Arrays is to investigate longer duration implants and extend what is known about nerve degeneration and regeneration following 1-7 month implants.[10-12]

The work presented in this dissertation was focused on neuromodulation via electrical stimulation of the nervous system, but many new nerve stimulation methods are being developed, including magnetic,[13,14] infrared,[15] and optical stimulation.[16] These neuromodulation techniques may surpass electrical stimulation in their ability to provide safe stimulation of neural tissue as well as highly selective stimulation of neural circuits. For example, multiwaveguide arrays have been developed for light delivery to multiple locations and depths in the cortex,[17] similar to the Utah Array technologies for delivery of electrical stimulation. The combination of optogenetics—whereby specific neural networks are targeted for activation (via transgenic manipulation of select neurons)—with multiwaveguide arrays provides an exciting example of combining new neuromodulation techniques and electrodes for functional restoration after nerve injury.

8.3 Increasing the lifetime of indwelling Utah Arrays

Combination devices may include any number of drugs or surface modifications to a device, such that a given physiological response to that device is inhibited or

activated. One example is cardiac pacemakers that deliver dexamethasone to decrease the fibrotic encapsulation of the device, which can effectively remove it from the distances needed to provide clinically useful electrical stimulation. Such combinations of devices and drugs have become commonplace in the clinic, from antibiotic containing sutures to vascular stents with anticoagulation modifications.

Future Utah Array technologies will likely benefit by incorporating some of these strategies, which may help increase the lifetime of these devices and/or the number of viable neurons surrounding the devices. In our chronic rat and human studies, we systemically administered dexamethasone and minocycline. However, local slow release of dexamethasone is more effective at attenuating the inflammatory response and reducing neural loss.[18] Thus, the next generation Utah Arrays may see enhanced effectiveness for long duration (months to years) indwelling devices if surface chemical modifications can be used to provide local delivery of drugs. Another strategy for increasing the effectiveness of these devices may be hydrogel matrix coatings, which have been shown to decrease cell loss surrounding neural probe-type cortical electrode arrays.[19]

One factor that is unique to nerve cuff and USEA-type interfaces is that the nerve and electrodes are wrapped with a containment system. New theories are emerging that postulated the inhibition of normal flow of molecules and cells at the device-tissue interface may lead to supra-physiological concentration of immune cells and signaling molecules, augmenting the chronic foreign body response.[19] Thus, decreasing the surface area or utilizing hydrogel matrices may improve the long-term functioning of Utah Arrays.

To this end, we tested a novel organic nerve wrap containment system in our rat studies, a system that was already FDA approved for use as a neuroprotective wrap or conduit in people with injured or severed nerves, respectively. In contrast to the systems previously used to contain USEAs (silicone or gortex-based wraps[10,20]), this wrap consisted of decellularized intestinal submucosa of the pig.[21] By the nature of such material, cells and signaling molecules would be able to diffuse through the material, and therefore, supraphysiological concentrations of immune cells and molecules would not accumulated at the wrap-tissue interface.[22] In addition, using this organic nerve wrap would directly translate to human studies, as the material was nonimmunogenic, FDA approved, and could be explanted after semichronic time periods (< 2 months). The results of both our rat and human studies support the use of this material as a containment system for Utah Arrays implanted for up to two months. Future studies are now warranted to investigate the use of such wraps to contain arrays in actively behaving animals for many months or even years postimplantation.

8.4 Final remarks

Utah Array technologies were being used worldwide prior to the work presented in this dissertation; however, applications were only available for medium-sized peripheral nerve animal studies. As a consequence of this work, we have designed an array that can be implanted in smaller nervous system structures, and validated the use of such high-density devices for up to two-month time periods. We have also expanded the potential clinical applications for Utah Array-based prostheses as an interface for neural recording and stimulation to restore urinary function in animal models and to develop the

next generation prosthetic limbs in humans. We hope this work will continue to open doors in basic research and clinical applications that utilize Utah Array-based neural interfaces for the restoration of function in people who have suffered from nerve injury or disease.

8.5 References

1 Hebb DO. The organization of behavior; a neuropsychological theory. Oxford, England. Wiley, 1949.

2 Bliss T, Collingridge GL. A synaptic model of memory: long-term potentiation in the hippocampus. Nature 1993;361(7):31-39.

3 Tom VJ, Sandrow-Feinberg HR, Miller K, et al. Combining peripheral nerve grafts and chondroitinase promotes functional axonal regeneration in the chronically injured spinal cord. J Neurosci 2009;29:14881–14890.

4 Huang J, Zhang Y, Lu L, et al. Electrical stimulation accelerates nerve regeneration and functional recovery in delayed peripheral nerve injury in rats. Eur J Neurosci 2013;38:3691–3701.

5 Popovic MR, Kapadia N, Zivanovic V, et al. Functional electrical stimulation therapy of voluntary grasping versus only conventional rehabilitation for patients with subacute incomplete tetraplegia: a randomized clinical trial. Neurorehabil Neural Repair 2011;25:433–442.

6 Thrasher TA, Popovic MR. Functional electrical stimulation of walking: function, exercise and rehabilitation. Ann Readapt Med Phys 2008;51:452–460.

7 Courtine G, Gerasimenko Y, van den Brand R, et al. Transformation of nonfunctional spinal circuits into functional states after the loss of brain input. Nat Neurosci 2009;12:1333–1342.

8 Sharma A, Rieth L, Tathireddy P, et al. Long term in vitro stability of fully integrated wireless neural interfaces based on Utah slant electrode array. Applied Physics Letters 2010;96:73702.

9 Hochberg LR, Serruya MD, Friehs GM, et al. Neuronal ensemble control of prosthetic devices by a human with tetraplegia. Nature 2006;442:164–171.

10 Branner A, Stein RB, Fernandez E, et al. Long-term stimulation and recording with a penetrating microelectrode array in cat sciatic nerve. IEEE Transact Biomedical Eng 2004;51:146–157.

11 Wark H, Mathews KS, Normann RA, et al. Behavioral and cellular consequences of high-electrode count Utah Arrays chronically implanted in rat sciatic nerve. *In revision* J Neural Eng Apr 2014.

12 Christensen MB. Doctoral Thesis: Evaluation of inflammation and morphometric parameters associated with neural device implantation in the sciatic nerve. University of Utah 2011.

13 Maccabee PJ, Nagarajan SS, Amassian VE, et al. Influence of pulse sequence,

polarity and amplitude on magnetic stimulation of human and porcine peripheral nerve. J Phys 1998;513 (Pt 2):571–585.

14 Rossi S, Hallett M, Rossini PM. Safety, ethical considerations, and application guidelines for the use of transcranial magnetic stimulation in clinical practice and research. Clinical Neurophys 2009.

15 Wells J, Konrad P, Kao C, et al. Pulsed laser versus electrical energy for peripheral nerve stimulation. J Neurosci 2007.

16 Pashaie R, Anikeeva P, Lee JH, et al. Optogenetic brain interfaces. IEEE Rev Biomed Eng 2014;7:3–30.

17 Zorzos AN, Scholvin J, Boyden ES, et al. Three-dimensional multiwaveguide probe array for light delivery to distributed brain circuits. Optics Letters 2012.

18 Zhong Y, Bellamkonda RV. Dexamethasone-coated neural probes elicit attenuated inflammatory response and neuronal loss compared to uncoated neural probes. Brain Research 2007;1148:15–27.

19 Skousen JL. Doctoral Thesis: Novel design strategies to reduce the foreign body response to central nervous system implants. University of Utah 2013.

20 Normann RA, Dowden BR, Frankel MA, et al. Coordinated, multijoint, fatigue-resistant feline stance produced with intrafascicular hind limb nerve stimulation. J Neural Eng 2012;9:6019.

21 Kokkalis ZT, Pu C, Small GA, et al. Assessment of processed porcine extracellular matrix as a protective barrier in a rabbit nerve wrap model. J Reconst Microsurg 2011;27:19–28.

22 Skousen JL, Merriam SME, Srivannavit O, et al. Reducing surface area while maintaining implant penetrating profile lowers the brain foreign body response to chronically implanted planar silicon microelectrode arrays. Progress Brain Research 2011;194:167–180.